POLITECNICO DI TORINO

Corso di Laurea Magistrale in Ingegneria Elettronica

Tesi di Laurea Magistrale

A quantum computation model for molecular nanomagnets

Relatori:
Prof. Maurizio Zamboni
Prof. Mariagrazia Graziano

Candidato:
Giovanni Amedeo Cirillo

Aprile 2018

Summary

Molecular nanomagnets can be candidates for the implementation of quantum computers: qubits are defined on their spins and they can be brought together through supramolecular chemistry (the domain of chemistry focusing on assembled molecular systems) to make quantum gates.
In this thesis, a supramolecular complex with Cr_7Ni rings has been exploited for the definition of quantum processors with two and three qubits. When a magnetostatic field B is applied on the molecule, a two-level ($S = \pm\frac{1}{2}$) spin qubit is associated to each ring and the interaction of adjacent qubits is tuned through a Co switchable link with its own $\pm\frac{1}{2}$ spin. Qubits can reach decoherence times - *i.e.* the dynamic randomization of the qubit phase, affecting the result of a quantum operation - of tens of microsecond, comparable with values of leading technology based on superconductor devices.
The thesis is organized in four chapters. In the first chapter, quantum computation theory is introduced and its mathematical model is discussed. The attention is focused on fundamental concepts as quantum superposition and entanglement, qubit description on the Bloch sphere, unitary evolution operators and the fundamental quantum gates. Moreover, an overview of some possible implementations of quantum computers is given, after introducing the DiVincenzo criteria for the realization of quantum computers.
Second chapter focuses its attention of Cr_7Ni supramolecular complexes, after introductions to spin quantum computing and the state of the art of molecular magnets in quantum computation. Electron Paramagnetic Resonance (EPR), the spin rotation technique based on oscillating Amplitude-Modulated fields, is controlled by classical processors and it is exploited to implement single-qubit gates with switch spin equal to $-\frac{1}{2}$ and the Controlled-phase (C-ϕ) gate through the interaction of adjacent qubits, enabled by changing the spin of the switch from $-\frac{1}{2}$ to $+\frac{1}{2}$. The combination of C-ϕ and single-qubit gates implements the CNOT gate, which forms with single-qubit rotations a set of universal quantum gates.
In the third chapter a quantum computer architecture is proposed, starting from the DiVincenzo criteria. The attention is focused on the molecular quantum execution unit, where single-qubit rotations and C-ϕ are treated as microinstrutions of a more complex instruction set. The instruction set has been proved to implement a reversible half-adder and to execute two quantum algorithms: the Quantum Fourier Transform (QFT) and Grover's search algorithm. A preliminary proposal of quantum teleportation with the three-qubits molecule is also presented.

Similarly to what happens for other types of quantum computers, qubits in molecular nanomagnets are affected by dynamic non-idealities (spin relaxation, decoherence and residual inter-qubit interaction) that impinge on the fidelity of the results on timescales even in the order of few millisecond. In order to establish the validity of the architecture, a MATLAB model for the molecular nanomagnets has been defined and it is discussed in the fourth chapter. Model includes transition frequencies in function of the static field B, EPR parameters for spin manipulation and timescales of non-idealtities. The estimated parameters can be useful for the definition of an optimal operating point where the behavior of molecules can be considered quasi-ideal.

According to the obtained values, complex operations as the QFT can be executed on available molecules with negligible dynamic errors on timescales of hundreds of nanosecond. In order to complete the architecture, it is required to design the front-end (spin manipulation architecture) and the back-end (spin measurement). On the other hand, chemical engineering can optimize the synthesis of molecules with longer timescales for non-idealities, so programs with more instructions than the actual ones can be executed with negligible errors.

Contents

List of Tables

List of Figures

Chapter 1

Introduction to Quantum Computing

Quantum computing is a discipline that exploits quantum physics phenomena for computation and algorithms execution. It can be seen as a combination of quantum physics, information and computer science, where the fundamental unit of information, named **quantum bit** or **qubit**, is physically mapped on a quantum state.
The idea of quantum computation emerged in 1980s. The idea of a quantum computer was proposed by the Russian mathematician Yuri Manin in 1980. In 1981 Richard Feynman observed that the simulation of nature should be done quantum mechanically. A fundamental milestone for quantum computing is the publication of BB84, the world's first quantum cryptography protocol, by IBM scientists Charles Bennett and Gilles Brassard in 1984. In the following decade the first quantum circuits were demonstrated: in 1993, an international group of six scientists, including Charles Bennett, showed quantum teleportation, then in 1994 Peter Shor demonstrated an algorithm for factorizing integer numbers (there is not any efficient algorithm solving this problem with classical qubits) through a quantum computer - implemented to factorize 15 using a seven-qubits NMR computer in 2001 - and in 1995 Lov Grover showed that the problem of unstructured database search can be solved on a quantum computer with a computational cost lower than on a classical computer. The first solid-state processors were realized in the second half of 2000s and these results have been exploited in this decade for the first quantum computing applications available to the public: D-Wave systems and the IBM Quantum Experience, a quantum computer programmable via-cloud.
From an electronic point of view, quantum computing could be a possible solution to overcome the contemporary limitations of Moore's law, related to the exponential increasing of power consumption in silicon integrated circuits, thus limiting the

speed-up of digital processors.

1.1 Basic Concepts of Quantum Mechanics

Quantum mechanics explains the behavior of matter and its interactions with energy on the scale of atoms and subatomic particles. The goal of this section is to present the mathematical model of quantum mechanics, that is also exploited in quantum computation and information theories. In fact, state vectors and operators are used in the quantum world to describe physical phenomena; moreover, this representation permits to simulate quantum systems and circuits on a classical computer.

1.1.1 Linear Algebra of Quantum Mechanics

Hilbert spaces and the Dirac notation

Any quantum state can be described by a **state vector** or a **wave function**. The state vector belongs to an **Hilbert space**, that is a generalization of an Euclidean space not limited to three dimensions. A Hilbert vector space can have any number of dimensions and every vector belonging to this space can be multiplied by a complex scalar or by another vector of the same dimension, since an inner complex scalar product, whose result depends on the order in which the vectors are taken, is available

$$\mathbf{v} \cdot \mathbf{u} = (\mathbf{u} \cdot \mathbf{v})^* = \alpha \in \mathbb{C}. \tag{1.1}$$

The results of scalar product - differing from the order of vectors - are complex conjugate. Equivalently to the Euclidean space, the inner product of a vector belonging to an Hilbert space with itself $\mathbf{u} \cdot \mathbf{u}$ is real and it is the square value of its norm $\|\mathbf{u}\|$, a quantity that can be interpreted as the vector's length. Each vector can be written as linear combination of orthonormal basis vectors

$$\mathbf{v} = \sum_i \alpha_i \mathbf{u}_i, \tag{1.2}$$

where $\mathbf{u}_i \cdot \mathbf{v} = \alpha_i$ and $\mathbf{u}_i \cdot \mathbf{u}_j = \delta_{ij}$, where δ_{ij} is the Kronecker delta, equal to 1 if $i = j$ and to 0 otherwise.

In quantum mechanics, the **Dirac notation** is employed for the description of a state vector, since it clearly distinguishes between vectors appearing on the right hand side - called **ket** vectors - and on the left hand side - called **bra** vectors - of scalar products. The state vector is expressed as a *ket*

$$|\psi\rangle = \begin{bmatrix} a_1 \\ a_2 \\ \vdots \\ a_n \end{bmatrix}, \tag{1.3}$$

where a_i are complex coefficients, each one associated to one state $|\psi_i\rangle$ belonging to the vector basis. The square value of magnitude $|a_i|^2$ gives the probability for the quantum state of being in the basis state $|\psi_i\rangle$

$$|a_i|^2 = P(|\psi\rangle = |\psi_i\rangle). \tag{1.4}$$

Since every vector in a space is a linear combination of the corresponding basis set, it is possible to say that the sum of the probabilities of being in these states must be equal to 1

$$\sum_{i=1}^{n} |a_i|^2 = 1. \tag{1.5}$$

A *bra* vector is the transposed conjugate of the corresponding *ket*

$$\langle\psi| = [a_1^*, a_2^*, \cdots, a_n^*] = (|\psi\rangle')^*. \tag{1.6}$$

The inner product of a *bra* and a *ket* is represented by the **bra-ket** notation

$$\langle\phi\,|\,\psi\rangle = \langle\phi| \cdot |\psi\rangle = \sum_i \phi_i^* \psi_i. \tag{1.7}$$

Operators

In linear algebra, an operator is any transformation A between two vector spaces V and W linear in its inputs

$$A\left(\sum_i a_i \mathbf{v}_i\right) = \sum_i a_i A(\mathbf{v}_i). \tag{1.8}$$

Linearity implies that the sum of two operators applied on the same vector can be written as

$$(A+B)\mathbf{v} = A\mathbf{v} + B\mathbf{v} \tag{1.9}$$

Linear operators are tipically represented as matrices that map a vector $\mathbf{v}_j$ belonging to the basis of V into a vector $\mathbf{w}_i$ belonging to the basis of W.

$$A\mathbf{v}_j = \sum_i A_{ij}\mathbf{w}_i. \tag{1.10}$$

The matrix representation of a linear operator needs the definition of basis states for the input and output vector spaces. In the case of vectors belonging to an Hilbert space, the transformation done by a linear operator maps the result vector in the same Hilbert space.
In the Dirac notation, a linear operator transforms kets into other kets according to

$$A\left|\psi\right\rangle = \left|\psi'\right\rangle. \tag{1.11}$$

An equivalent transformation on bras is done

$$\left\langle\psi\right| A = \left\langle\psi'\right|. \tag{1.12}$$

Given an operator A, its Hermitian conjugate or **adjoint** $A^\dagger$ is an operator such that

$$\left\langle\psi\right| A^\dagger = A\left|\psi\right\rangle. \tag{1.13}$$

or equivalently

$$\left\langle\psi|A^\dagger|\phi\right\rangle = \left\langle\phi|A|\psi\right\rangle^*. \tag{1.14}$$

The Hermitian conjugate is nothing but the transposed conjugate of the matrix A

$$A^{\dagger}_{ij} = A^{*}_{ji}. \tag{1.15}$$

It is possible to prove that $(A^{\dagger})^{\dagger} = A$. Most physical processes are described by **Hermitian** or **unitary** operators: the Hermitian ones are equal to their adjoint

$$H = H^{\dagger} \tag{1.16}$$

and the unitary ones have their inverse equal to their adjoint, so that

$$UU^{\dagger} = U^{\dagger}U. \tag{1.17}$$

The **identity** operator is the most evident example of Hermitian operator ($I^{\dagger} = I$).

Eigenvalues and eigenvectors

An **eigenvector** - or **eigenket**, according to Dirac notation - of a linear operator A on a vector space is a non-zero vector $|\psi\rangle = [\psi_1, \psi_2, \cdots, \psi_i, \cdots, \psi_j, \cdots, \psi_n]'$ such that

$$A|\psi\rangle = \lambda|\psi\rangle \tag{1.18}$$

where λ is a scalar named **eigenvalue**. Using the matrix formalism, in a n-dimension Hilbert space, equation 1.18 is equivalent to n simultaneous equations of the form

$$\sum_j A_{ij}\psi_j = \lambda\psi_i \tag{1.19}$$

or

$$\sum_j (A_{ij} - \lambda\delta_{ij})\psi_j = 0 \tag{1.20}$$

The set of equations - described by the coefficient matrix $A - \lambda I$ - has non-trivial solutions if $\det|A - \lambda I| = 0$. The determinant is in fact an n^{th} order polynomial in λ, whose roots are the eigenvalues of A. According to the fundamental theorem of algebra, every polynomial has at least one complex root, thus ensuring the existence of one eigenvalue and a corresponding eigenvector for a linear operator A. Once

the eigenvalues $\{\lambda_1, \cdots, \lambda_i, \cdots, \lambda_n\}$ have been determined, it is possible to find the **eigenvector** corresponding to each eigenvalue λ_i by solving the set of equations

$$\sum_j (A_{ij} - \lambda_i \delta_{ij}) \psi_j = 0, \tag{1.21}$$

with coefficients of the eigenvector $|\psi_j\rangle$ as solutions.
The problem of finding eigenvalues and eigenvector of a matrix A is equivalent to the diagonalization of A

$$A = S \Lambda S^{-1}, \tag{1.22}$$

where Λ is a diagonal matrix with the eigenvalues of A and S is a matrix formed by the eigenvectors of A.

$$S = \left[|\psi_1\rangle, |\psi_2\rangle, \cdots, |\psi_n\rangle \right]. \tag{1.23}$$

It is possible to prove that an **Hermitian operator has real eigenvalues and mutually orthogonal eigenvectors** (their inner product is null). Moreover, for any Hermitian operator in an n dimensional Hilbert space n orthonormal eigenvectors always exist, thus providing a natural basis for describing the operator, where each basis vector has a single nonzero entry with norm equal to 1. **For a unitary operator, the eigenvalues have magnitude one and the corresponding eigenvectors are orthogonal**.

Tensor product

Given two vector spaces V and W of dimension m and n respectively, the tensor product $V \otimes W$ linearly combines the elements of V and W, thus obtaining a mn dimensional vector space. A convenient representation of the tensor product is the **Kronecker product**, based on matrices. Given two matrices A (m by n) and B (p by q), the Kronecker product is

$$A \otimes B = \begin{bmatrix} A_{11}B & \cdots & A_{1n}B \\ A_{21}B & \cdots & A_{2n}B \\ \vdots & \vdots & \vdots \\ A_{m1}B & \cdots & A_{mn}B \end{bmatrix}. \tag{1.24}$$

An example is reported, with two column vectors of dimension 3 and 2 respectively.

$$\begin{bmatrix} a_1 \\ a_2 \\ a_3 \end{bmatrix} \otimes \begin{bmatrix} b_1 \\ b_2 \end{bmatrix} = \begin{bmatrix} a_1 b_1 \\ a_1 b_2 \\ a_1 b_3 \\ a_2 b_1 \\ a_2 b_2 \\ a_2 b_3 \\ a_3 b_1 \\ a_3 b_2 \\ a_3 b_3 \end{bmatrix}.$$

Linearity of tensor product ensures that the it satisfies the following basic properties:

1. Given a scalar z and two vectors $|v\rangle$ and $|w\rangle$ belonging to V and W respectively

$$z(|v\rangle \otimes |w\rangle) = (z\,|v\rangle) \otimes |w\rangle = |v\rangle \otimes (z\,|w\rangle). \tag{1.25}$$

2. Given two vectors $|v_1\rangle$ and $|v_2\rangle$ in V and $|w\rangle$ in W

$$(|v_1\rangle + |v_2\rangle) \otimes |w\rangle = (|v_1\rangle \otimes |w\rangle) + (|v_2\rangle \otimes |w\rangle). \tag{1.26}$$

3. Given $|v\rangle$ in V and two vectors $|w_1\rangle$ and $|w_2\rangle$ in W

$$|v\rangle \otimes (|w_1\rangle + |w_2\rangle) = (|v\rangle \otimes |w_1\rangle) + (|v\rangle) \otimes |w_2\rangle). \tag{1.27}$$

Tensor product can be also applied on linear operators. In fact, given two linear operators A and B applied to $|v\rangle$ and $|w\rangle$ belonging V and W respectively, it is possible to define an operator $A \otimes B$ on the $V \otimes W$ vector space

$$(A \otimes B)(|v\rangle \otimes |w\rangle) \equiv A\,|v\rangle \otimes B\,|w\rangle\,. \tag{1.28}$$

Linearity permits to represent an arbitrary linear operator mapping $V \otimes W$ to $V' \otimes W'$ as a linear combination of tensor products of operators mapping V to V' and W to

W'

$$C = \left(\sum_i c_i A_i \otimes B_i \right) |v\rangle \otimes |w\rangle = \sum_i (c_i A_i |v\rangle \otimes B_i |w\rangle). \tag{1.29}$$

These properties are exploited in the definition of quantum logic gates and quantum computing algorithms.

Trace

The **trace** of a matrix A is a function, defined to be the sum of the diagonal elements of A

$$\mathrm{tr}(A) = \sum_i A_{ii}. \tag{1.30}$$

It is possible to prove that trace is cyclic

$$\mathrm{tr}(AB) = \mathrm{tr}(BA) \tag{1.31}$$

and linear

$$\mathrm{tr}(aA + bB) = a\,\mathrm{tr}(A) + b\,\mathrm{tr}(B). \tag{1.32}$$

where A and B are two arbitrary matrices and a and b are two complex numbers. Trace can be extended to the matrix representation of any operator described by matrix A and the invariance of the trace under unitary transformations $A \to UAU^\dagger$

$$\mathrm{tr}(UAU^\dagger) = \mathrm{tr}(A) \tag{1.33}$$

ensures the well-definition of the trace of an operator.

Operator exponential

An important link between unitary and Hermitian operators is provided by matrix exponentiation. It is possible to prove that, **given a unitary operator U, there is an Hermitian operator** A such that

$$U = \mathrm{e}^{-\mathrm{i}A}. \tag{1.34}$$

The demonstration is related to the fact that the eigenvalues λ_i of a unitary operator have modulus equal to 1, so they are writable as e^{-ia_i}, where a_i are real numbers that can be though of as the eigenvalues of an Hermitian operator A. The **exponentiation of a matrix** A is generally computed through a series expansion

$$\mathrm{e}^A = I + A + \frac{1}{2!}AA + \frac{1}{3!}AAA + \cdots = \sum_{k=0}^{+\infty} \frac{A^k}{k!}, \tag{1.35}$$

that it is generally an hard operation from the computational point of view. However, since the **exponentiation of a diagonal matrix** is very simple

$$\exp\left(\begin{bmatrix} a & 0 \\ 0 & b \end{bmatrix}\right) = \begin{bmatrix} \mathrm{e}^a & 0 \\ 0 & \mathrm{e}^b \end{bmatrix}, \tag{1.36}$$

the exponential of a general matrix can be calculated in a similar way by first diagonalizing the matrix and then noting that

$$\mathrm{e}^{S\Lambda S^{-1}} = S\mathrm{e}^{\Lambda}S^{-1}. \tag{1.37}$$

It is also possible to define an equivalent of the **Euler's formula for matrices**, that is strictly related to the evolution of a quantum system

$$\mathrm{e}^{\mathrm{i}A} = \cos(A) + \mathrm{i}\sin(A), \tag{1.38}$$

with

$$\cos(A) = I - \frac{A^2}{2!} + \frac{A^4}{4!} + \cdots = \sum_{k=0}^{+\infty} \frac{(-1)^k A^{2k}}{(2k)!},$$
$$\sin(A) = A - \frac{A^3}{3!} + \frac{A^5}{5!} + \cdots = \sum_{k=0}^{+\infty} \frac{(-1)^k A^{2k+1}}{(2k+1)!}.$$

1.1.2 The Schrödinger equation

The time evolution of a closed quantum system is described by the **Schrödinger equation**

$$\mathrm{i}\hbar\frac{\partial}{\partial t}|\psi\rangle = H(t)|\psi\rangle \tag{1.39}$$

where $\hbar$ is the **Planck's constant** divided by 2π and H is an Hermitian operator known as the **Hamiltonian** of the closed system. The general solution is

$$|\psi(t)\rangle = \mathrm{e}^{-\mathrm{i}\cdot\frac{1}{\hbar}\cdot\int_0^t H(t')\mathrm{d}t'}\,|\psi(0)\rangle\,. \tag{1.40}$$

When the Hamiltonian is constant during the time interval of integration

$$|\psi(t)\rangle = \mathrm{e}^{-\mathrm{i}\frac{H}{\hbar}t}\,|\psi(0)\rangle\,. \tag{1.41}$$

Since H is Hermitian, the expression is equivalent to

$$|\psi(t)\rangle = U(t)\,|\psi(0)\rangle\,, \tag{1.42}$$

so the **evolution** of a quantum state can be described by a unitary operator U usually called **propagator**. In the context of quantum circuits, quantum gates applied to single qubits are unitary. It has been assumed that the Hamiltonian is time-independent, but complex systems are controlled by varying the Hamiltonian, so the previous assumption is not valid anymore. In many cases, however, the Hamiltonian is piecewise constant in time domain, so the evolution can be described using a series of N propagators

$$|\psi\rangle = \left(\prod_{k=N}^{1} U_i\right)|\psi\rangle \tag{1.43}$$

with $U_i = \mathrm{e}^{-\mathrm{i}\frac{H_i}{\hbar}t_i}$. While the sequence of Hamiltonians is written with time running from left to right, the sequence of propagators is written from right to left, *i.e.* the rightmost propagator is the first to be applied. When the Hamiltonian varies continuously with time, the piecewise constant model does not describe the quantum system accurately; in that case, it is possible to write down a formal solution but it is not generally a useful approach in terms of computation and simulation.
The fact that any propagator describing the evolution of a quantum system is unitary has significant consequences:

- every propagator has an inverse, so quantum evolution - with the exception of measurement - is reversible, *i.e.* the cascade of two reciprocally inverse

transformations restores the initial state;

- unitary transformations preserve the length of the state vector, thus ensuring their description as rotations of the vector.

1.2 Fundamentals of Quantum Computation

In this section the fundamentals of quantum computing are presented with a comparison between classical computing and quantum computing. The mathematical model previously described is employed for the definition of the time evolution of the qubit and for the definition of quantum gates.

1.2.1 The qubit

In classical Information Theory the **bit** is a unit of information describing a two-dimensional classical system. A bit is properly a physical state representable as a 2-by-1 matrix

$$\begin{aligned} |0\rangle &= \begin{bmatrix} 1 \\ 0 \end{bmatrix}, \\ |1\rangle &= \begin{bmatrix} 0 \\ 1 \end{bmatrix}. \end{aligned} \tag{1.44}$$

Examples of bits are electricity travelling through a circuit, with corresponding voltages V_{DD} and GND, and a switch turned ON or OFF. The basic element used in quantum information is the quantum bit, or **qubit**, a physical system with two basis states - tipically named $|0\rangle$ and $|1\rangle$ - implemented in many ways, as spin states of electrons or atomic nuclei, atomic energy levels, polarization states of photons, or paths in an interferometer; however, in quantum circuit and information theories the qubit is abstracted from physical details. The main difference between a qubit and a classical bit is that the first is not confined to two states $|0\rangle$ and $|1\rangle$, but can be found in arbitrary superposition states

$$|\psi\rangle = c_0 |0\rangle + c_1 |1\rangle = c_0 \cdot \begin{bmatrix} 1 \\ 0 \end{bmatrix} + c_1 \cdot \begin{bmatrix} 0 \\ 1 \end{bmatrix} = \begin{bmatrix} c_0 \\ c_1 \end{bmatrix} \tag{1.45}$$

where c_0 and c_1 are two complex numbers. The square of the absolute value of each complex coefficient provides the probability of finding the qubit in that state

$$\begin{aligned} |c_0|^2 &= P(|\psi\rangle = |0\rangle), \\ |c_1|^2 &= P(|\psi\rangle = |1\rangle), \\ |c_0|^2 + |c_1|^2 &= 1. \end{aligned} \tag{1.46}$$

Equations 1.45 and 1.48 can be generalized to a *quantum word* of N qubits with 2^N superposing states

$$|\psi\rangle = \begin{bmatrix} c_0 \\ c_1 \\ c_2 \\ \vdots \\ c_i \\ \vdots \\ c_{2^N-1} \end{bmatrix}, \tag{1.47}$$

with

$$\begin{aligned} |c_i|^2 &= P(|\psi\rangle = |\psi_i\rangle), \\ \sum_{i=0}^{2^N-1} |c_i|^2 &= 1. \end{aligned} \tag{1.48}$$

Superposition is the property for which quantum bits are more powerful than their classical equivalents, since an equivalent higher degree of parallelism can be exploited. Parallelism ensures the reduction of the computational cost for some problems, *e.g.* finding an element in an unsorted array of length N has a computational cost $O(\sqrt{N})$ with a quantum computer and $O(N)$ with a classical computer.
The description of a single qubit is typically done through the **Bloch sphere** (Figure 1.1). The qubit can be written in the vector form

$$|\psi\rangle = \cos\left(\frac{\theta}{2}\right)|0\rangle + \mathrm{e}^{\mathrm{i}\phi}\sin\left(\frac{\theta}{2}\right)|1\rangle = \begin{bmatrix} \cos\left(\frac{\theta}{2}\right) \\ \mathrm{e}^{\mathrm{i}\phi}\sin\left(\frac{\theta}{2}\right) \end{bmatrix}, \tag{1.49}$$

where $0 \leq \theta \leq \pi$ is the co-latitude angle and $0 \leq \phi \leq 2\pi$ is the azimuth angle. Any state of the qubit can be represented as a unit vector connecting the origin

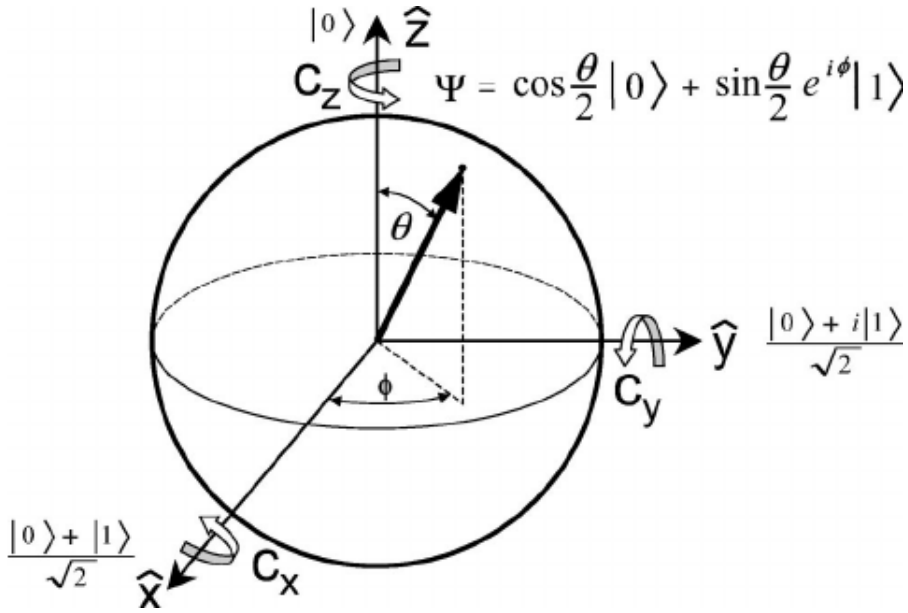

Figure 1.1: Bloch sphere. From Martinis *et al.*, 2003.

and a point on the Bloch sphere. The two basis states $|0\rangle$ ($\theta = 0$) and $|1\rangle$ ($\theta = \pi$) - corresponding to the states 0 and 1 of a classical bit - lie at the poles of the sphere; in these cases the value of ϕ is irrelevant. **A qubit can lie anywhere on the surface of the Bloch sphere and points on the same latitude have the same probabilities** $|c_0|^2$ and $|c_1|^2$; for example, points on the equator of the sphere present equally weighted superposition, *i.e.* $|c_0|^2 = |c_1|^2 = \frac{1}{2}$.
Operations on a qubit correspond to rotations of this vector. The vector rotation is obtained by rotating a certain number of degrees along the x, y or z axis. It is possible to define three matrices performing the task:

$$R_x(\theta) = \begin{bmatrix} \cos\left(\frac{\theta}{2}\right) & -\mathrm{i}\sin\left(\frac{\theta}{2}\right) \\ -\mathrm{i}\sin\left(\frac{\theta}{2}\right) & \cos\left(\frac{\theta}{2}\right) \end{bmatrix}, \tag{1.50}$$

$$R_y(\theta) = \begin{bmatrix} \cos\left(\frac{\theta}{2}\right) & -\sin\left(\frac{\theta}{2}\right) \\ \sin\left(\frac{\theta}{2}\right) & \cos\left(\frac{\theta}{2}\right) \end{bmatrix}, \tag{1.51}$$

$$R_z(\theta) = \begin{bmatrix} \mathrm{e}^{-\mathrm{i}\frac{\theta}{2}} & 0 \\ 0 & \mathrm{e}^{\mathrm{i}\frac{\theta}{2}} \end{bmatrix}. \tag{1.52}$$

1.2.2 Multipartite systems and entanglement

A **multipartite** quantum system is composed by two **separate** different states, each one belonging to a different Hilbert space. From a mathematical point of view, the Hilbert space of a multipartite system can be written as

$$\mathcal{H} = \mathcal{H}_1 \otimes \mathcal{H}_2 \otimes \cdots \otimes \mathcal{H}_i \otimes \cdots \otimes \mathcal{H}_N. \tag{1.53}$$

A general state vector can be written as the tensor product of separate state vectors

$$|\psi\rangle = |\psi\rangle_1 \otimes |\psi\rangle_2 \otimes \cdots \otimes |\psi\rangle_i \otimes \cdots \otimes |\psi\rangle_N, \tag{1.54}$$

each one belonging to one Hilbert space. The dimension of the total space is the product of the dimensions of each Hilbert subspace

$$\dim \mathcal{H} = \prod_i \dim \mathcal{H}_i. \tag{1.55}$$

A state composed by separate states is called **separable** and it admits a classical interpretation, *i.e.* it is possible to treat each system independently from the others. For example in a separable system with a global state $|\psi\rangle = |\psi_1\rangle \otimes |\psi_2\rangle$, it is possible to say that the first system is in the state $|\psi_1\rangle$ and the second one is in $|\psi_2\rangle$.
In quantum physics, it is not ensured that quantum states are separable. **Entanglement** is a quantum interacting phenomenon for which it is not possible to treat quantum states separately; a perturbation on a state can provide variations on the others entangled with that state, even when the particles are separated by a large distance. The consequence of entanglement is that a quantum state for the system as a whole must be described. An example of two entangled state is the following

$$|\psi\rangle = \frac{|00\rangle + |11\rangle}{\sqrt{2}}.$$

Supposing that it is possible a decomposition

$$\begin{aligned} |\psi\rangle &= (c_{10}\,|0\rangle + c_{11}\,|1\rangle) \otimes (c_{20}\,|0\rangle + c_{21}\,|1\rangle) \\ &= c_{10}c_{20}\,|00\rangle + c_{10}c_{21}\,|01\rangle + c_{11}c_{20}\,|10\rangle + c_{11}c_{21}\,|11\rangle\,, \end{aligned}$$

where $|ij\rangle = |i\rangle \otimes |j\rangle$, it is possible to prove that the decomposition is not permitted since it would be required

$$\begin{aligned} c_{10}c_{21} = c_{11}c_{20} = 0, \\ c_{10}c_{20} = c_{11}c_{21} = \frac{1}{\sqrt{2}} \end{aligned}$$

but the equation set does not have solution.

1.2.3 Measurements

Measuring is the act of carrying out an observation on a given physical system. By making a measurement on a system, the state vector is projected to one of the basis vectors that the measurement equipment defines. Assuming that measuring is done in the computational basis, the result of the measurement will be that the qubit is either in state $|0\rangle$ or $|1\rangle$ - depending on probabilities $|c_0|^2$ and $|c_1|^2$ - so the

qubit will be found in the appropriate state and superposition will be suppressed. It is possible to define a **measurement operator** M_m related to the probability of obtaining the outcome m in the state

$$P(m) = \left\langle \psi \,\middle|\, M_m^\dagger M_m \,\middle|\, \psi \right\rangle . \tag{1.56}$$

The state of the system after the measurement is

$$|m\rangle = \frac{M_m \,|\psi\rangle}{\sqrt{P(m)}}. \tag{1.57}$$

The measurement of a qubit in the computational basis is defined by projection operators

$$\begin{aligned} M_0 &= |0\rangle \langle 0| = \begin{bmatrix} 1 & 0 \\ 0 & 0 \end{bmatrix}, \\ M_1 &= |1\rangle \langle 1| = \begin{bmatrix} 0 & 0 \\ 0 & 1 \end{bmatrix}. \end{aligned} \tag{1.58}$$

For M_0, it is possible to prove that

$$P(0) = \left\langle \psi \,\middle|\, M_0^\dagger M_0 \,\middle|\, \psi \right\rangle = |c_0|^2, \tag{1.59}$$

$$\frac{M_0 \,|\psi\rangle}{\sqrt{P(0)}} = \frac{c_0}{|c_0|} \,|0\rangle \simeq |0\rangle . \tag{1.60}$$

It must be noted that $\frac{c_0}{|c_0|} = \mathrm{e}^{i\phi}$ presents a phase contribution that does not play any role. These results can be similarly obtained for M_1. According to the completeness equation

$$\sum_m M_m^\dagger M_m = I, \tag{1.61}$$

it is possible to prove that the probabilities sum

$$\sum_m P(m) = \sum_m \left\langle \psi \,\middle|\, M_m^\dagger M_m \,\middle|\, \psi \right\rangle = \sum_m \langle \psi \,|\, \psi \rangle = 1, \tag{1.62}$$

thus proving that the measurement results can only belong to the basis. Considering a generic two-qubit state

$$|\psi\rangle = a\,|00\rangle + b\,|01\rangle + c\,|10\rangle + d\,|11\rangle \tag{1.63}$$

the measurement operators acting on the first qubit are

$$\begin{aligned} M_0 &= |0\rangle\langle 0| \otimes I, \\ M_1 &= |1\rangle\langle 1| \otimes I. \end{aligned} \tag{1.64}$$

Moreover, the state after the first-qubit measurement can be

$$\frac{M_0}{\sqrt{P(0)}} = |0\rangle \otimes \left(\frac{a}{u}|0\rangle + \frac{b}{u}|1\rangle\right), \tag{1.65}$$

$$\frac{M_1}{\sqrt{P(1)}} = |1\rangle \otimes \left(\frac{c}{v}|0\rangle + \frac{d}{v}|1\rangle\right), \tag{1.66}$$

where $u = \sqrt{|a|^2 + |b|^2}$ and $v = \sqrt{|c|^2 + |d|^2}$ are the square root of the probabilities of measuring for the second qubit 0 or 1 respectively. When a measurement on a subsystem (*e.g.* two qubits $|q_i\rangle$ and $|q_j\rangle$) is done, the measurement operator for the whole system would be

$$M = I_1 \otimes I_2 \otimes \cdots \otimes |q_i\rangle\langle q_i| \otimes \cdots \otimes |q_j\rangle\langle q_j| \otimes \cdots \otimes I_N, \tag{1.67}$$

where $|q_i\rangle\langle q_i|$ and $|q_j\rangle\langle q_j|$ can be obviously $|0\rangle\langle 0|$ or $|1\rangle\langle 1|$. When qubits are entangled, the measurement of one qubit affects the outcome of the measurement on the others, so there exists a strong correlation between them. For example, for the entangled state

$$|\psi\rangle = \frac{|00\rangle + |11\rangle}{\sqrt{2}}$$

if the first qubit is measured to be 0 (1), then the outcome of the measurement of the second qubit is definitely 0 (1). On the other hand, for the non-entangled state

$$|\psi\rangle = \frac{|00\rangle + |01\rangle}{\sqrt{2}}$$

the measurement of the first qubit definitely yields 0, while the second qubit is measured to be 0 or 1 with probability $\frac{1}{2}$, independently of whether the first qubit is measured or not.
It must also be taken into account that **non-orthogonal states** cannot be reliably distinguished by measurement operators. Considering two non-orthogonal states $|\psi_1\rangle$ and $|\psi_2\rangle$ forming a basis for a generic quantum state $|\psi\rangle = a\,|\psi_1\rangle + b\,|\psi_2\rangle$, since $|\psi_2\rangle$ can be decomposed into a non-zero component $b_\parallel$ parallel to $|\psi_1\rangle$ and a component $b_\perp$ orthogonal to $|\psi_1\rangle$

$$b\,|\psi_2\rangle = b_\parallel\,|\psi_1\rangle + b_\perp\,|\psi_{1_\perp}\rangle\,, \tag{1.68}$$

the quantum state can be written as

$$|\psi\rangle = \left(a + b_\parallel\right)|\psi_1\rangle + b_\perp\,|\psi_{1_\perp}\rangle\,, \tag{1.69}$$

with $|b|^2 = |b_\parallel|^2 + |b_\perp|^2$. The consequence is that measurement can provide $|\psi_1\rangle$ as result even though $|\psi\rangle = |\psi_2\rangle$ has been prepared.

1.2.4 Quantum gates

In the quantum circuit model of computation, a quantum gate is a basic quantum circuit operating on qubits. Complex quantum circuits are obtained by combining quantum gates, equivalently to classical logic gates for digital circuits.

Pauli matrices

A two by two matrix can always be expanded as a weighted sum of four basic matrices, in particular the indentity matrix with the Pauli matrices.

$$I = \begin{bmatrix} 1 & 0 \\ 0 & 1 \end{bmatrix}, \qquad X = \begin{bmatrix} 0 & 1 \\ 1 & 0 \end{bmatrix}, \qquad Y = \begin{bmatrix} 0 & -\mathrm{i} \\ \mathrm{i} & 0 \end{bmatrix}, \qquad Z = \begin{bmatrix} 1 & 0 \\ 0 & -1 \end{bmatrix}. \tag{1.70}$$

As the Pauli matrices are Hermitian, a density matrix can be written as weighted sum - with real matrix coefficients - of the matrix basis 1.70. Moreover, Pauli

matrices are unitary, thus corresponding to possible propagators and to quantum logic gates. It is possible to prove that

$$\sigma_\alpha^2 = I \tag{1.71}$$

where σ_α is a generic Pauli matrix and

$$\mathrm{e}^{-\mathrm{i}\theta\sigma_\alpha} = \cos(\theta)I - \mathrm{i}\sin(\theta)\sigma_\alpha \tag{1.72}$$

so exponentiation does not require diagonalizing any matrix, making it easy to calculate many single qubit propagators.

Overview of fundamental quantum gates

According to the vector representation of a bit, logic gates can be seen as matrices to be multiplied to an input vector. Some examples of matrix representations of classical logic gates are the following.

$$\mathrm{NOT}\,|0\rangle = \begin{bmatrix} 0 & 1 \\ 1 & 0 \end{bmatrix} \begin{bmatrix} 1 \\ 0 \end{bmatrix} = \begin{bmatrix} 0 \\ 1 \end{bmatrix}$$

$$\mathrm{AND}\,|11\rangle = \begin{bmatrix} 1 & 1 & 1 & 0 \\ 0 & 0 & 0 & 1 \end{bmatrix} \begin{bmatrix} 0 \\ 0 \\ 0 \\ 1 \end{bmatrix} = \begin{bmatrix} 0 \\ 1 \end{bmatrix}$$

$$\mathrm{OR}\,|01\rangle = \begin{bmatrix} 1 & 0 & 0 & 0 \\ 1 & 1 & 1 & 0 \end{bmatrix} \begin{bmatrix} 0 \\ 1 \\ 0 \\ 0 \end{bmatrix} = \begin{bmatrix} 0 \\ 1 \end{bmatrix}$$

If A is an operation with m input bits and n output bits, its size is 2^n-by-2^m. Sequential operations - as sequential unitary transformations - can be represented as a product matrix from the matrix of the last operator to the initial one, so the first gate applied is the rightmost. For example, the a cascade of a AND and a NOT

makes a NAND gate

$$\text{NOT} \cdot \text{AND} = \begin{bmatrix} 0 & 1 \\ 1 & 0 \end{bmatrix} \cdot \begin{bmatrix} 1 & 1 & 1 & 0 \\ 0 & 0 & 0 & 1 \end{bmatrix} = \begin{bmatrix} 0 & 0 & 0 & 1 \\ 1 & 1 & 1 & 0 \end{bmatrix} = \text{NAND}.$$

In classical computing {AND, NOT} (consequently NAND by itself) form a set of **universal logic gates**, *i.e.* these gates are sufficient for implementing all logic gates (OR, multiplexer, *etc.*). Just as logic gates on classical bits, quantum gates take qubits from one state to another. **Quantum gates** are obtained by modifying the system Hamiltonian through additional control fields that will cause **qubit evolution under unitary reversible transformations**. Identity gate I and NOT - equivalent to the X Pauli gate - are reversible. Linearity permits to extend reversible logic gates on superposition states. The **NOT** applied on a qubit provides

$$\begin{bmatrix} 0 & 1 \\ 1 & 0 \end{bmatrix} \begin{bmatrix} \cos\left(\frac{\theta}{2}\right) \\ \mathrm{e}^{\mathrm{i}\phi} \sin\left(\frac{\theta}{2}\right) \end{bmatrix} = \begin{bmatrix} \mathrm{e}^{\mathrm{i}\phi} \sin\left(\frac{\theta}{2}\right) \\ \cos\left(\frac{\theta}{2}\right) \end{bmatrix} = \begin{bmatrix} \cos\left(\frac{\pi-\theta}{2}\right) \\ \mathrm{e}^{-\mathrm{i}\phi} \sin\left(\frac{\pi-\theta}{2}\right) \end{bmatrix}. \tag{1.73}$$

NOT is equivalent to a π-rotation of the Bloch sphere around the x axis. Considering Equation 1.72, an ideal X unitary evolution cannot be achieved. However, if

$$U = \mathrm{e}^{-\mathrm{i}\frac{\pi}{2}X} = -\mathrm{i}X,$$

the probabilistic behaviour of this gate is exactly the same, since the phase contribution $-\mathrm{i}$ does not provide any significant contribution - in terms of probability - to each coefficient ($|-\mathrm{i}|^2 = 1$). It must be observed that $-\mathrm{i}X$ is obtained from Equation 1.50 with $\theta = \pi$.

More in general, the effect of applying some Hamiltonian to a qubit is to rotate it around the Bloch sphere by an angle depending on both the intrinsic strength of the Hamiltonian and the time for which it is applied. For example, a $\frac{\pi}{2}$-rotation around the x axis generates an evolution equivalent the $\sqrt{\text{NOT}}$ (**SQUARE-ROOT-OF-NOT**) gate

$$U = \mathrm{e}^{-\mathrm{i}\frac{\pi}{4}X} = \frac{1}{\sqrt{2}} \begin{bmatrix} 1 & -\mathrm{i} \\ -\mathrm{i} & 1 \end{bmatrix}.$$

The cascade of two gates of this type is equivalent to a $-\mathrm{i}X$ gate. The same approach can be used with the Y and Z Pauli gates in Equation 1.70 and the unitary evolutions

are equivalent to Equations 1.51 and 1.52.
The **Hadamard** gate is a useful reversible gate working on single qubits with matrix

$$H = \frac{1}{\sqrt{2}} \begin{bmatrix} 1 & 1 \\ 1 & -1 \end{bmatrix}. \tag{1.74}$$

After applying this gate to $|0\rangle$ or $|1\rangle$, a measurement will have equal probabilities to become 0 or 1

$$|0\rangle \to \frac{1}{\sqrt{2}}(|0\rangle + |1\rangle), \qquad |1\rangle \to \frac{1}{\sqrt{2}}(|0\rangle - |1\rangle). \tag{1.75}$$

Hadamard gate is typically employed at the beginning of quantum algorithms, in order to exploit superposition of states. It is possible to prove that the Hadamard is equivalent to a $R_z(\pi)$ operation followed by a $R_y\left(\frac{\pi}{2}\right)$ operation, or to a $R_y\left(-\frac{\pi}{2}\right)$ followed by a $R_x(\pi)$.
The **Phase shift** gate adds a phase ϕ to the complex coefficient associated to the 1 state

$$\phi = \begin{bmatrix} 1 & 0 \\ 0 & \mathrm{e}^{\mathrm{i}\phi} \end{bmatrix}. \tag{1.76}$$

Quantum gates can also involve more qubits. The SWAP gate is the easiest two-qubit gate, that swaps the two inputs on the output. The matrix corresponding to SWAP is

$$\mathrm{SWAP} = \begin{bmatrix} 1 & 0 & 0 & 0 \\ 0 & 0 & 1 & 0 \\ 0 & 1 & 0 & 0 \\ 0 & 0 & 0 & 1 \end{bmatrix}. \tag{1.77}$$

Figure 1.2: Circuit representation of the SWAP gate.

Quantum gates involving multiple entangled qubits are typically **controlled operations**, *i.e.* the operation on a target qubit is done if the control qubit is true.

A generic controlled U gate has the form

$$\mathrm{C}(U) = \begin{bmatrix} 1 & 0 & 0 & 0 \\ 0 & 1 & 0 & 0 \\ 0 & 0 & u_{00} & u_{01} \\ 0 & 0 & u_{10} & u_{11} \end{bmatrix}. \tag{1.78}$$

The simplest controlled gate gate is the **Controlled-NOT** or **Feynman** gate, whose matrix is

$$\mathrm{CNOT} = \begin{bmatrix} 1 & 0 & 0 & 0 \\ 0 & 1 & 0 & 0 \\ 0 & 0 & 0 & 1 \\ 0 & 0 & 1 & 0 \end{bmatrix}. \tag{1.79}$$

The action of the CNOT is $|c\rangle\,|t\rangle \to |c\rangle\,|t \oplus c\rangle$, so the target qubit is flipped when the control is 1.

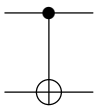

Figure 1.3: Circuit representation of the CNOT gate.

The **controlled-phase** (C-ϕ) gate

$$\text{C-}\phi = \begin{bmatrix} 1 & 0 & 0 & 0 \\ 0 & 1 & 0 & 0 \\ 0 & 0 & 1 & 0 \\ 0 & 0 & 0 & \mathrm{e}^{\mathrm{i}\phi} \end{bmatrix} \tag{1.80}$$

is nothing but the controlled version of the phase gate, that adds a phase term to $|1\rangle$. For a two-qubits state, C-ϕ adds a scalar phase contribution $\mathrm{e}^{\mathrm{i}\phi}$ to c_{11}.

When $\phi = \pi$, the **controlled-Z** (C-Z) gate is obtained

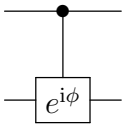

Figure 1.4: Circuit representation of the C-ϕ gate.

$$\text{C-}Z = \begin{bmatrix} 1 & 0 & 0 & 0 \\ 0 & 1 & 0 & 0 \\ 0 & 0 & 1 & 0 \\ 0 & 0 & 0 & -1 \end{bmatrix} \tag{1.81}$$

employed in quantum algorithms (*e.g.* in Grover's search) and to make the CNOT gate. In fact, if a C-Z gate is put between two Hadamard gates on the target qubit network, a CNOT gate is obtained.

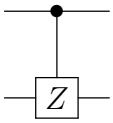

Figure 1.5: Circuit representation of the C-Z gate.

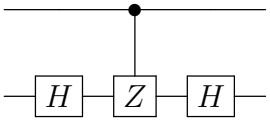

Figure 1.6: CNOT gate constructed with Hadamard and C-Z gates.

A fine set of **universal quantum gates** that can simulate all quantum gates is made by CNOT and single-qubit rotations or the Hadamard, CNOT and phase shift gates. Similarly to the classical computing, the definition of quantum gates involving more than two qubits could be convenient in terms of resources and costs. The easiest three-qubits gate is the **Toffoli** or Controlled-Controlled-NOT gate

$$\text{CCNOT} = \begin{bmatrix} 1 & 0 & 0 & 0 & 0 & 0 & 0 & 0 \\ 0 & 1 & 0 & 0 & 0 & 0 & 0 & 0 \\ 0 & 0 & 1 & 0 & 0 & 0 & 0 & 0 \\ 0 & 0 & 0 & 1 & 0 & 0 & 0 & 0 \\ 0 & 0 & 0 & 0 & 1 & 0 & 0 & 0 \\ 0 & 0 & 0 & 0 & 0 & 1 & 0 & 0 \\ 0 & 0 & 0 & 0 & 0 & 0 & 0 & 1 \\ 0 & 0 & 0 & 0 & 0 & 0 & 1 & 0 \end{bmatrix}. \tag{1.82}$$

The action of Toffoli gate is $|c_1\rangle |c_2\rangle |t\rangle \rightarrow |c_1\rangle |c_2\rangle |t \oplus (c_1 \cdot c_2)\rangle$, so the target qubit is flipped when the control qubits are both 1, so it can be employed to make an AND gate when $|t\rangle = |0\rangle$.

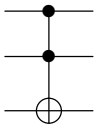

Figure 1.7: Circuit representation of the Toffoli gate.

Fredkin gate is nothing but the Controlled-SWAP gate

$$\text{CSWAP} = \begin{bmatrix} 1 & 0 & 0 & 0 & 0 & 0 & 0 & 0 \\ 0 & 1 & 0 & 0 & 0 & 0 & 0 & 0 \\ 0 & 0 & 1 & 0 & 0 & 0 & 0 & 0 \\ 0 & 0 & 0 & 1 & 0 & 0 & 0 & 0 \\ 0 & 0 & 0 & 0 & 1 & 0 & 0 & 0 \\ 0 & 0 & 0 & 0 & 0 & 0 & 1 & 0 \\ 0 & 0 & 0 & 0 & 0 & 1 & 0 & 0 \\ 0 & 0 & 0 & 0 & 0 & 0 & 0 & 1 \end{bmatrix}. \tag{1.83}$$

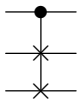

Figure 1.8: Circuit representation of the Fredkin gate.

The action of Fredkin gate is $|c\rangle |t_1\rangle |t_2\rangle \rightarrow |c\rangle |c \cdot t_1 + \overline{c} \cdot t_2\rangle |\overline{c} \cdot t_1 + c \cdot t_2\rangle$.
For the definition of complex quantum circuits, the definition of the unitary evolution of a N qubits system subjected to a rotation of a single qubit is required. Given a generic circuit

The unitary evolution can be written as

$$U = I_1 \otimes I_2 \otimes \cdots \otimes I_{j-1} \otimes A_j \otimes I_{j+1} \otimes \cdots \otimes I_N \tag{1.84}$$

where I_k refers to the identity matrix for the k^{th} term of the Kronecker product (remember that wire corresponds to the identity gate). Linearity of quantum circuits ensures that parallel rotations of different qubits can be associated to a global unitary evolution matrix given by

$$U = I_1 \otimes A_2 \otimes \cdots \otimes I_{j-1} \otimes B_j \otimes I_{j+1} \otimes \cdots \otimes I_N. \tag{1.85}$$

1.2.5 No-cloning theorem and quantum teleportation

According to the **no-cloning theorem**, it is impossible to clone an exact quantum state without destroying the original. It means that quantum gates cannot mimic the *fanout* operation, even Toffoli gate, that does this operation with classical bits. It is possible to prove it *ad absurdum*: suppose that a unitary operator U that makes a clone of a quantum state $|\phi\rangle$ on another state initialized to $|0\rangle$

$$U : |\phi 0\rangle \rightarrow |\phi\phi\rangle \,. \tag{1.86}$$

Let $|\phi\rangle$ and $|\varphi\rangle$ two states linearly independent. The unitary readout must provide $U|\phi 0\rangle = |\phi\phi\rangle$ and $U|\varphi 0\rangle = |\varphi\varphi\rangle$ as outputs. When the quantum state is an equal superposition $|\psi\rangle = \frac{|\phi\rangle+|\varphi\rangle}{\sqrt{2}}$, the cloning transformation must provide for linearity

$$U\left|\frac{|\phi\rangle + |\varphi\rangle}{\sqrt{2}}0\right\rangle = \frac{1}{\sqrt{2}}(U|\phi 0\rangle + U|\varphi 0\rangle) = \frac{|\phi\phi\rangle + |\varphi\varphi\rangle}{\sqrt{2}}.$$

However, if U were a cloning transformation, the cloning transformation must also provide

$$U|\psi 0\rangle = |\psi\psi\rangle = \frac{1}{2}(|\phi\phi\rangle + |\phi\varphi\rangle + |\varphi\phi\rangle + |\varphi\varphi\rangle)$$

as output, but this output state is different from the previous one. Therefore, the fanout behaviour is not satisfied when the input is in a superposition of states, while $|0\rangle$ and $|1\rangle$ can be cloned by an operator $U|00\rangle \rightarrow |00\rangle$ and $|10\rangle \rightarrow |11\rangle$, that is nothing but a CNOT gate where the qubit to be read is the control bit and the output is the target.

In contrast to cloning, **there is no problem transporting arbitrary quantum states from one system to another**. This procedure is fundamental for **quantum teleportation**, that exploits the entanglement between two remote qubits to transmit an unknown quantum state. The information required to reproduce the transmitted quantum state is properly sent on a classical channel, *i.e.* by the measurement of top qubits in Figure 1.9, with a destruction of the original state since quantum teleportation is not in contradiction with the no-cloning theorem.

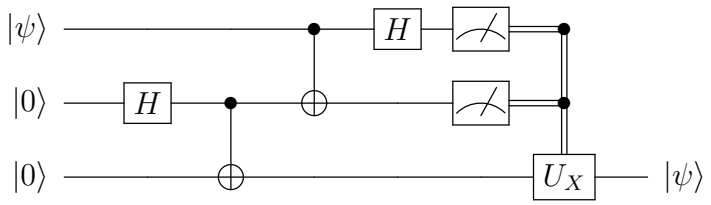

Figure 1.9: Quantum teleportation circuit.

For these reasons, according to no-cloning theorem and quantum teleportation it is possible to "**cut-and-paste**" a state but not to "copy-and-paste" it.

1.2.6 Decoherence

Decoherence refers to the phenomenon of dynamic randomization of qubit phase. In Section 1.2.1 the qubit state has been written as

$$|\psi\rangle = \begin{bmatrix} \cos\left(\frac{\theta}{2}\right) \\ e^{i\phi}\sin\left(\frac{\theta}{2}\right) \end{bmatrix},$$

where ϕ is the qubit phase. In an ideal case, ϕ does not change in time; unfortunately, this condition is not satisfied in reality. Even though the probability of being $|0\rangle$ or $|1\rangle$ is not changed by phase variation, since the quantum state affected by decoherence is kept on the same parallel of the Bloch sphere, the effect of the same quantum gate on them can be completely different, so decoherence can influence dramatically the result of a quantum gate or algorithm. Two qubit states characterized by the same $|c_0|^2$ and $|c_1|^2$ are taken as example

$$|\psi_1\rangle = \begin{bmatrix} \frac{1}{\sqrt{2}} \\ \frac{1}{\sqrt{2}} \end{bmatrix},$$

$$|\psi_2\rangle = \begin{bmatrix} \frac{1}{\sqrt{2}} \\ i\frac{1}{\sqrt{2}} \end{bmatrix}.$$

If a H gate is applied on these qubits the outputs do not have the same probabilities

$$\frac{1}{\sqrt{2}}\begin{bmatrix}1 & 1\\ 1 & -1\end{bmatrix}\cdot\begin{bmatrix}\frac{1}{\sqrt{2}}\\ \frac{1}{\sqrt{2}}\end{bmatrix}=\begin{bmatrix}1\\ 0\end{bmatrix},$$
$$\frac{1}{\sqrt{2}}\begin{bmatrix}1 & 1\\ 1 & -1\end{bmatrix}\cdot\begin{bmatrix}\frac{1}{\sqrt{2}}\\ \mathrm{i}\frac{1}{\sqrt{2}}\end{bmatrix}=\begin{bmatrix}\frac{1}{\sqrt{2}}\\ -\mathrm{i}\frac{1}{\sqrt{2}}\end{bmatrix}.$$

This example puts in evidence that a phase variation is significant for quantum computation, especially when many gates are applied on a qubit.
Decoherence is typically described by a time exponential model that takes into account some time constant T_2 (typical notation). If the time duration of a quantum gate or circuit is much lower than T_2, the decoherence errors can be neglected. This is actually the most critical problem for the realization of a quantum computer and researchers are focusing their attention on the definition of a technology and error correction techniques to minimize the effect of decoherence on qubits.

1.2.7 DiVincenzo criteria

The concepts previously discussed have been collected by David DiVincenzo in his criteria, suggested in [6], that must be satisfied by a potential technology for the implementation of a quantum computer:

1. "*A scalable physical system with well characterized qubits*". The state space of each qubit must be accessed to realize unitary transformations and processor must be upgraded by adding further qubits (scalability).

2. "*The ability to initialize of the state of the qubits to a simple fiducial state, such as* $|00\cdots0\rangle$". The initial state must be a pure state; this operation is fundamental for the execution of any quantum program by applying quantum gates.

3. "*Long relevant decoherence times, much longer than the gate operation time*", thus ensuring the execution of quantum computations with negligible error.

4. "*A "universal" set of quantum gates*"", exploitable to implement all quantum gates required for the execution of any quantum program.

5. "*A qubit-specific measurement capability*".

The technologies proposed for quantum computation have been several since 2000. The most reliable technology is based on superconducting devices [5]. Superconductivity is a quantum mechanical phenomenon of exactly zero electrical resistance and expulsion of magnetic flux fields occurring in certain materials, called superconductors, when cooled below a characteristic critical temperature. It is characterized by the Meissner effect, *i.e.* the complete ejection of magnetic field lines from the interior of the superconductor; the occurrence of the Meissner effect indicates that superconductivity cannot be understood simply as the idealization of classical conductivity.

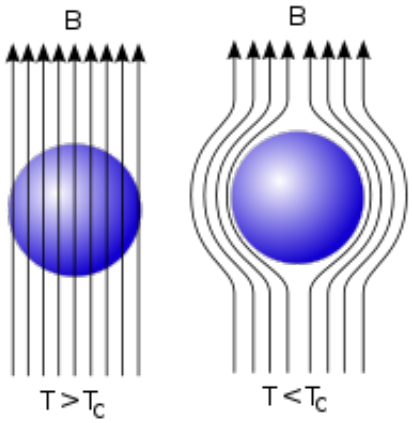

Figure 1.10: Meissner effect. From https://en.wikipedia.org/wiki/Meissner_effect.

The qubit is defined on an artificial atom obtained by anharmonic oscillator circuits, based on capacitors, inductors and a Josephson junction, which is a tunnel junction made of a superconductor (Aluminum typically), a thin insulator (Aluminum oxide typically) and another superconducting electrode (again Aluminum typically). In superconductivity regime ($T < T_c$) the conduction through the insulator barrier does not respect the Ohm's law because the charges responsible of the current flux through the junction are not electrons in a conduction energy band, but tunneling Cooper pairs of electrons or holes presenting an attractive interaction that dominates the electrostatic repulsion. When a bias current I_b is applied between the

two electrodes of the junction, Cooper pairs can tunnel through the barrier provided by the insulator without any voltage drop between the two electrodes. In the circuit

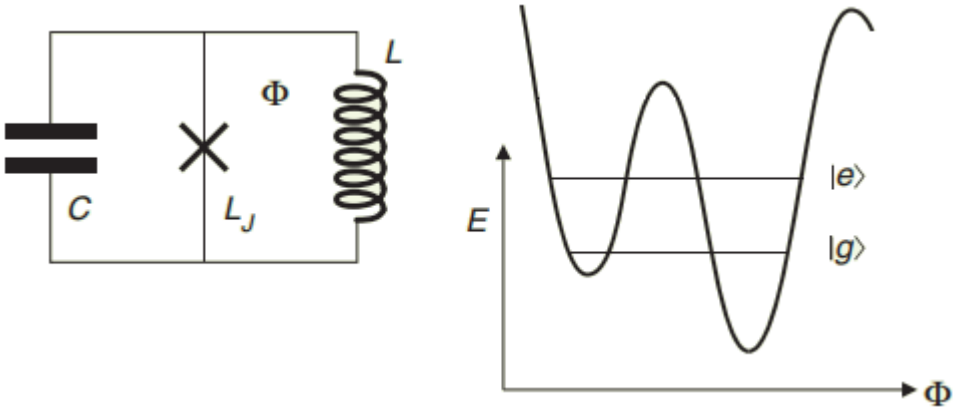

Figure 1.11: Superconducting qubit implemented on an anharmonic quantum circuit. Devoret *et al.*, 2013.

in Figure 1.11, the Josephson junction behaves as a non-linear inductor. In a pure LC quantized circuit, energy levels are equally spaced (ΔE is constant), so it is not possible to select a specific transition; the non-linear inductance forces unequally spaced levels, thus providing to the circuit the behavior of a true artificial atom, for which the lowest two energy levels ($|g\rangle$ and $|e\rangle$) serve as the computational states $|0\rangle$ and $|1\rangle$ and transitions can be selectively excited. The results are so promising that an equivalent Moore's law for quantum computing has been defined, where an exponential scaling in time of decoherence time constant and of number of qubits is observed (Figure 1.12).

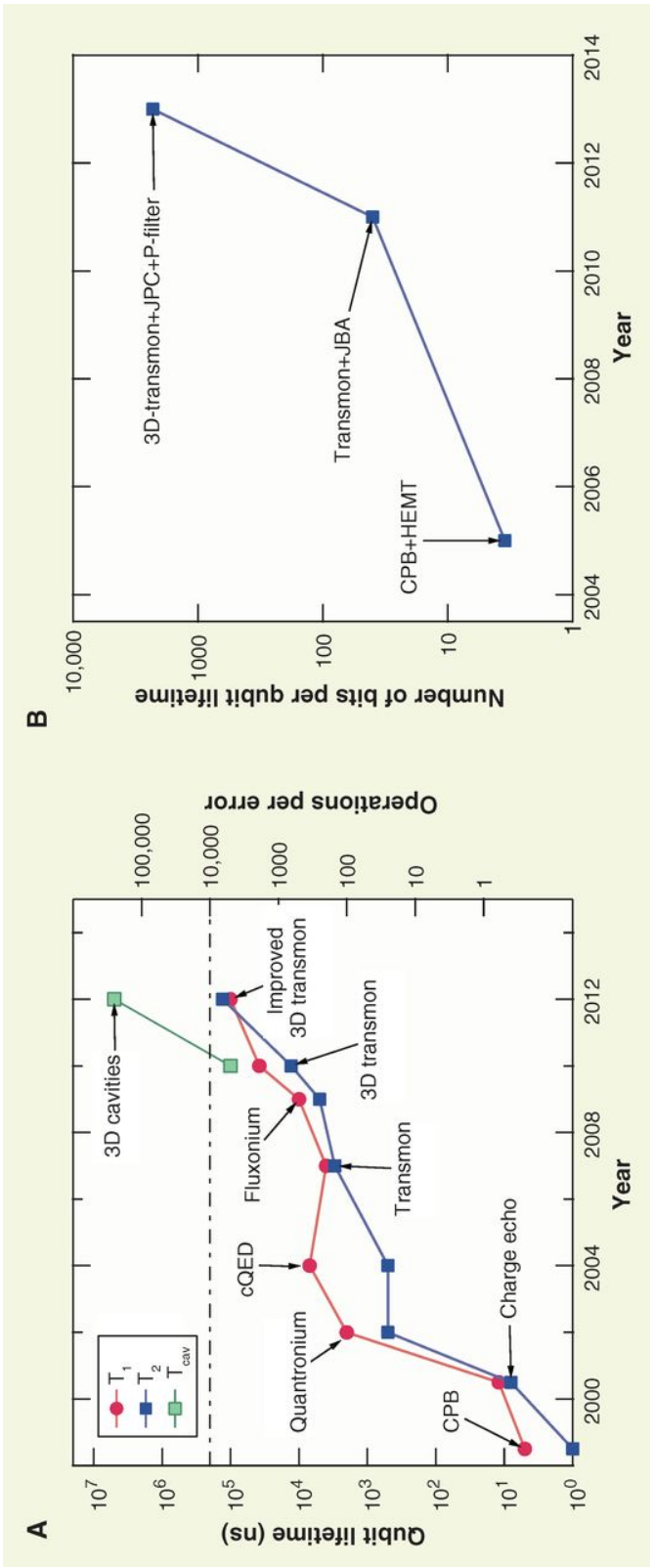

Figure 1.12: "Moore's law" for quantum computing. Image taken from Devoret *et al.*, 2013.

A problem of superconducting devices is the low operating temperature, close to 0 K. However, other technologies based on magnetic resonance in silicon devices [17] or supramolecular complexes do not work on temperature ranges much higher (some kelvin). For the high costs for reaching low temperatures and the costs of control and manipulation, quantum computing is actually thought for supercomputing applications rather than personal computers. Research on superconducting quantum computers is at an advantage stage and the first quantum computers have been realized using this technology:

- IBM Quantum Experience, a web-based educational tool hosted on the IBM Cloud, which allows users to learn about and run quantum circuits and algorithms in a simulation mode and even on a real five-qubits quantum processor. Through the web tool, the user is given a set of quantum operations - settable via-cloud - to manipulate qubits.

- D-Wave Systems, Inc. a Canadian company, the first one in the world to sell quantum computers. Their systems are being used by world-class organizations and institutions - including Lockheed Martin, Google and NASA - and they implement a quantum annealing algorithm, which solves problems by searching for the global minimum of a function. These computer architectures have their own quantum Assembly and they can be programmed through high-level languages (C/C++, MATLAB, Python).

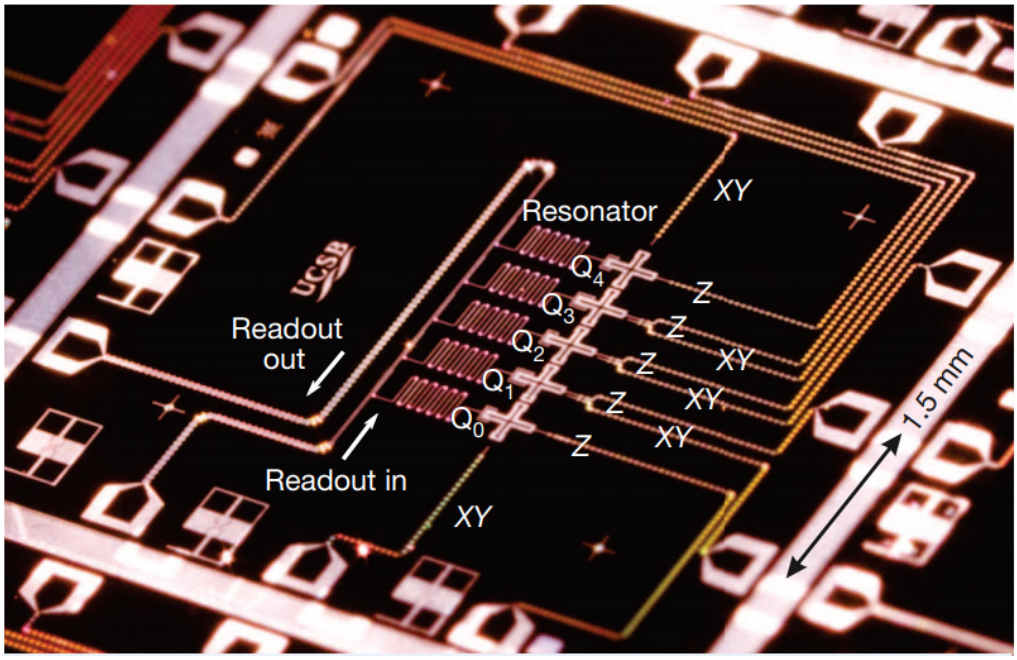

(a) Superconducting processor with five Xmon qubits (cross-shaped devices) placed in a linear array. Barends *et al.*, 2014.

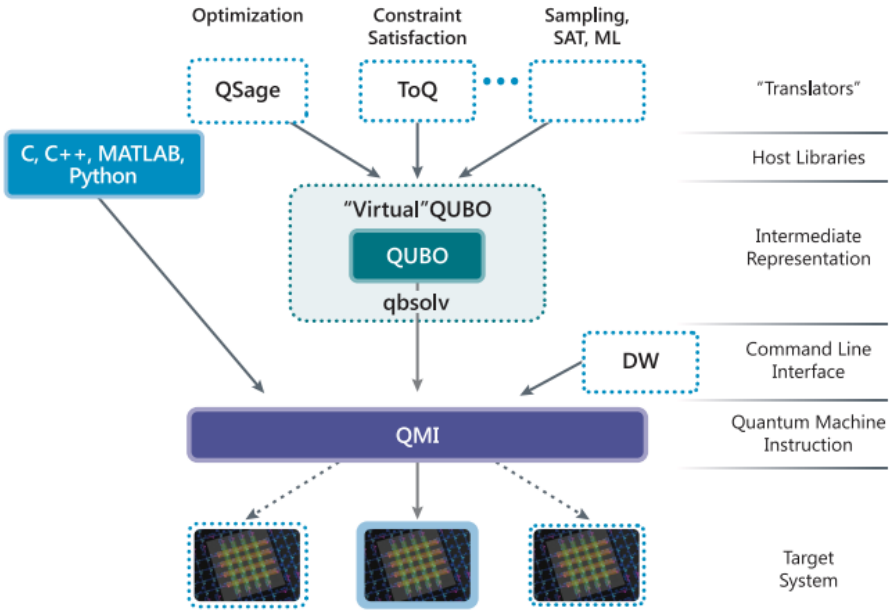

(b) D-Wave software infrastucture. From official D-Wave documentation.

Figure 1.13: Examples of real quantum computers.

Other proposed technologies for quantum computers are based on spins and their manipulation through magnetic resonance. This technique is considered in this thesis, where the discussed architecture is based on spins of molecular nanomagnets. It is interesting to observe that silicon has been recently proposed for the definition of qubits, in order to make on the same substrate a quantum computing unit and a sophisticated classical processor. Silicon spin qubits can be realized in two ways:

- **Donors**, where electrons are bounded to individual donor atoms (typically ^{31}P [17]) at low temperature. The electron spin is the qubit to be manipulated while the atom nuclear spin - characterized by lower magnetic moment and longer relaxation timescales - can be employed to store the quantum information. Through a combination of resonant microwave and radio frequency pulses, the state of a P donor's electron spin may be coherently swapped with that of the ^{31}P nuclear spin in "read" and "write" operations.

- **Quantum dots**, where spins can be confined in lithographically-defined artificial atoms. An example of this architecture is reported in [12]. The qubit device (Figure 1.15) is derived from silicon nanowire MOSFET fabricated on 300 mm silicon-on-insulator (SOI) wafers. It consists of a 10 nm × 20 nm undoped silicon channel and p-doped source and drain contact regions. Over the channel, two parallel top gates of width 30 nm enable the formation of two quantum dots in series - named QD1 and QD2 - whose occupancy is controlled by voltages V_{g_1} and V_{g_2}, one per each gate. The qubit is the related to the spin of the carrier in QD1. Gate 1 is subjected to a static gate voltage V_{g_1} and to a high-frequency modulation ($f \sim 20$ GHz) necessary for the spin qubit initialization and manipulation. Gate 2 is employed for the readout: if the spin value in the second quantum dot is different from the first one, a tunneling current from Q1 to Q2 takes place and it is possible to measure a drain current due to both charges, otherwise - because of Pauli exclusion principle - spin qubit is blocked in Q1 and a lower current is measured. This phenomenon is named **Pauli spin blockade**.

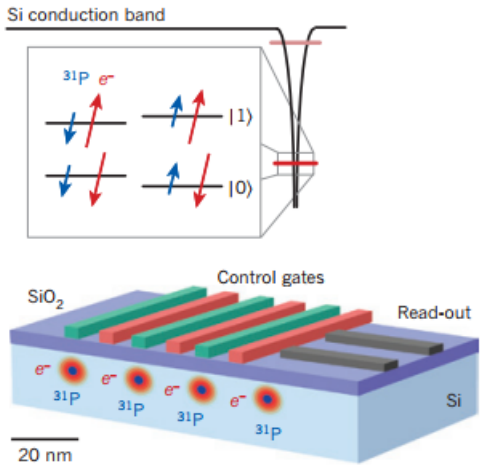

Figure 1.14: Donor-based silicon quantum computing. Morton *et al.*, 2011.

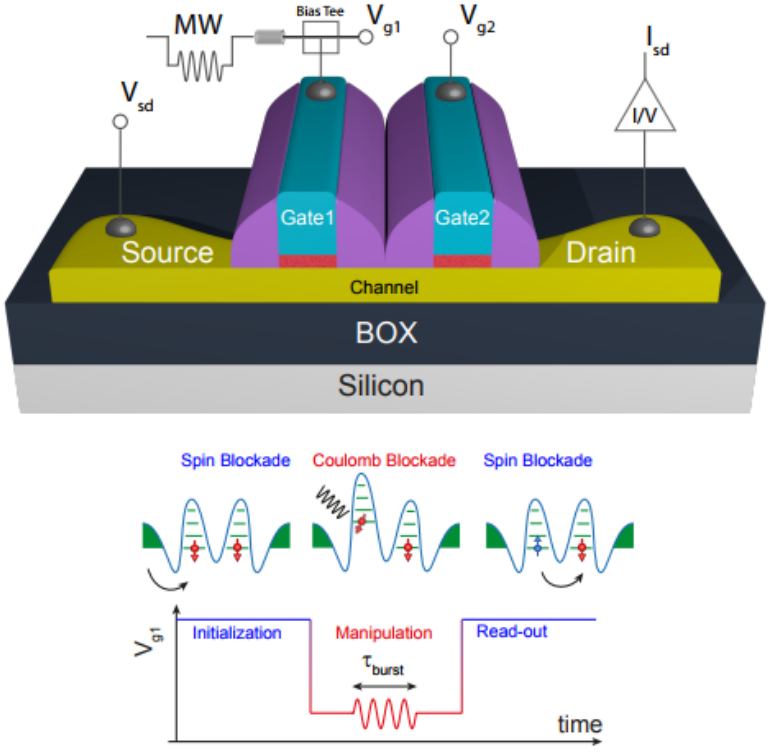

Figure 1.15: Quantum dot architecture. R. Maurand *et al.*, 2016.

Chapter 2

Molecular magnets

2.1 Spin fundamentals

Spin is a quantum mechanical form of angular momentum carried by elementary particles, atomic nuclei and composite particles. It refers to the rotation of a particle around an axis and it is described by a **spin angular momentum** vector and a **spin quantum number**. According to classical electrodynamics, a rotating electrically charged body (*e.g.* an electron) creates a magnetic dipole, so it behaves like a magnet. In other words, the particle has a **magnetic moment** and - in presence of an external magnetic field $B\mathbf{z}$ - a torque on it is exerted, depending on its orientation with respect to the field, while the spin vector is subjected to a precession around the z-axis (Figure 2.1(a)). The **spin angular momentum** $\mathbf{S} = S\mathbf{u}_S$ is quantized and defined as

$$\|\mathbf{S}\| = \sqrt{S_Z(S_Z+1)}\hbar, \tag{2.1}$$

where S_Z is the spin quantum number. The allowed values for S_Z are non-negative integers or half-integers: fermions (electron, proton and neutron) have half-integer values, whereas bosons (photon, mesons) have integer spin values. The **spin magnetic dipole moment** can be written as

$$\mu\mathbf{u}_S = \gamma\mathbf{S} \tag{2.2}$$

where γ is the gyromagnetic ratio

$$\gamma = 1.761 \times 10^{11}\,\mathrm{rad\,s^{-1}\,T^{-1}},$$
$$\frac{\gamma}{2\pi} = 2.802\,494\,4\,\mathrm{MHz\,G^{-1}}.$$

Since the electron gyromagnetic factor can be written as

$$\gamma = \frac{g\mu_B}{\hbar}, \tag{2.3}$$

where g is the **g-factor**, characteristic of each particle (for the electron $g \approx -2$) and

$$\mu_B = 5.788 \times 10^{-5}\,\mathrm{eV\,T^{-1}}$$

is the **Bohr's magneton**, its spin magnetic moment can be written as

$$\mu\mathbf{u}_S = \gamma\mathbf{S} = \frac{g\mu_B}{\hbar}\mathbf{S} \tag{2.4}$$

or equivalently, since the electron has $g < 0$

$$\mu\mathbf{u}_S = -\frac{|g|\mu_B}{\hbar}\mathbf{S} = -|g|\mu_B\sqrt{S_Z(S_Z+1)}\mathbf{u}_S. \tag{2.5}$$

The negative sign in Equation 2.5 puts in evidence that the magnetic momentum of electron is antiparallel to the spin. It can be also proved by the alternative definition of the electron magnetic moment

$$\mu\mathbf{u}_S = \frac{e^-\hbar}{2m_e}\mathbf{u}_S, \tag{2.6}$$

where the electron charge $e^- < 0$. In general, the sign of the magnetic moment - depending on γ - determines the sense of spin precession with the same applied field. The spin angular momentum z-projection (Figure 2.1(b)) is given by

$$s_z = \hbar S_z, \tag{2.7}$$

where S_z is the **secondary spin quantum number**, ranging from $-S_Z$ to $+S_Z$ in steps of one, so $2S_Z + 1$ different values are admitted. It is possible to define the **projection of the magnetic dipole moment along the z-axis** as

$$\mu_z = \gamma s_z = \hbar\gamma S_z, \tag{2.8}$$

or equivalently for the electron

$$\mu_z = -|g|\mu_B S_z. \tag{2.9}$$

According to Equations 2.5 and 2.8, the spin magnetic moment has constant magnitude μ and - since the number of its projections on the z-axis is finite - it can only belong to a finite set of circles on a sphere of radius μ (Figure 2.1(b)). Moreover, the angle between $\mathbf{S}$ and $\mathbf{u}_z$ vectors depends on the secondary spin quantum number S_z. Electron has only two admitted z-projections: the two different spin orientations are

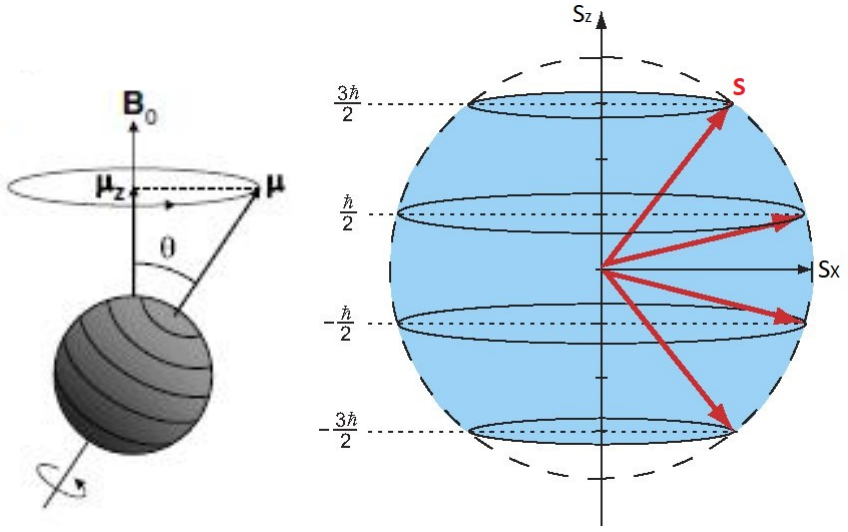

(a) From https://tinyurl.com/ya6fm94l. (b) From https://tinyurl.com/y7cd4sg7.

Figure 2.1: Magnetic dipole moments.

sometimes called "spin-up" ($+\frac{1}{2}$, with z-projection parallel to $\mathbf{B}$) and "spin-down" ($-\frac{1}{2}$, with z-projection antiparallel to $\mathbf{B}$) and they can be associated to counter-clockwise and clockwise rotations around the z-axis. In the context of Spintronics, different spin states are exploited to encode information. Since spin is characterized by superposition, it can be also exploited for the definition of the qubit. The object of this thesis is the description of a **quantum architecture with spin qubits on molecular magnets**. A preliminary overview of the quantum computation model with spin-$\frac{1}{2}$ qubits is required.

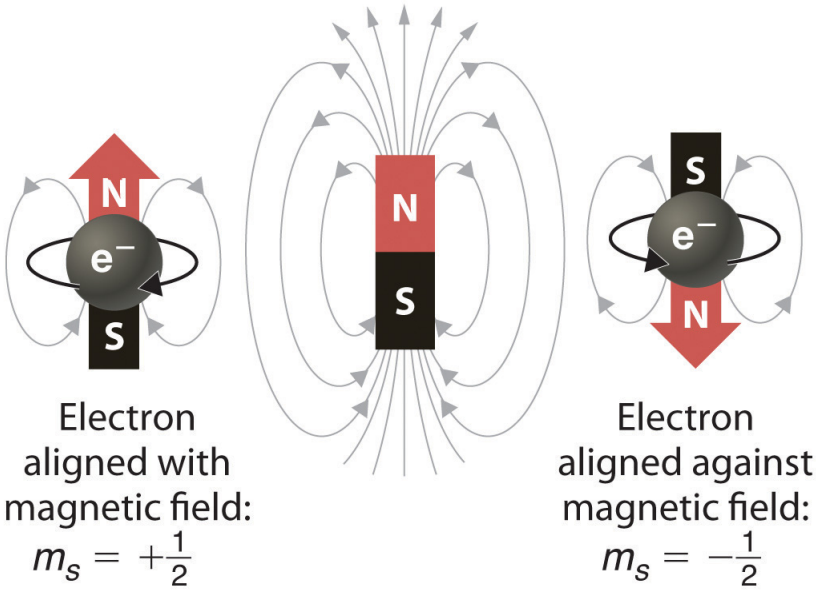

Figure 2.2: Electron spin. From https://tinyurl.com/y9kuzahf.

2.2 Magnetic resonance and spin manipulation

A magnetic dipole moment μ in a magnetic field B will presents a potential energy which depends upon its orientation with respect to the magnetic field

$$U = -\mu B. \tag{2.10}$$

When a static magnetic field $\mathbf{B} = B\mathbf{z}$ is applied on a spin-$\frac{1}{2}$ quantum system as an electron, the magnetic moment aligns itself either antiparallel or parallel to field and states are separated by an energy difference ΔE. If an external energy amount ΔE is provided to the system, it can change the energy state (*i.e.* its spin orientation); this technique is named **magnetic resonance** and it is employed for both nuclear (**Nuclear Magnetic Resonance** or NMR) and electron (**Electron Paramagnetic Resonance** or EPR) spins. In the context of quantum computation, it is employed to implement quantum gates on spin qubits.
Two different energy levels with energy difference $\Delta E = E_1 - E_0$ are admitted for the system and they can be exploited to encode $|0\rangle$ and $|1\rangle$, associated in the following to low and high-energy states respectively. The energy splitting is named **Zeeman effect** and it can be described by the Hamiltonian matrix

$$H = -\frac{1}{2}\hbar\gamma BZ = -\hbar\frac{\omega_0}{2}Z \tag{2.11}$$

where Z is one of the Pauli matrices and $\omega_0 = \frac{\Delta E}{\hbar} = \gamma B$ is the transition frequency or **Larmor frequency**, that is for electron spin $\omega_0 = \frac{g\mu_B B}{\hbar}$. Equation 2.11 is nothing but the quantum version of Equation 2.10 for the potential energy U_z of the magnetic moment projection $\mu_z\mathbf{z}$. In fact, $\frac{1}{2}Z$ is a matrix representation for S_z, so $\mu_z = \hbar\gamma S_z$ (Equation 2.8) and

$$U_z = -\mu_z B = -\hbar\gamma S_z B. \tag{2.12}$$

It is possible to compute the eigenvalues related to the eigenstates $|0\rangle$ and $|1\rangle$

$$E_0 = -\frac{\hbar\omega_0}{2}, \qquad E_1 = +\frac{\hbar\omega_0}{2}. \tag{2.13}$$

Eigenvalues and Equation 2.12 put in evidence that a particle with $\gamma > 0$ is in the lower energy state for $S_z = +\frac{1}{2}$ ("spin up"), while the electron is in ground state for $S_z = -\frac{1}{2}$ ("spin down"). In both cases, the energy is lowest when the magnetic moment is aligned with the magnetic field (Figure 2.3), *i.e.* $\mu B > 0$. The Larmor

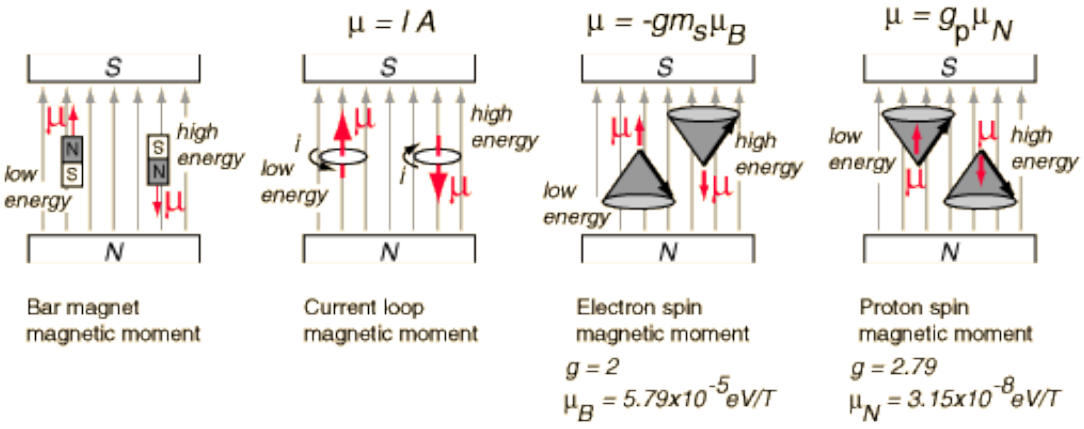

Figure 2.3: Spin-$\frac{1}{2}$ energy is lowest when μ is aligned with $\mathbf{B}$. From http://hyperphysics.phy-astr.gsu.edu/hbasees/Nuclear/nmr.html.

frequency is related to the angular velocity of the the magnetic moment exhibiting precession about the z axis, that is equivalent to the motion of the qubit vector on a parallel of the Bloch sphere. Precession does not change $|c_0|^2$ and $|c_1|^2$ - so the probabilities do not change - but it changes qubit phase in time. The spin state can be modified by applying a radio frequency (in NMR) or microwave (in EPR) magnetic field in the xy-plane, that forces an additional spin precession with angular frequency proportional to the gyromagnetic ratio γ of the system and to the external field

$$\omega_1 = \gamma B_1. \tag{2.14}$$

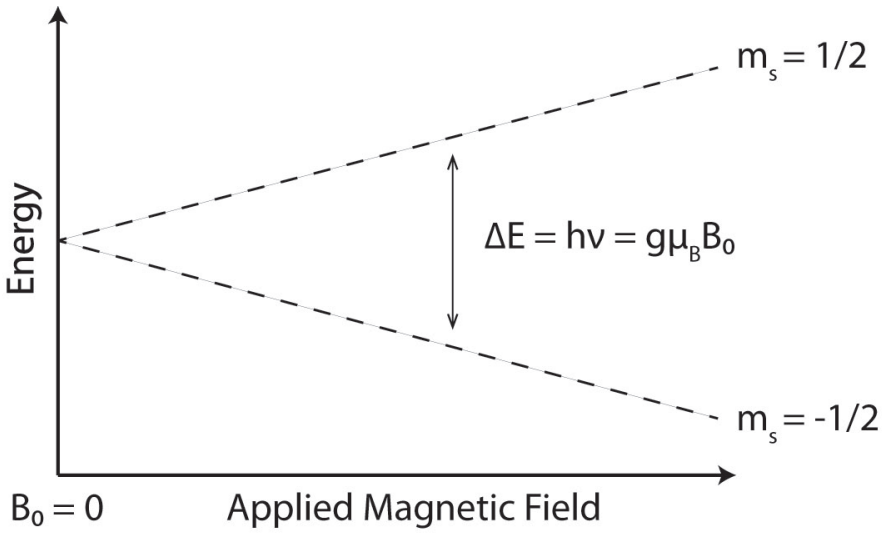

Figure 2.4: Zeeman effect for an electron. The spin values are swapped nuclear spin. From https://tinyurl.com/y9kfgcbk.

The driving field can be a rotating field in the xy plane[1] at angular frequency ω as

$$\mathbf{B}_1(t) = B_1 \cos(\omega t - \phi)\mathbf{x} + B_1 \sin(\omega t - \phi)\mathbf{y}, \tag{2.15}$$

or as a field oscillating in the x direction

$$\mathbf{B}_1(t) = 2B_1 \cos(\omega t - \phi)\mathbf{x}. \tag{2.16}$$

The oscillating field can be decomposed as

$$\mathbf{B}_{1_+} + \mathbf{B}_{1_-} \tag{2.17}$$

where

$$\mathbf{B}_{1_\pm} = B_1 \cos(\omega t - \phi)\mathbf{x} \pm B_1 \sin(\omega t - \phi)\mathbf{y}. \tag{2.18}$$

It is possible to prove that in a rotating frame moving with one of these fields, the other contribution varies rapidly with time, so its effect on the spin expected value is averaged out and it can be neglected, according to the **rotating wave approximation**. In the following analysis, Equation 2.16 is exploited, remembering that a field with double amplitude $2B_1$ with the respect to the rotating field 2.15 is required to obtain the same spin rotation amount. The Hamiltonian contribution of the transverse field is

$$H_1 = 2\hbar\omega_1 \cos(\omega t - \phi)X \tag{2.19}$$

where $\hbar\omega_1 = \hbar\gamma B_1$. The total Hamiltonian is reported for both $\mathbf{B}_1(t)$ cases, remembering that the attention is focused on the model involving the oscillating field (Equation 2.16)

$$\begin{aligned} H &= -\hbar\frac{\omega_0}{2}Z + \hbar\frac{\omega_1}{2}[\cos(\omega t - \phi)X + \sin(\omega t - \phi)Y] = \frac{\hbar}{2}\begin{bmatrix} -\omega_0 & \omega_1 \mathrm{e}^{-(\mathrm{i}\omega t - \phi)} \\ \omega_1 \mathrm{e}^{\mathrm{i}(\omega t - \phi)} & \omega_0 \end{bmatrix}, \\ H &= -\hbar\frac{\omega_0}{2}Z + \hbar\omega_1 \cos(\omega t - \phi)X = \hbar\begin{bmatrix} -\frac{\omega_0}{2} & \omega_1 \cos(\omega t - \phi) \\ \omega_1 \cos(\omega t - \phi) & \frac{\omega_0}{2} \end{bmatrix}. \end{aligned} \tag{2.20}$$

[1] The rotating field can be seen as a static field of magnitude B_1 subjected to a uniform circular motion in the xy plane.

Since it has explicit time-dependence, that is inconvenient in terms of integration for obtaining the evolution of the quantum system, the frame of reference is changed from the laboratory frame with vector basis ($\mathbf{e}_x$,$\mathbf{e}_y$,$\mathbf{e}_z$) to a frame rotating with angular frequency $\omega_{\text{frame}} = \omega$ around the z-axis. A new vector basis ($\mathbf{e}'_x$,$\mathbf{e}'_y$,$\mathbf{e}'_z$) is required where $\mathbf{e}'_x$ always coincides with the direction of $B_1(t)$. Let

$$U_R = \mathrm{e}^{\mathrm{i}\hbar\frac{\omega t}{2}Z} = \begin{bmatrix} \mathrm{e}^{\mathrm{i}\hbar\frac{\omega t}{2}} & 0 \\ 0 & \mathrm{e}^{-\mathrm{i}\hbar\frac{\omega t}{2}} \end{bmatrix} \tag{2.21}$$

be a unitary transformation to a rotating frame with angular velocity ω. The equivalent Schrödinger equation has Hamiltonian

$$\tilde{H} = U_R H U_R^\dagger - \mathrm{i}\hbar U_R \frac{\partial U_R^\dagger}{\partial t}. \tag{2.22}$$

The first term is the transformation of H into a new vector basis, while the second one is a corrective term required when working in non-inertial systems. The matrix form of Hamiltonian 2.22 is

$$\tilde{H} = \frac{\hbar}{2}\begin{bmatrix} \omega - \omega_0 & \omega_1\left[\mathrm{e}^{\mathrm{i}(\phi-2\omega t)} + \mathrm{e}^{-\mathrm{i}\phi}\right] \\ \omega_1\left[\mathrm{e}^{-\mathrm{i}(\phi-2\omega t)} + \mathrm{e}^{\mathrm{i}\phi}\right] & \omega_0 - \omega \end{bmatrix} \tag{2.23}$$

On the antidiagonal there are contributions oscillating at angular frequency $2\omega_0$ that averaged out on a time duration much longer than $\frac{2\pi}{\omega_0}$ according to the rotating wave approximation, so they can be neglected and the Hamiltonian can be approximated as

$$\tilde{H} = \frac{\hbar}{2}\begin{bmatrix} \delta & \omega_1\mathrm{e}^{-\mathrm{i}\phi} \\ \omega_1\mathrm{e}^{\mathrm{i}\phi} & -\delta \end{bmatrix} = \frac{\hbar}{2}\{\delta Z + \omega_1[\cos(\phi)X - \sin(\phi)Y]\} \tag{2.24}$$

where $\delta = \omega - \omega_0$. From a practical point of view, the driving field $\mathbf{B}_1(t)$ is ideally generated by an Amplitude Modulation (AM) technique with pulse carrier ω - typically resonant with the Larmor angular frequency ω_0 and a rectangular modulating waveform of amplitude $\propto \frac{\omega_1}{\gamma}$. The unitary evolution associated to Hamiltonian 2.24 on a time duration τ is

$$\tilde{U} = \begin{bmatrix} \cos\left(\frac{\Omega\tau}{2}\right) - \mathrm{i}\frac{\delta}{\Omega}\sin\left(\frac{\Omega\tau}{2}\right) & -\mathrm{i}\frac{\omega_1}{\Omega}\sin\left(\frac{\Omega\tau}{2}\right)\mathrm{e}^{-\mathrm{i}\phi} \\ -\mathrm{i}\frac{\omega_1}{\Omega}\sin\left(\frac{\Omega\tau}{2}\right)\mathrm{e}^{\mathrm{i}\phi} & \cos\left(\frac{\Omega\tau}{2}\right) + \mathrm{i}\frac{\delta}{\Omega}\sin\left(\frac{\Omega\tau}{2}\right) \end{bmatrix} \tag{2.25}$$

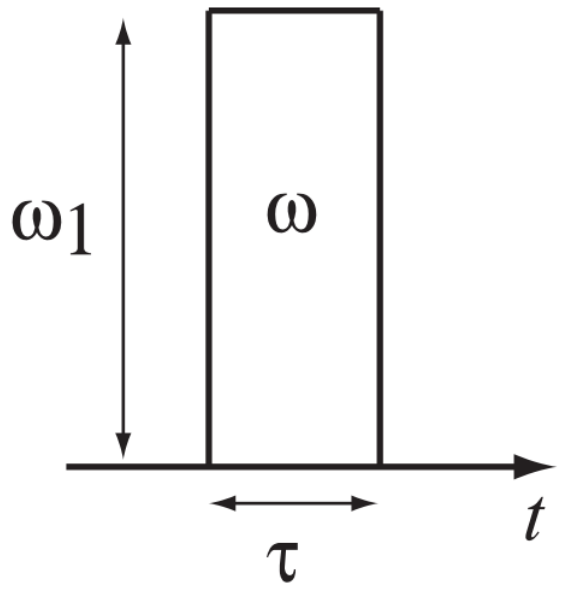

Figure 2.5: Magnetic field amplitude modulation, with carrier frequency Ω, amplitude proportional to ω_1 and duration τ. Adapted from Nakahara *et al.*, 2008.

with $\Omega = \sqrt{\omega_1^2 + \delta^2}$ named **Rabi frequency**. In terms of spin motion in the rotating frame of reference, the unitary evolution is related to the precession about the direction of the **effective field**

$$\mathbf{B}_{\text{eff}} = B_0 \left(1 - \frac{\omega}{\omega_0}\right) \mathbf{e}'_z + B_1 \mathbf{e}'_x, \tag{2.26}$$

at frequency equal to the Rabi frequency

$$\Omega = \gamma |\mathbf{B}_{\text{eff}}|. \tag{2.27}$$

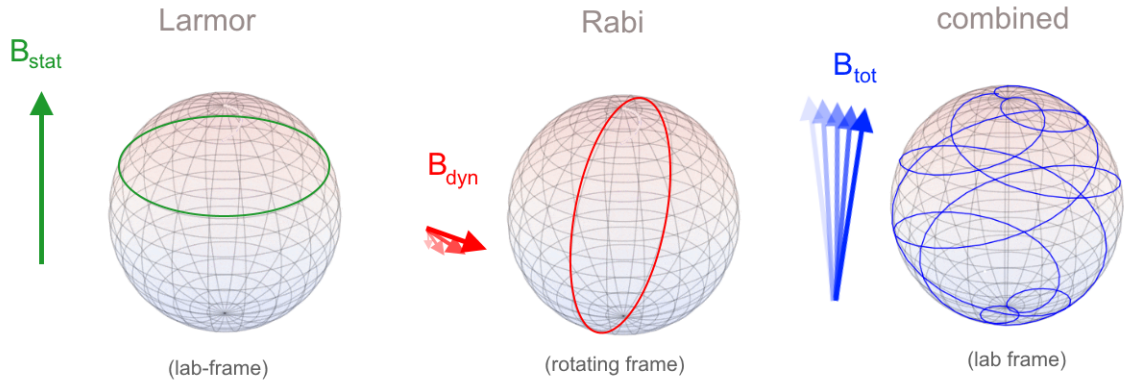

Figure 2.6: Larmor and Rabi precessions in laboratory and rotating frames of reference respectively and their superposition. From http://i.imgur.com/Es7YDP3.png.

When the carrier signal is resonant with the transition - *i.e.* $\delta = 0$ and $\Omega = \omega_1$ - the unitary evolution matrix can be simplified

$$\begin{aligned} \tilde{U} &= \begin{bmatrix} \cos\left(\frac{\omega_1 \tau}{2}\right) & -\mathrm{i}\sin\left(\frac{\omega_1 \tau}{2}\right) \mathrm{e}^{-\mathrm{i}\phi} \\ -\mathrm{i}\sin\left(\frac{\omega_1 \tau}{2}\right) \mathrm{e}^{\mathrm{i}\phi} & \cos\left(\frac{\omega_1 \tau}{2}\right) \end{bmatrix} \\ &= \cos\left(\frac{\omega_1 \tau}{2}\right) I - \mathrm{i}\sin\left(\frac{\omega_1 \tau}{2}\right) [\cos(\phi) X + \sin(\phi) Y]. \end{aligned} \tag{2.28}$$

The precession would be around $\mathbf{e}'_x$ with angular frequency ω_1. Rotation matrices

1.50 and 1.51 can be derived from matrix 2.28

$$\begin{aligned} R_x(\pi) &= \tilde{U}(\theta = \pi, \phi = 0) = -\mathrm{i}X, \\ R_y(\pi) &= \tilde{U}\left(\theta = \pi, \phi = \frac{\pi}{2}\right) = -\mathrm{i}Y. \end{aligned} \tag{2.29}$$

The angle θ related to the amount of the rotation is nothing but

$$\theta = \omega_1 \tau \tag{2.30}$$

so it is possible to vary the rotation angle by keeping constant one variable and varying the other one or both. In the proposed description model, τ is kept constant and ω_1 (*i.e.* the magnetic field intensity) is supposed to be variable. According to Equation 2.28, when $\omega_1 \tau = \pi$ it is possible to obtain $-\mathrm{i}X$ and $-\mathrm{i}Y$ gates with $\phi = 0$ and $\phi = \frac{\pi}{2}$ respectively. Rotation gates around the z axis must be derived by a sequence of rotations around x and y axes. For example, it is possible to prove that

$$-\mathrm{i}Z = -\mathrm{i}X \cdot -\mathrm{i}Y \tag{2.31}$$

so the π rotation around the z axis is obtained by a sequence of π rotations around the y and x axes. Hadamard-like gates can be implemented by exploiting either a single pulse with anti-resonant carrier frequency ($\delta = \omega_1$ and $\Omega\tau = \pi$) or a couple of resonant pulses

$$R_x(\pi) \cdot R_y\left(\frac{\pi}{2}\right) = -\frac{\mathrm{i}}{\sqrt{2}} \begin{bmatrix} 1 & 1 \\ 1 & -1 \end{bmatrix} = -\mathrm{i}H, \tag{2.32}$$

that is the implementation chosen for the proposed architecture. It is also possible to write an equation for transition probability

$$P_{0\to 1} = \left| \frac{\omega_1}{\Omega} \sin\left(\frac{\Omega\tau}{2}\right) \right|^2 \tag{2.33}$$

that is nothing but the square magnitude of the terms on the antidiagonal of the unitary evolution operator. When there is not any pulse applied on the qubit, the system must be still observed in the rotating frame reference ($\delta = 0$); it is equivalent

to say that a pulse with carrier resonant with ω_0 and null amplitude ($\omega_1 = 0$) is applied on the qubit, so that the unitary evolution $U = I$.
When the carrier signal is strongly anti-resonant with the respect to the Larmor frequency, for $\delta\tau \gg 2\pi$ and $\delta \gg \omega_1$, Hamiltonian 2.24 can be approximated as

$$\tilde{H} \approx \frac{\hbar}{2}\delta Z. \tag{2.34}$$

The Hamiltonian has the same form of the laboratory frame; the only difference is that in the rotating frame the precession angular frequency is $\delta < \omega_0$. The unitary evolution can be written as

$$\tilde{U} \approx \begin{bmatrix} \cos\left(\frac{\delta\tau}{2}\right) - \mathrm{i}\sin\left(\frac{\delta\tau}{2}\right) & 0 \\ 0 & \cos\left(\frac{\delta\tau}{2}\right) + \mathrm{i}\sin\left(\frac{\delta\tau}{2}\right) \end{bmatrix} = \begin{bmatrix} \mathrm{e}^{-\mathrm{i}\frac{\delta\tau}{2}} & 0 \\ 0 & \mathrm{e}^{\mathrm{i}\frac{\delta\tau}{2}} \end{bmatrix} = \mathrm{e}^{-\mathrm{i}\frac{\delta\tau}{2}} \begin{bmatrix} 1 & 0 \\ 0 & \mathrm{e}^{\mathrm{i}\delta\tau} \end{bmatrix},$$

and the rotating wave approximation would permit to write this unitary evolution as

$$\begin{bmatrix} \mathrm{e}^{-\mathrm{i}\frac{\delta\tau}{2}} & 0 \\ 0 & \mathrm{e}^{\mathrm{i}\frac{\delta\tau}{2}} \end{bmatrix} = \mathrm{e}^{-\mathrm{i}\frac{\delta\tau}{2}} \begin{bmatrix} 1 & 0 \\ 0 & \mathrm{e}^{\mathrm{i}\delta\tau} \end{bmatrix} \approx \begin{bmatrix} 1 & 0 \\ 0 & 1 \end{bmatrix},$$

with $\tau \gg \frac{2\pi}{\delta}$.
A more formal derivation is obtained by exploiting the Hamiltonian in the rotating frame, supposing that ω_{frame} is equal to ω_0, instead of ω, thus implying that the terms on the main diagonal of $\tilde{H}$ are always null and $\delta = \omega - \omega_{\text{frame}} = \omega - \omega_0$. For $\delta\tau \gg 2\pi$ the rotating wave approximation is applied on two waves, rotating at frequencies δ and $(\omega + \omega_0)$, so that the Hamiltonian can be approximated as

$$\begin{aligned} \tilde{H} &= \frac{\hbar}{2} \begin{bmatrix} 0 & \omega_1 \left\{ \mathrm{e}^{-\mathrm{i}[(\omega-\omega_0)t+\phi]} + \mathrm{e}^{-\mathrm{i}[(\omega+\omega_0)t-\phi]} \right\} \\ \omega_1 \left\{ \mathrm{e}^{\mathrm{i}[(\omega-\omega_0)t+\phi]} + \mathrm{e}^{\mathrm{i}[(\omega+\omega_0)t-\phi]} \right\} & 0 \end{bmatrix} \\ &= \frac{\hbar}{2} \begin{bmatrix} 0 & \omega_1 \left\{ \mathrm{e}^{-\mathrm{i}(\delta t+\phi)} + \mathrm{e}^{-\mathrm{i}[(\omega+\omega_0)t-\phi]} \right\} \\ \omega_1 \left\{ \mathrm{e}^{\mathrm{i}(\delta t+\phi)} + \mathrm{e}^{\mathrm{i}[(\omega+\omega_0)t-\phi}} \right\} & 0 \end{bmatrix} \approx \frac{\hbar}{2} \begin{bmatrix} 0 & 0 \\ 0 & 0 \end{bmatrix}, \end{aligned} \tag{2.35}$$

and the unitary evolution would be

$$\tilde{U} = \mathrm{e}^{-\mathrm{i}\frac{\tilde{H}}{\hbar}\tau} \approx \begin{bmatrix} 1 & 0 \\ 0 & 1 \end{bmatrix}. \tag{2.36}$$

Figures 2.7 and 2.8 report the spin evolution in laboratory and rotating frames by changing the carrier frequency, and consequently δ and Ω.
The reported quantum computation model refers to the Nuclear Magnetic Resonance. For the Electron Paramagnetic Resonance - since $\gamma < 0$ - it would be required to replace γ with $-|\gamma|$ and the sign of the Hamiltonian would be opposed. However the application of a static field $\mathbf{B}' = -\mathbf{B}$ - permits to exploit the same equations. In general, if precession frequencies $\omega_{0,1} = \gamma B_{0,1}$ are supposed to be greater than 0, it is sufficient to set properly the verse of the magnetic fields depending on the sign of γ to avoid problems due to the signs of Hamiltonians and unitary operators.
In magnetic resonance applications, the typical measurement units are megahertz and gauss ($1\,\mathrm{G} = 1 \times 10^{-4}\,\mathrm{T}$, employed for the peak of magnetic pulses). In order to establish the frequency or field required to rotate in EPR a spin not belonging to an electron (as in molecular magnets), the megahertz-to-gauss conversion can be easily computed as

$$f\,[\mathrm{MHz}] \Leftrightarrow 2.8024944 \frac{g}{g_\mathrm{e}} \cdot B\,[\mathrm{G}], \tag{2.37}$$

where g and g_e are the g-factors of the spin to be manipulated and of the electron spin respectively, so the conversion is roughly

$$f\,[\mathrm{MHz}] \Leftrightarrow 1.4 \cdot g \cdot B\,[\mathrm{G}]. \tag{2.38}$$

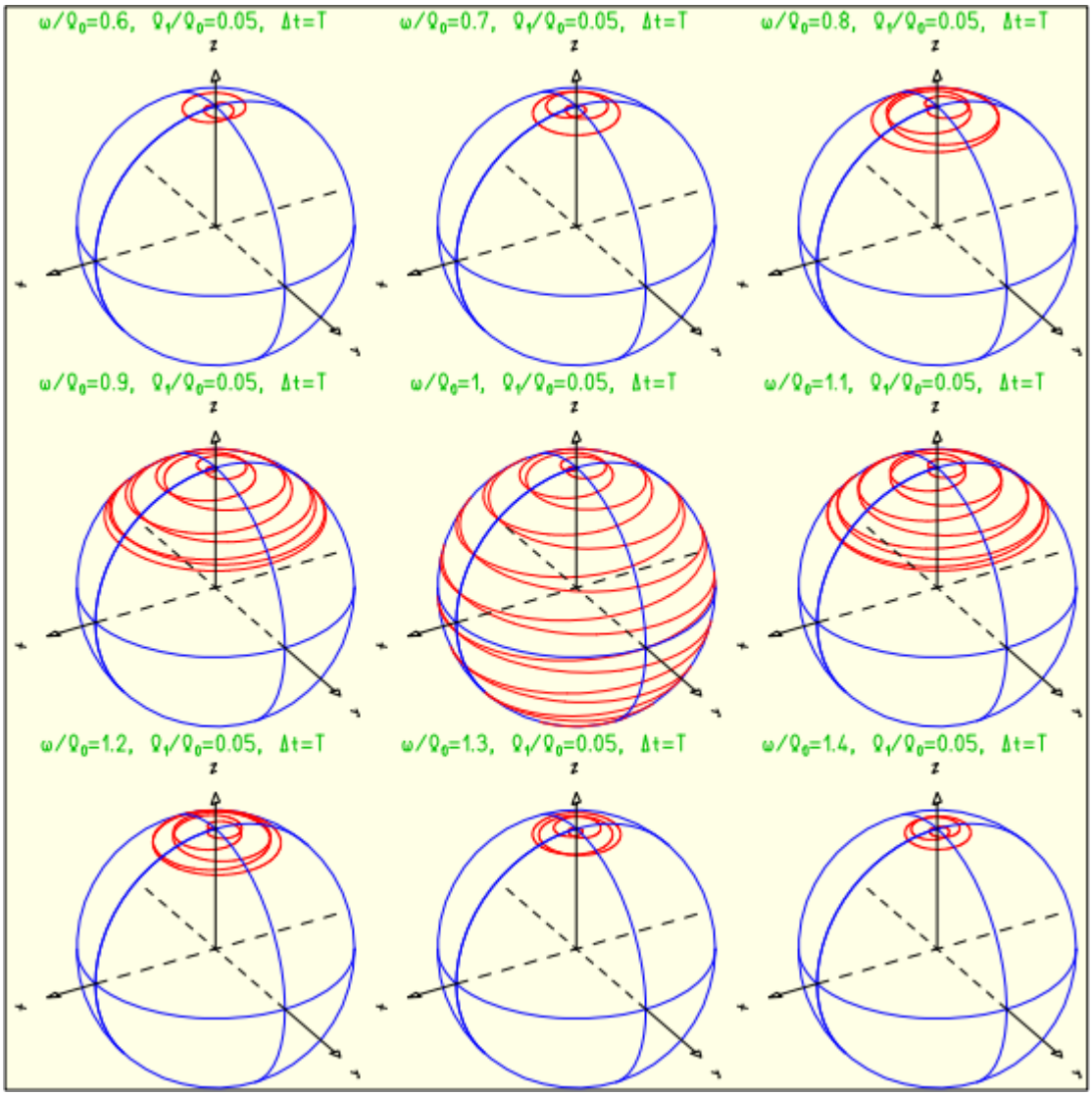

Figure 2.7: Trajectory of the expectation value of the spin vector within one period T in the laboratory frame of reference. The value of ω is varied from plot to plot, while ω_0 and ω_1 are constant. The plot in the middle of the figure corresponds to $\delta = 0$. Brandt and Dahmen, 2012.

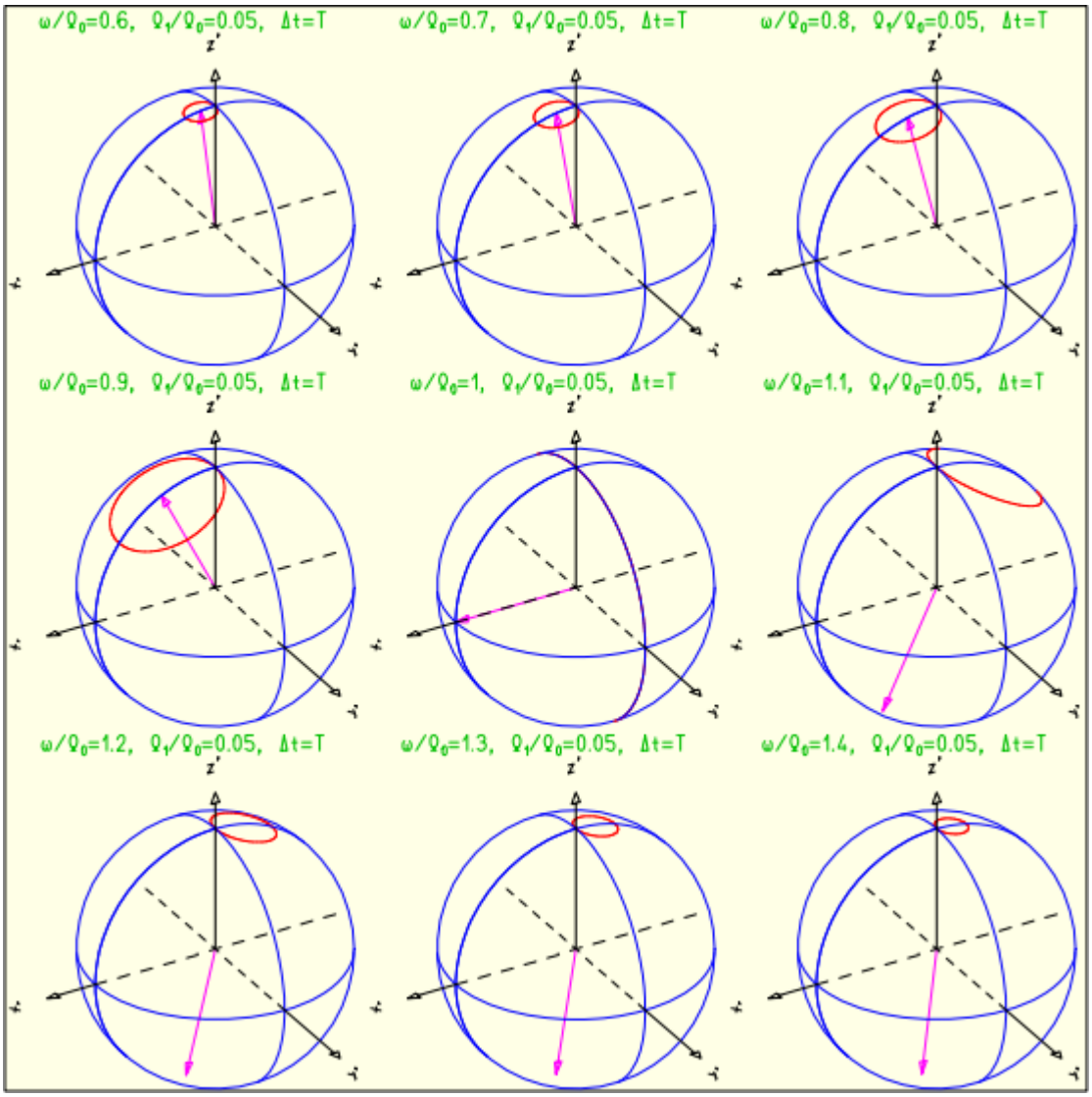

Figure 2.8: Trajectory of the expectation value of the spin vector within one period T in the rotating frame of reference. The arrow is the vector of the effective field $\mathbf{B}_{\text{eff}}$. The tip of the expectation value of the spin vector precesses around that direction. Its initial position is on the z' axis. Brandt and Dahmen, 2012.

2.3 Spin relaxation and decoherence

The corruption of a spin qubit state can be separated into two timescales:

- T_1 - describing the variation of θ - related to **spin relaxation**;
- T_2 - describing the randomization of ϕ - that is nothing but **decoherence** discussed in 1.2.6.

Relaxation is the phenomenon for which - when the exciting EM field is switched off - spin tends to its lower energy state. From a probabilistic point of view, the variation of θ implies the variation of the probabilities of being $|0\rangle$ and $|1\rangle$, even in absence of rotation pulses. In terms of magnetization, the time response for T_1 -

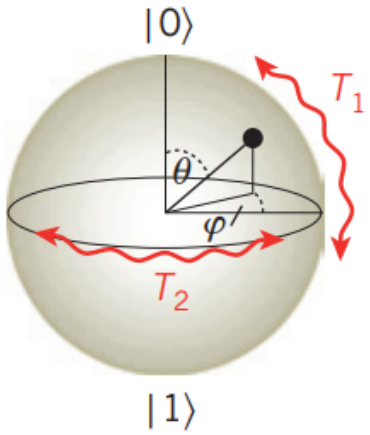

Figure 2.9: Effects of relaxation and decoherence on the Bloch sphere. Morton *et al.*, 2011.

parallel to the applied static magnetic field - is exponential, as the voltage transient of a capacitor

$$\begin{aligned} M_z(t) &= M_{z_\infty} - (M_{z_\infty} - M_0)e^{-\frac{t}{T_1}}, \\ M_0 &= M(|1\rangle), \\ M_{z_\infty} &= M(|0\rangle). \end{aligned} \tag{2.39}$$

The time duration Δt for a quantum gate/program must be sufficiently short to

make these effects negligible

$$\Delta t \ll \min\{T_1, T_2\}. \tag{2.40}$$

In the cases of interest [4, 17], T_1 is always greater than T_2, so the most significant error contribution is related to decoherence. Relaxation and decoherence can be

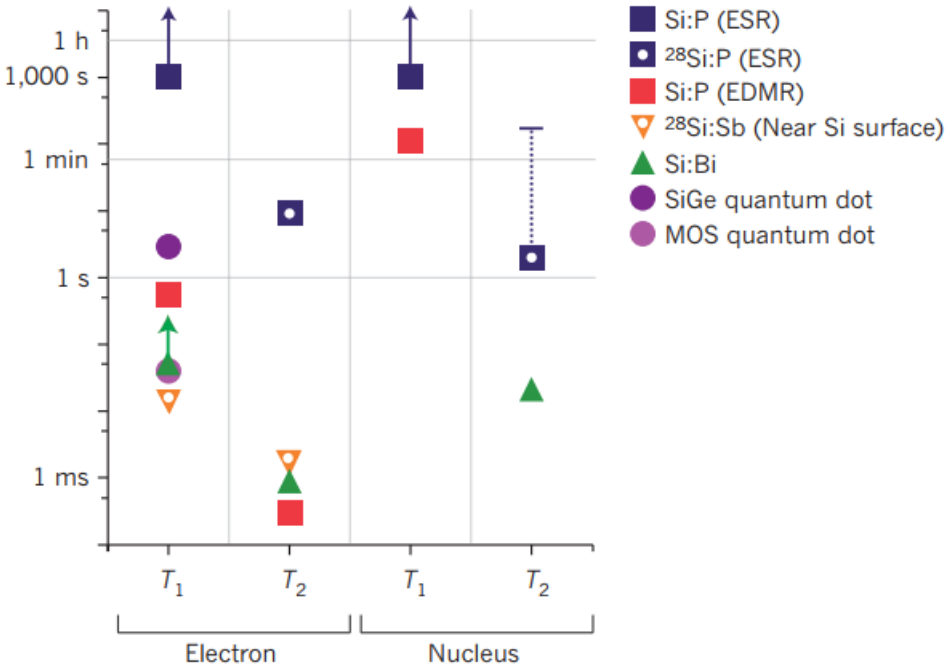

Figure 2.10: Relaxation and decoherence times of spin qubits in silicon. Morton *et al.*, 2011.

measured in magnetic resonance experiments. In the case of T_1, a π rotation to the qubit initialized in $|0\rangle$ is done in order to toggle the spin state (Figure 2.12(a)); then the spin is left in free evolution and the exponential reductions of the magnetization parallel to $\mathbf{B}$ and of the probability of being $|1\rangle$, also named population

$$P_e = |c_1|^2 = \mathrm{e}^{-\frac{t}{T_1}}, \tag{2.41}$$

are observed. T_2 can be measured in two different ways:

- **Ramsey fringes**. Two $\frac{\pi}{2}$ pulses are applied on the qubit (detuning frequency

$\delta = 0$), separated by a delay Δt during which the spin can freely precess around z-axis ($\delta \neq 0$). Different Δt values imply different populations; it is possible to plot the population in function of Δt and an exponential envelope will be observed, with time constant T_2. The beating frequency of the envelope (Figure 2.13) is proportional to δ.

- **Spin echo**. A π pulse between two $\frac{\pi}{2}$ pulses inverts the population of the two sites, thus reversing low-frequency phase dynamics. In this case it is possible to plot an envelope of population in function of the time interval between the first $\frac{\pi}{2}$ and π pulses (Figure 2.13). The beating period is shorter than the corresponding with Ramsey fringes since low frequency fluctuations are eliminated; the higher beating frequency is related to a time constant T_2^* for population in function of the sequence length $\Delta t_{xy} = \Delta t_{\text{free evolution}} + \Delta t_\pi + \Delta t_{\text{refocusing}}$

$$P_e = \frac{1}{2}\left(1 - \mathrm{e}^{-\frac{\Delta t_{xy}}{T_2^*}}\right) \tag{2.42}$$

Spin echo manipulations increase the coherence timescale, even though additional correction pulses are involved. For example, the identity gate made by a sequence of two X gates

$$I = XX$$

is an example of echo-like gate. It is possible to prove that echo-like gates have a lower error than the corresponding without echo [21] (Figure 2.14).

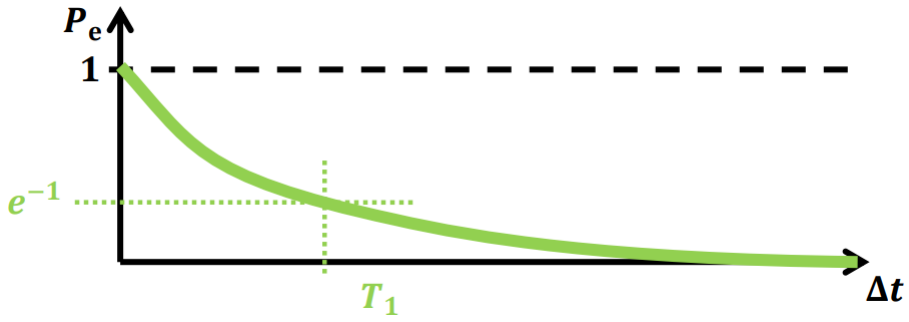

(a) Spin relaxation.

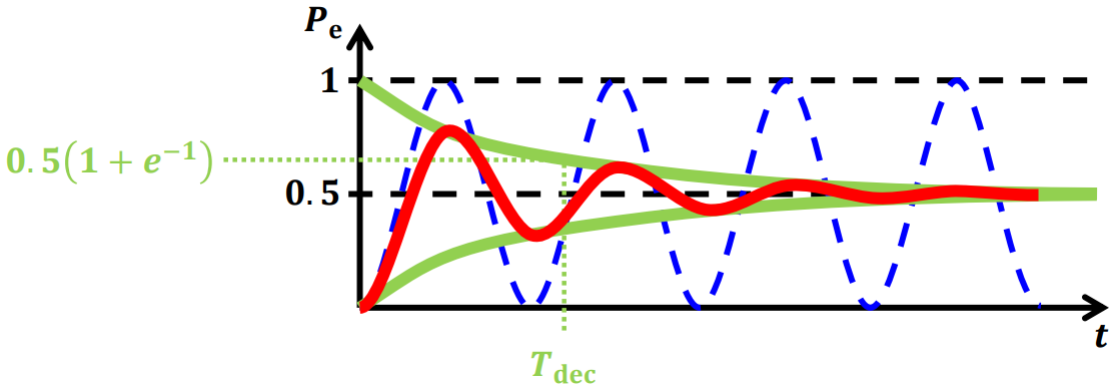

(b) Spin decoherence.

Figure 2.11: Effects of relaxation and decoherence on population. From http://www.wmi.badw.de/teaching/Lecturenotes/AS/AS2013_Chapter10_2_Slides.pdf.

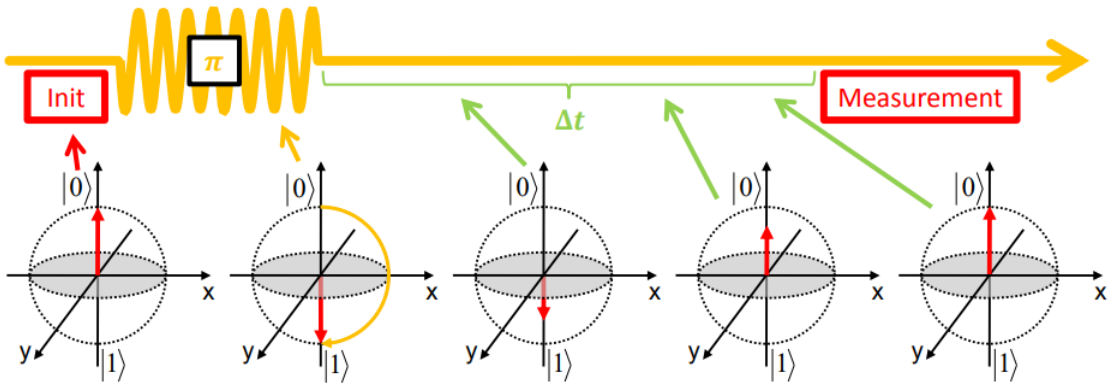

(a) Relaxation experiment.

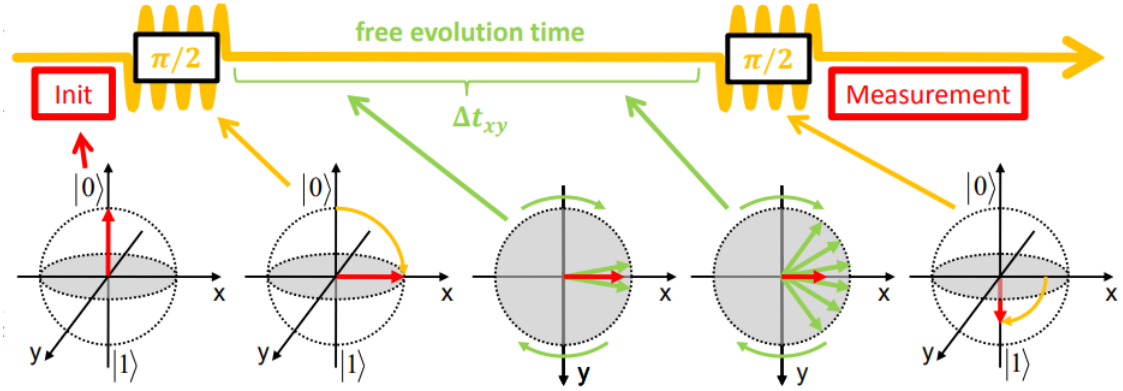

(b) Ramsey fringes.

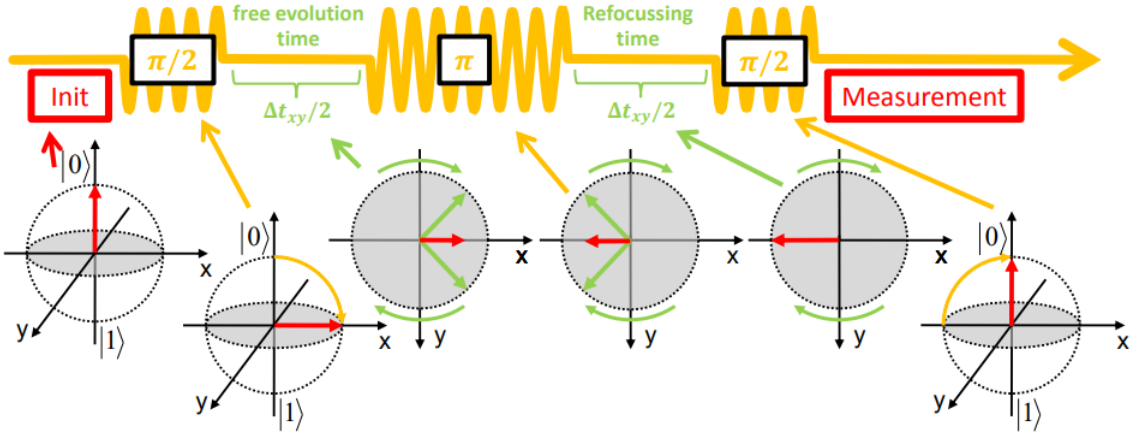

(c) Spin echo.

Figure 2.12: Measurement techniques for T_1 and T_2. From http://www.wmi.badw.de/teaching/Lecturenotes/AS/AS2013_Chapter10_2_Slides.pdf.

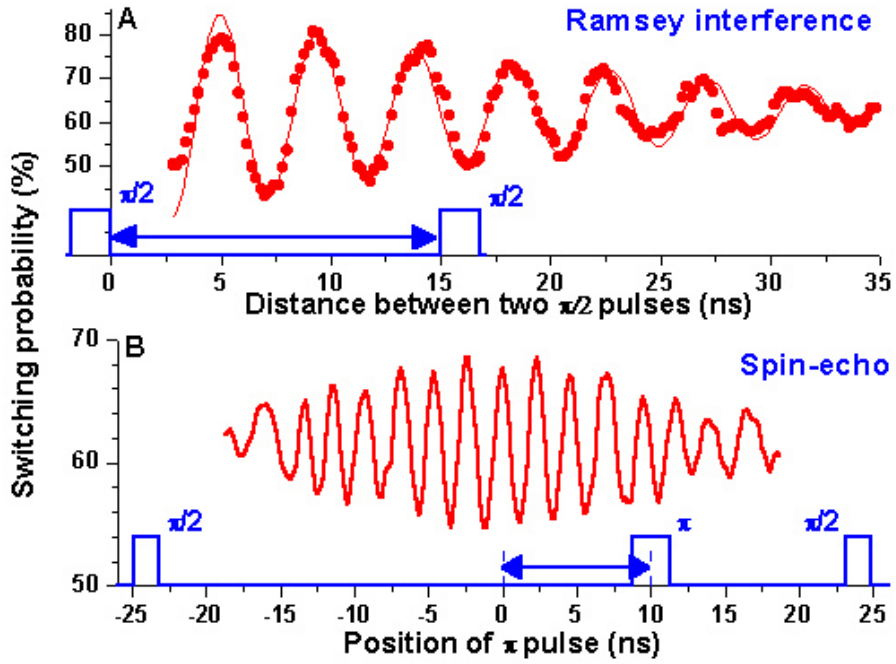

Figure 2.13: Ramsey and spin echo experiments envelopes. From http://qsd.magnet.fsu.edu/oldpage/fluxqubit.

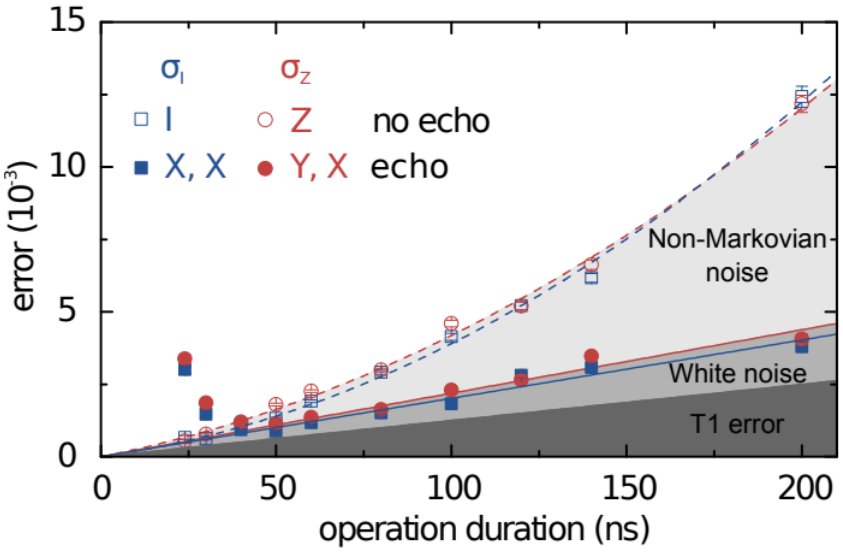

Figure 2.14: Operation error of I and Z in superconducting qubits, implemented with (filled symbols) and without (empty symbols) echoing. O'Malley, 2016.

2.4 Molecular Nano-Magnets for QIP

Single-molecule magnets are molecular compounds based on macromolecules, containing a core of magnetic ions surrounded by organic ligands. From an historical point of view, Fe_8 and Mn_{12} have been the most studied molecular nanomagnets; they display hysteresis and slow relaxation of the magnetization at the single-molecule level, so when the molecule is magnetized in presence of a magnetic field, it will retain its magnetization on removal of the field. This feature is characteristic of the molecule, *i.e.* it does not involve any intermolecular interaction.

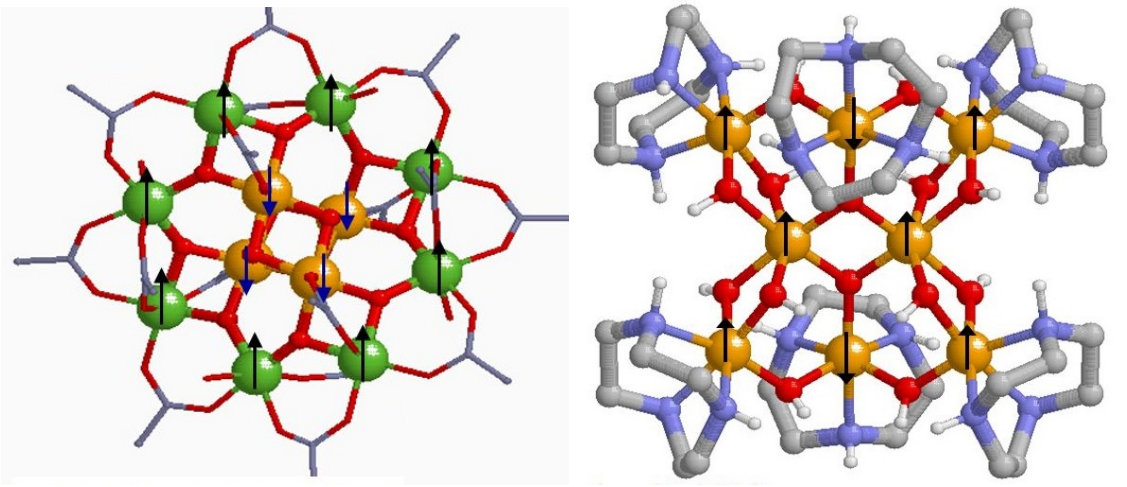

(a) Mn_{12}. Sessoli *et al.*, 1993.

(b) Fe_8. Image adapted from Weighardt *et al.*, 1984

Figure 2.15: Single Molecule Magnets.

Fe_8 and Mn_{12} are magnetically anisotropic, *i.e.* they align spontaneously along one direction, where the systems present the minimum energy. For the energy analysis of this system, supposed a static field $\mathbf{B} = B\mathbf{z}$ is supposed to be applied on the molecule. The quantum number S_z, related to the projection of the molecule's magnetic moment along the z-axis, is exploited. For Mn_{12} (Figure 2.15(a), made by four spins of Mn^{4+} sites (orange) with $S = \frac{3}{2}$ antiferromagnetically coupled to eight spins of Mn^{3+} sites (green) with $S = 2$, the spin angular momentum S_Z is

$$S_{z_{\max}} = S_Z = 8 \cdot 2 - 4 \cdot \frac{3}{2} = 10,$$

so the "boundary" values for S_z are ± 10. Fe_8 is made by eight Fe^{3+} ion with $S = \frac{5}{2}$ and two of them orientate anti-parallel to the other six

$$S_Z = (6 - 2) \cdot \frac{5}{2} = 10.$$

If energy is increased, the magnetization is not aligned along the z-axis anymore, but it is rotated of a certain angle $0 < \theta < \pi$ (Figures 2.16 and 2.17). The total

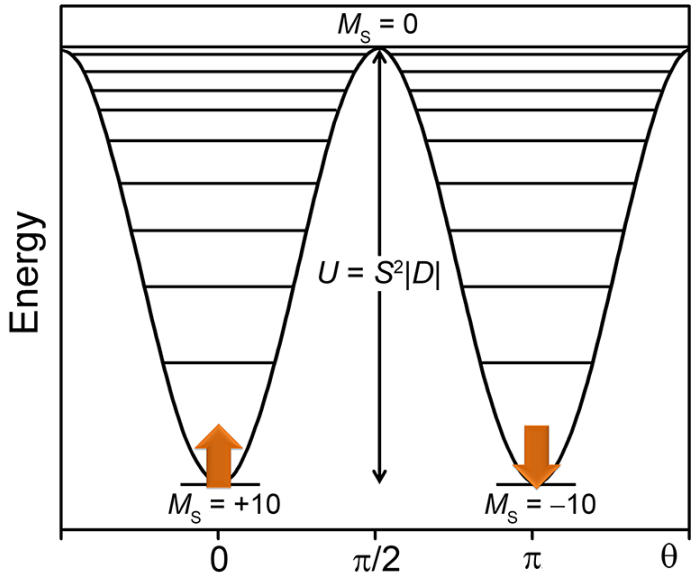

Figure 2.16: Energy of Mn_{12} in function of the orientation angle θ. Adapted from http://alchemy.cchem.berkeley.edu/magnetism/.

number of energy states is equal to $2S_Z + 1$, since $-S_Z \leq S_z \leq +S_Z$. Information can be encoded:

- on the energy states with $S_z = \pm S_Z$, *i.e.* $|0\rangle$ and $|1\rangle$ are defined on anti-parallel orientation. Spin can be changed by providing an energy amount either for overcoming the parabolic potential barrier in Figure 2.17 or sufficient for quantum tunneling, thus permitting the direct magnetization reversal from $-S_Z$ to $+S_Z$ (and vice versa);
- on two adjacent energy states (*e.g.* $|0\rangle \leftrightarrow S_z = -S_Z$ and $|1\rangle \leftrightarrow S_z = -S_Z + 1$);
- on more than two states, since a molecular magnet with $N = 2S_Z + 1$ states can be exploited to encode $\lfloor \log_2(N) \rfloor$ bits.

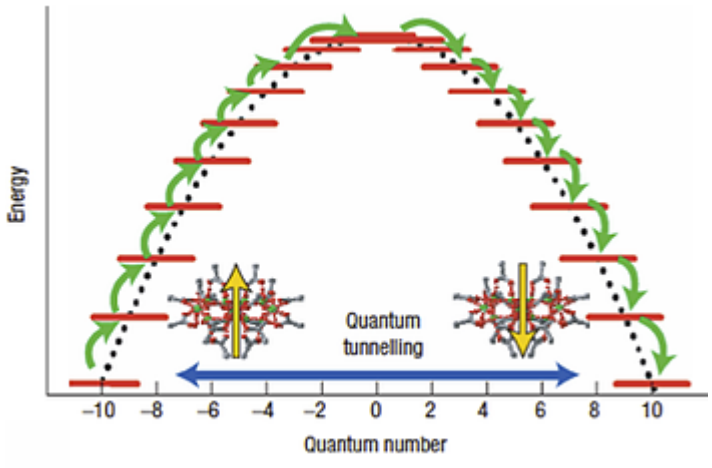

Figure 2.17: Energy of Mn_{12} in function of the spin quantum number S_z. Image adapted from Bogani *et al.*, 2008.

In 2001 it was proved that Fe_8 and Mn_{12} single molecule magnets are candidates for the realization of a quantum computer - according to the DiVincenzo's criteria [25] - capable to solve Grover's algorithm [11].

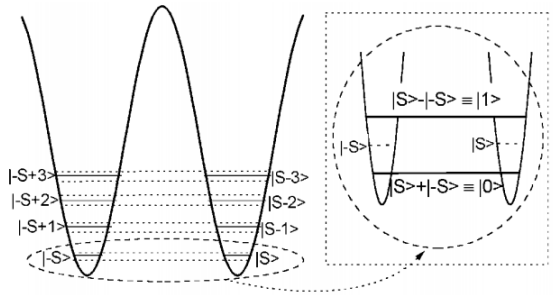

(a) Qubit states on ground states.

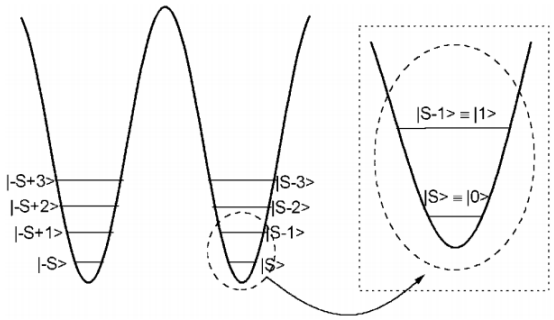

(b) Qubit adjacent states.

Figure 2.18: Qubits on Fe_8 and Mn_{12}. Tejada *et al.*, 2001.

Other molecules have been recently proposed as quantum computation units. In the case of GdW_{30} single-ion magnet [1, 8], a maximum quantum number $S_Z = \frac{7}{2}$ is associated to the Gd^{3+} ion, so it can be mapped onto the states of three addressable qubits with seven allowed transitions. Within this scheme, Rabi oscillations correspond to quantum operations between two of these logic states. For example - according to the employed Gray encoding - a π rotation tuned at transition 1 of Zeeman diagram in Figure 2.19 implements a Toffoli-like gate.

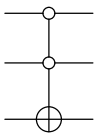

Differently than the standard Toffoli gate, the target qubit is flipped when the control qubits are '0' instead of '1'. In general, for a $S_Z > \frac{1}{2}$ molecule, an arbitrary encoding can be chosen.

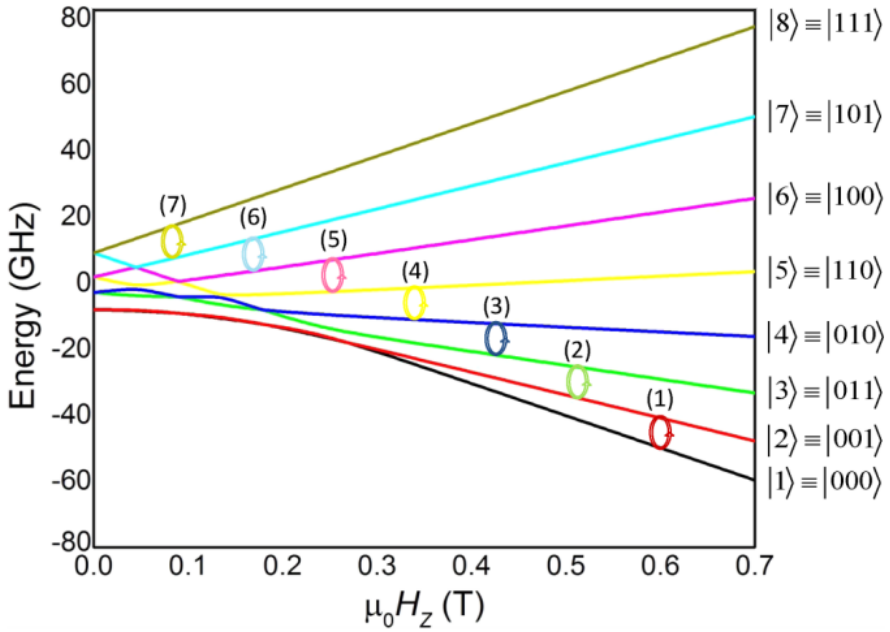

Figure 2.19: Zeeman diagram of the GdW_{30} single-ion magnet. Energy states are Gray-coded. Image adapted from Jenkins *et al.*, 2017.

If a molecule presents more spins, they can be exploited as independent qubits. This is the case of the dinuclear complex of Tb^{3+} (terbium) ions named [Tb_2] [22]. The zero-field energy level structure of [Tb_2] is reported in Figure 2.20. The ground state is a doublet which is separated more than 180 K from the first excited state (Figure 2.20(b)). The four states forming the doublet are separated by $\Delta E = 2.14$ K. As the easy axes of spins are not aligned and their effective gyromagnetic ratios g_1 and g_2 are different, they are magnetically anisotrope. If a static field is applied along one of the anisotropy axes, ions will couple differently to it, thus obtaining a four-level system, needed for performing quantum gates. The magnetic asymmetry

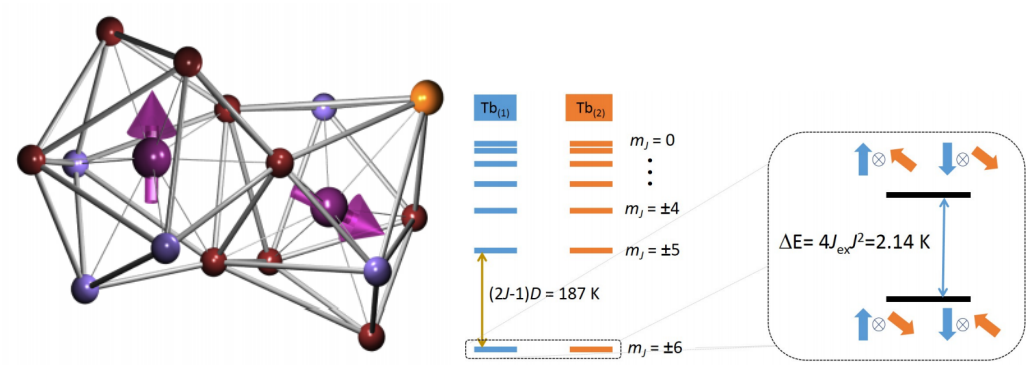

(a) Two qubits molecule.

(b) Computational basis.

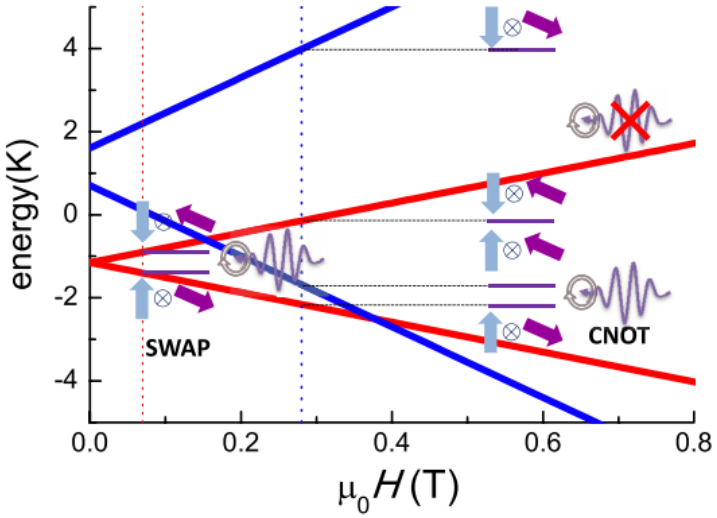

(c) Zeeman diagram and implementable gates.

Figure 2.20: [Tb_2] molecule. Repolles, 2016.

enables to univocally single out any of the desired transitions (Figure 2.20(c)):

- At $\mu_0 H = 0.07\,\mathrm{T}$, only transitions between states $|\Uparrow\rangle \otimes |\Downarrow\rangle$ and $|\Downarrow\rangle \otimes |\Uparrow\rangle$ (SWAP) would be resonant with $\nu = 9.8\,\mathrm{GHz}$ photons.

- At $\mu_0 H = 0.28\,\mathrm{T}$ the same transition frequency permits to change the state from $|\Uparrow\rangle \otimes |\Uparrow\rangle$ to $|\Uparrow\rangle \otimes |\Downarrow\rangle$ (CNOT).

SWAP and CNOT operations can be selected by tuning $\mu_0 H$, with the same photon energy. The state initialization can be carried out by cooling. For $T = 0.1\,\mathrm{K}$ and both field values, the ground state population amounts to 99.3% [22].
A molecular magnet similar to [Tb_2] is based on the two dysprosium groups, each one with its own spin qubit [22]. With a static field of 69 mT and an excitation of frequency 7.5 GHz (Figure 2.21(b)), it could perform a SWAP operation. CNOT operation could be carried out, for example, at 200 mT, by exciting with an energy frequency of 4.17 GHz.
The main problem of molecular magnets with $S_Z > \frac{1}{2}$ is their modeste decoherence timescale. It has been experimentally proved that T_2 values for molecules with $S_Z = \frac{1}{2}$ are some order of magnitude longer than those for $S_Z > \frac{1}{2}$, as it is possible to ascertain in Figure 2.22. Considering that EPR pulse durations are typically of some nanosecond, values of T_2 in the order of tens of microseconds permit to do some thousand of operations with negligible error; moreover, qubit decoherence timescale has an exponentially increasing trend. For these reasons, molecular magnets with $S_Z = \frac{1}{2}$ are serious candidates for the definition of a quantum computer architecture, even though there is not actually a well-defined model. A potential scalable architecture with individual molecular spins coupled to superconducting coplanar resonators and transmission lines has been proposed in [9]. Arbitrary operations on each spin qubit can be can performed and tunable interactions between pair of qubits can be induced, thus permitting the definition of single and two-qubits gates. A superconducting resonator with a magnetic field profile $\overrightarrow{b}_r$ of its ground $\frac{\lambda}{2}$ mode is eventually put in resonance with the spin qubits by an homogeneous in-plane magnetic field $\overrightarrow{B}$ and local magnetic fields $\overrightarrow{b}_i$ (Figure 2.23), thus permitting the definition of quantum gates. It is fundamental to accurately integrate qubits into specific areas of the device.

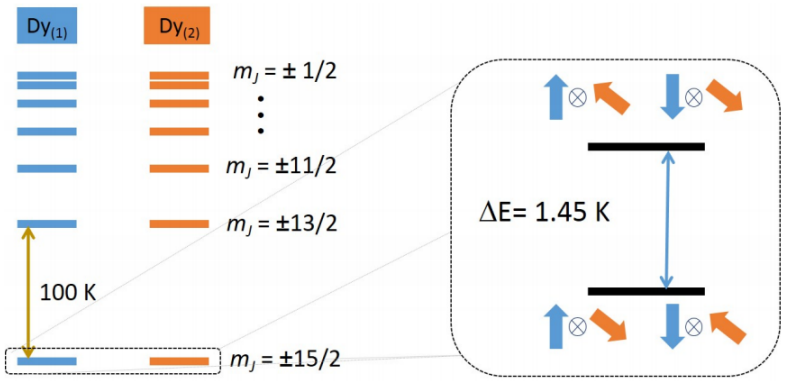

(a) Computational basis

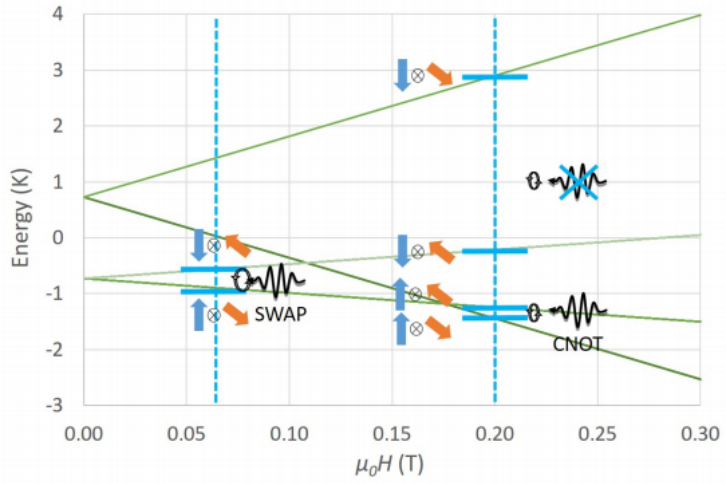

(b) Zeeman diagram and implementable gates.

Figure 2.21: [Dy2] molecule. Repolles, 2016.

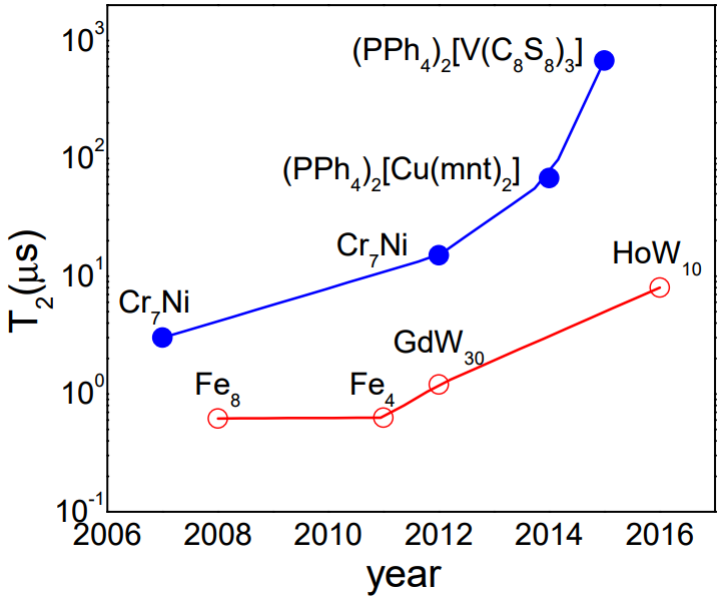

Figure 2.22: Decoherence of qubits based on molecular magnets. Image adapted from Jenkins *et al.*, 2016.

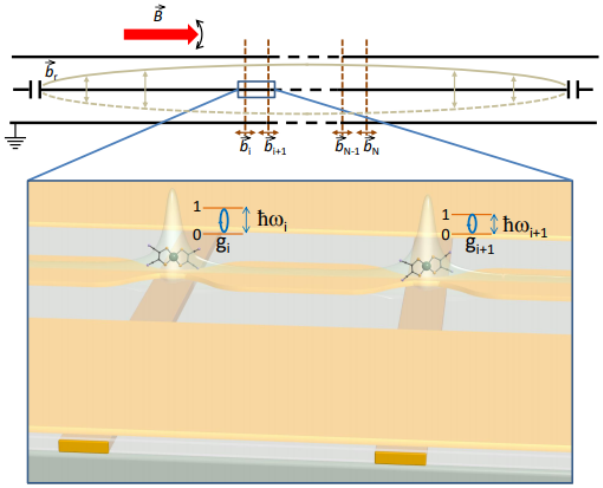

Figure 2.23: Quantum computer architecture proposed by Jenkins *et al.*, 2016.

2.4.1 Cr_7Ni-Co-Cr_7Ni supramolecular complex

In this thesis, the qubits defined on Cr_7Ni heterometallic rings are discussed: they are two-level systems ($S_Z = \frac{1}{2}$) with sufficiently long phase memory times (some microsecond) to allow many gate operations before state degradation occurs. Each ring defines a qubit and assemblies of low-spin coupling rings have been made through switchable links, that are also characterized by spin $S_z = \pm\frac{1}{2}$. Supramolecular chemistry is exploited to link individual components, characterized by different spatial configurations, thus influencing the properties of the resulting supramolecules. When the switch between two qubits is in its ground state ($S_z = \left|-\frac{1}{2}\right\rangle$), they can be

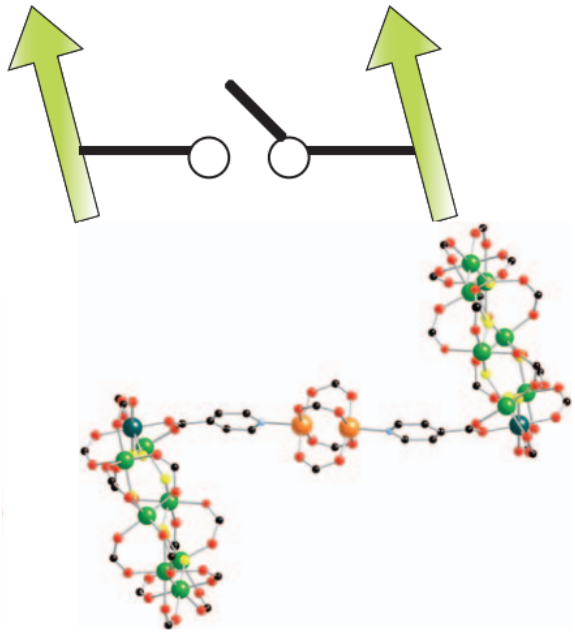

Figure 2.24: Two Cr_7Ni-qubit system with switchable coupling. Atoms legend: Cr (light green), Ni (dark green), Cu (orange), O (red), N (blue), F (yellow) and C (black). Timco *et al.*, 2009.

treated as decoupled and single qubit gates can be implemented by magnetic pulses resonant with the qubit gap. Conversely, conditional gates between neighboring pairs of qubits are performed by temporarily bringing the switch to an excited state - where the switch spin equals $\left|+\frac{1}{2}\right\rangle$ - by a microwave pulse of suitable phase and duration, thus turning on the qubit-qubit interaction. In general, a residual interaction among qubits is always present but it can be neglected on a timescale of 500 ns,

so it is possible to define quantum circuits involving quantum gates working on a time duration lower than that. The decoherence time can be significantly larger, up to $T_2 \sim 15\,\mu s$ [28].
A couple of Cr_7Ni rings is connected through high spin Co^{2+} ions, that presents $S_Z = \frac{1}{2}$ at low temperature ($T = 5\,K$). The spin Hamiltonian of a two-qubits molecule is

$$\frac{H}{\hbar} = -2\left[(\mathbf{S}_1 \cdot \underline{J}_{12} \cdot \mathbf{S}_2) + (\mathbf{S}_2 \cdot \underline{J}_{23} \cdot \mathbf{S}_3)\right] + \mu_B \left(\mathbf{S}_1 \cdot \underline{g}_1 + \mathbf{S}_2 \cdot \underline{g}_2 + \mathbf{S}_3 \cdot \underline{g}_3\right) \cdot \mathbf{B} \quad (2.43)$$

where $\mathbf{S}$ indicates the effective spin-$\frac{1}{2}$ operators of the Cr_7Ni qubits (1 and 3) and of the Co^{2+} switch (2), respectively, $\underline{g}$ are the spectroscopic (g-factor) tensors describing the interaction of the magnetic moments with an external magnetic field $\mathbf{B}$, and μ_B is the Bohr's magneton. Finally, each $\underline{J}$ is an exchange tensor describing a qubit-switch interaction. In Equation 2.43 the -2 coefficient is explicitly written (such as [7]), in other cases this term is already multiplied by the exchange tensor as in [4].
The Spin Hamiltonian of a three-qubits molecule would be

$$\begin{aligned}\frac{H}{\hbar} = &-2\left[(\mathbf{S}_1 \cdot \underline{J}_{12} \cdot \mathbf{S}_2) + (\mathbf{S}_2 \cdot \underline{J}_{23} \cdot \mathbf{S}_3) + (\mathbf{S}_3 \cdot \underline{J}_{23} \cdot \mathbf{S}_4) + (\mathbf{S}_4 \cdot \underline{J}_{12} \cdot \mathbf{S}_5)\right] \\ &+ \mu_B \left(\mathbf{S}_1 \cdot \underline{g}_1 + \mathbf{S}_2 \cdot \underline{g}_2 + \mathbf{S}_3 \cdot \underline{g}_3 + \mathbf{S}_4 \cdot \underline{g}_2 + \mathbf{S}_5 \cdot \underline{g}_1\right) \cdot \mathbf{B}\end{aligned} \quad (2.44)$$

where $\mathbf{S}_5$ is the third qubit, that interacts with the second qubit through the switch $\mathbf{S}_4$; in Equation 2.44 it is possible to observe that spectroscopic tensors $\underline{g}$ of $\mathbf{S}_5$ and $\mathbf{S}_4$ are equal to those of $\mathbf{S}_1$ and $\mathbf{S}_2$ respectively.
The spin-Hamiltonian parameters of the molecule employed in simulations are reported, coherently with the notation in Equation 2.43. The energy level diagrams for the two-qubits and three-qubits molecules are reported In Figures 2.25 and 2.26.

	g_x	g_y	g_z
{Cr_7Ni-O_2C-terpy} (1)	1.78	1.78	1.74
Co switch (2)	1.78	4.25	6.50
{Cr_7Ni-O_2C-py} (3)	1.74	1.78	1.78

Table 2.1: Terms on the main diagonal of each spectroscopic tensor $\underline{g}$. Ferrando *et al.*, 2016.

	J_x (cm^{-1})	J_y (cm^{-1})	J_z (cm^{-1})
J_{12}	-0.14	0.34	0.17
J_{23}	-0.07	0.17	0.43

Table 2.2: Terms on the main diagonal of each exchange tensor $\underline{J}$. Ferrando *et al.*, 2016.

	J_x (cm^{-1})	J_y (cm^{-1})	J_z (cm^{-1})
J_{12}	-0.048	0.113	0.056
J_{23}	-0.024	0.056	0.113

Table 2.3: Terms on the main diagonal of each exchange tensor $\underline{J}$. Chiesa *et al.*, 2016.

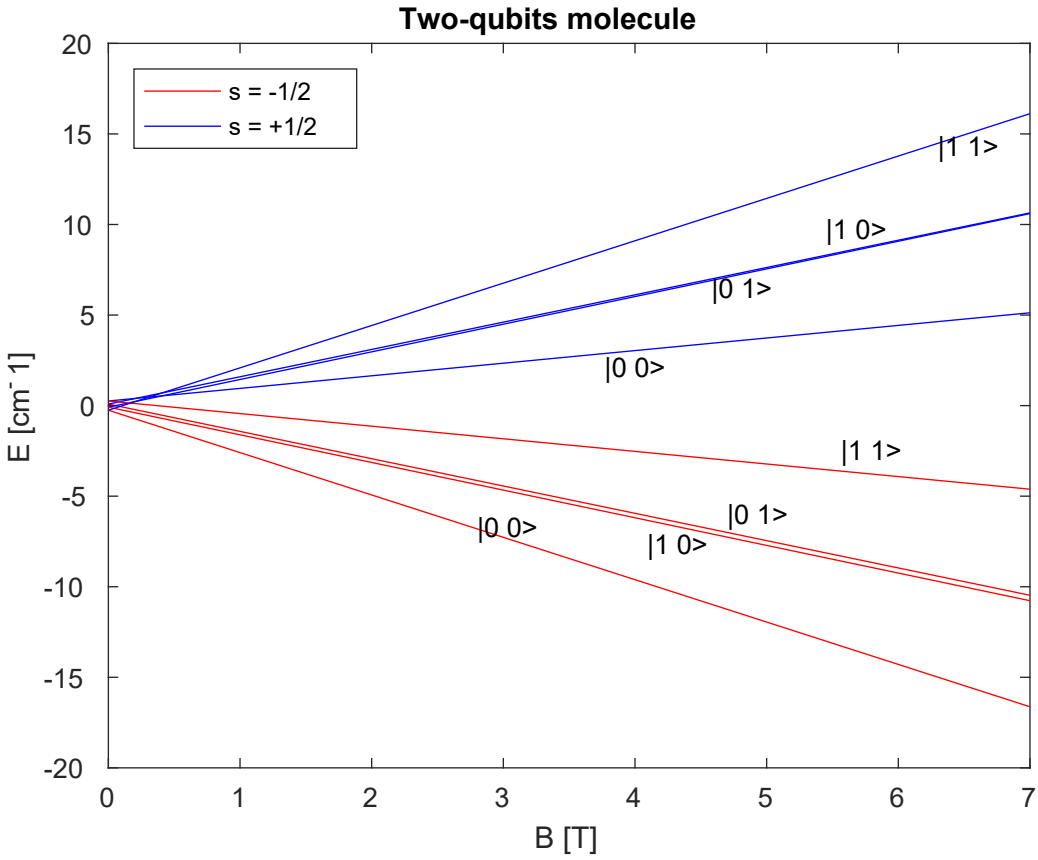

Figure 2.25: Energy levels for a two-qubits molecule.

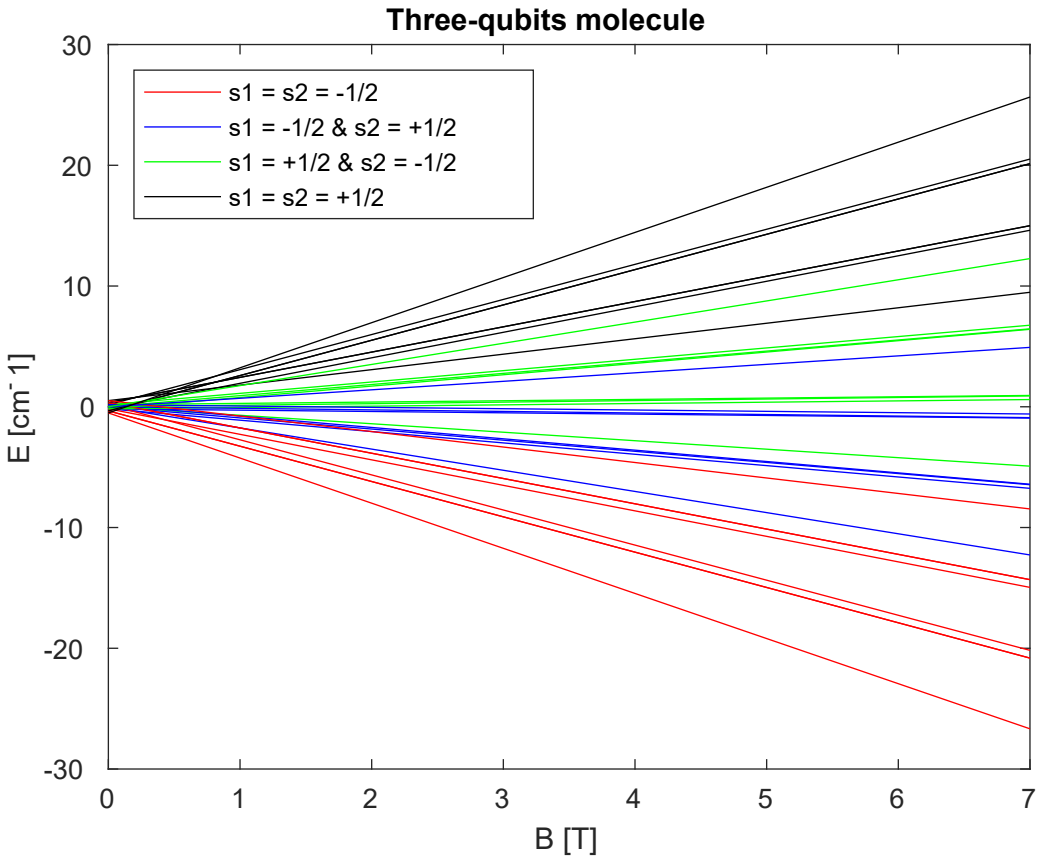

Figure 2.26: Energy levels for a three-qubits molecule.

The computational basis is defined for states where the spin of each switch is $S_z = \left|-\frac{1}{2}\right\rangle$ (red curves). It is possible to derive the transition frequencies

$$\Delta f \text{ [GHz]} \simeq 30 \cdot \Delta E \text{ [cm}^{-1}\text{]}, \tag{2.45}$$

in particular those required to rotate single qubits and the switch. In the architecture to be implemented, it must be assumed that a magnetic resonance infrastructure is associated to each spin (Figure 2.27). It can be also observed that for the transition from ground state $|000\rangle$ to a state with two or more qubits equal to $|1\rangle$, the total energy/frequency is the sum of those of each separate spin, *e.g.* for $|000\rangle \rightarrow |110\rangle$

$$\Delta E_{110} = \hbar \left(\omega_{100} + \omega_{010}\right). \tag{2.46}$$

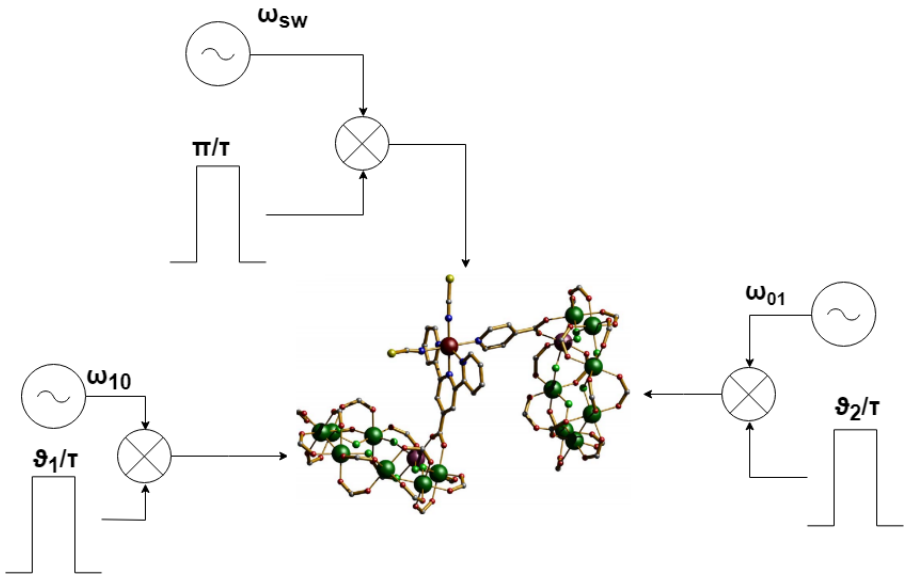

Figure 2.27: Manipulation of each spin in a two-qubits molecule. Adapted from Ferrando *et al.*, 2016.

In the range of interest for the magnetostatic field B, the required transitions all

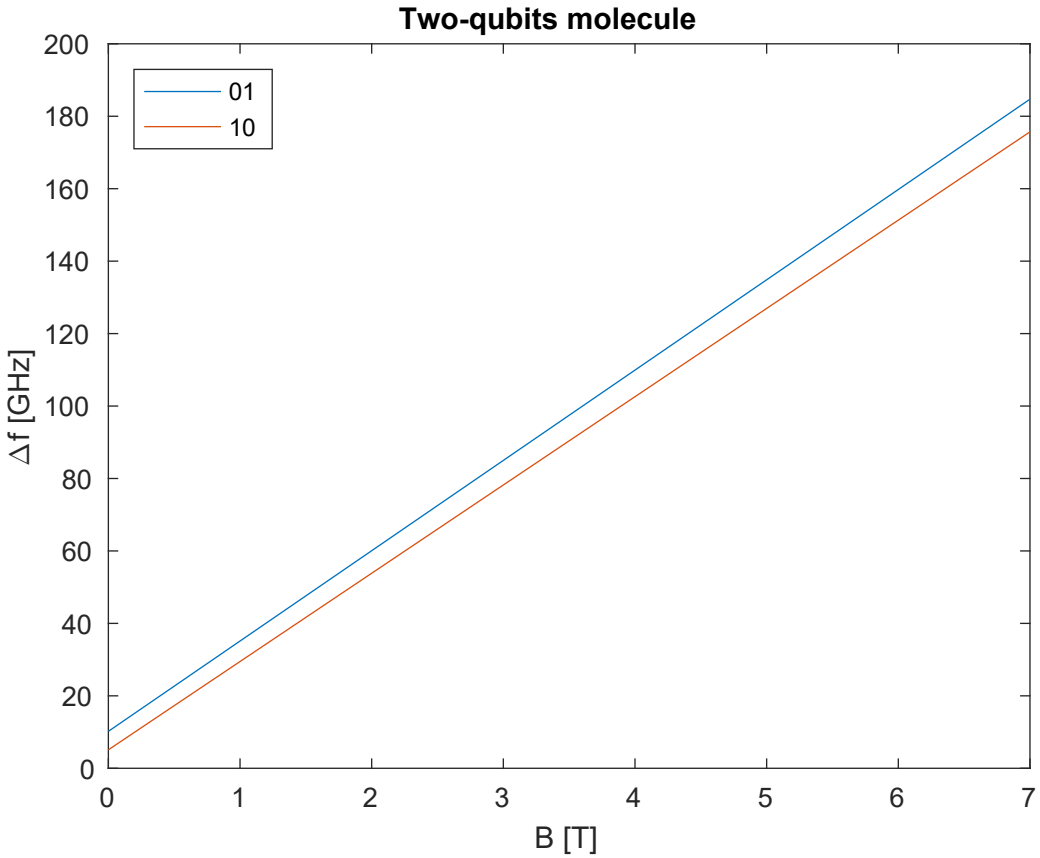

Figure 2.28: Rotation energies for a two-qubits molecule.

belong to the microwave spectrum. Since the first and the third qubit are identical, the same energy amount is required and their curves are superposed in Figure 2.29.

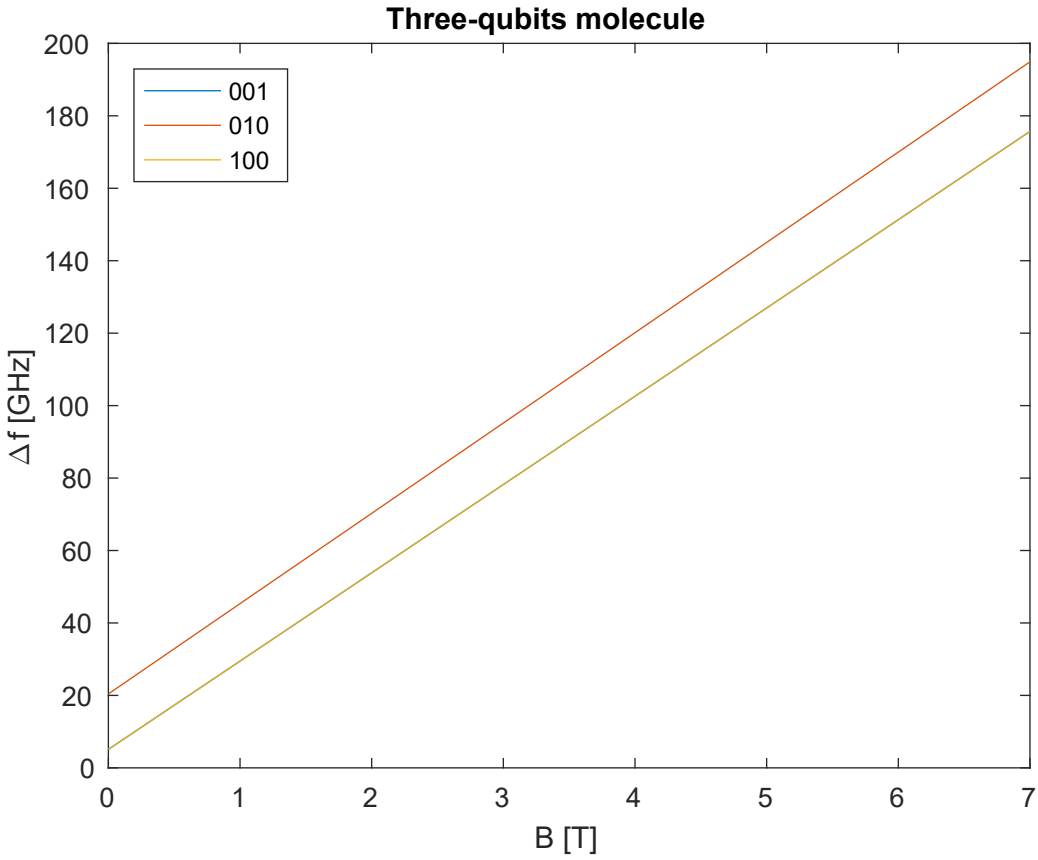

Figure 2.29: Rotation energies for a three-qubits molecule.

C-ϕ and CNOT gates with Cr_7Ni-Co-Cr_7Ni complex

The controlled-phase gate (see matrix 1.80) is realized by a couple of pulses resonant with the transition $|11\rangle \otimes S_{\text{sw}} = \left|-\frac{1}{2}\right\rangle \Rightarrow |11\rangle \otimes S_{\text{sw}} = \left|+\frac{1}{2}\right\rangle$ that does not affect the other states. According to [7], a couple of pulses - with carrier frequency resonant with that transition and modulated by a gaussian function with peak value of 50 G and 99% of area in about 6 ns - permits to obtain the evolution of a C-Z gate, *i.e.* a C-ϕ with $\phi = \pi$. In the proposed model, it has been assumed that the switch state can be changed by a rectangular modulation pulse with carrier frequency resonant with its transition and the transition probability can be computed from 2.33. It has been proved that the four transition frequencies of the switch are all different in the considered range for B (Figures 2.30, 2.31 and 2.32), so the molecule has been treated as a four two-level system

$$|ij\rangle \otimes \left[S_{\text{sw}} = \left|-\frac{1}{2}\right\rangle\right] \Rightarrow |ij\rangle \otimes \left[S_{\text{sw}} = \left|+\frac{1}{2}\right\rangle\right].$$

Transitions do not depend on the value of the qubit not connected to the switch of interest, *e.g.* for the switch linking the second and third qubits $\Delta E_{\text{sw}}(010) = \Delta E_{\text{sw}}(110)$, so there are four different transition frequencies for each switch.
For the implementation of the C-ϕ gate, the additional phase to the $|11\rangle$ coefficient of the two-qubits vector is provided by a couple of $\omega_1\tau = \pi$ pulses and the carrier of each pulse has phase $\frac{\phi}{2}$. In the case of resonant pulses, the switch will change two times and at the end of the pulse sequence $|11\rangle$ will have additional phase $e^{i\phi}$; in the other cases the switch will not change its state, so qubits are not affected by the pulse sequence. Because of unavailability of mathematical tools for solving the Schrödinger equation, a model for the description of the Controlled-ϕ dynamics was required. The initial idea was to treat the switch as a qubit vector with $|0\rangle = \left(S_{\text{sw}} = \left|-\frac{1}{2}\right\rangle\right)$ and $|1\rangle = \left(S_{\text{sw}} = \left|+\frac{1}{2}\right\rangle\right)$, so that the evolution at the end of the sequence of two pulses could be described as

$$|11\rangle \otimes \left[\left(S_{\text{sw}} = \left|-\frac{1}{2}\right\rangle\right) \cdot e^{i\phi}\right] = \left(e^{i\phi} \cdot |11\rangle\right) \otimes \left[S_{\text{sw}} = \left|-\frac{1}{2}\right\rangle\right].$$

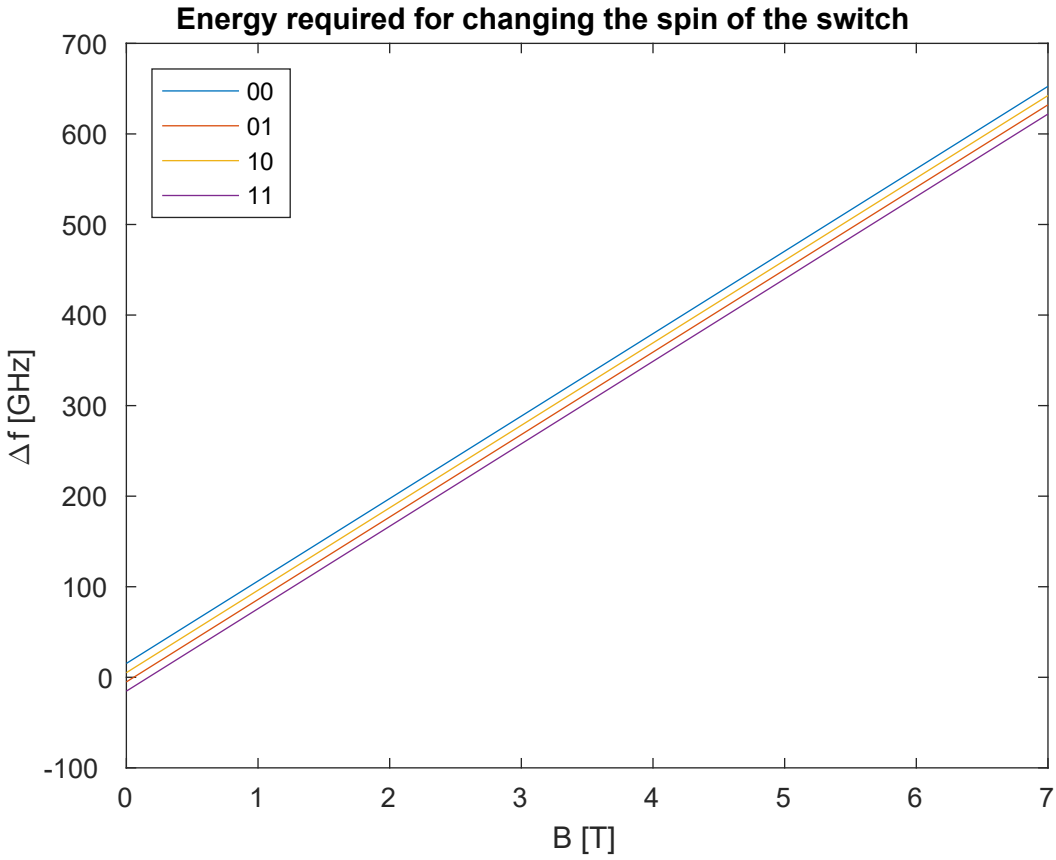

Figure 2.30: Rotation energies for the switch spin in the two-qubit complex.

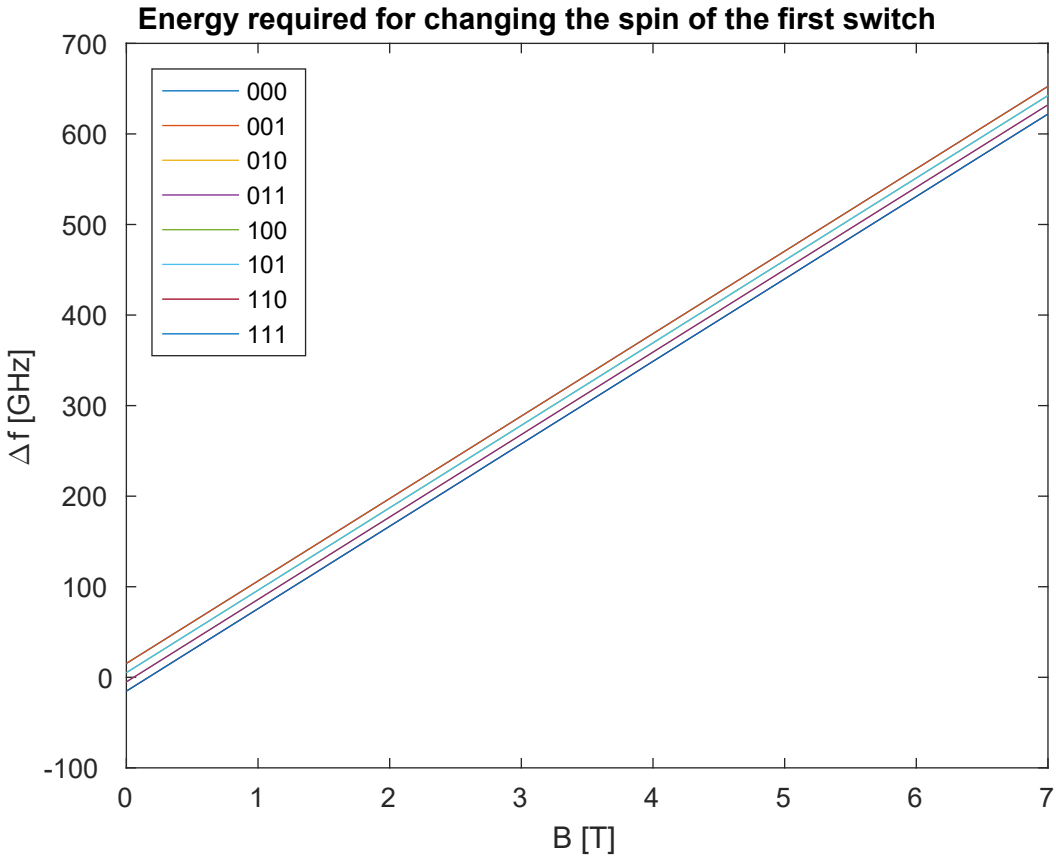

Figure 2.31: Rotation energies for the first switch spin in the three-qubit complex.

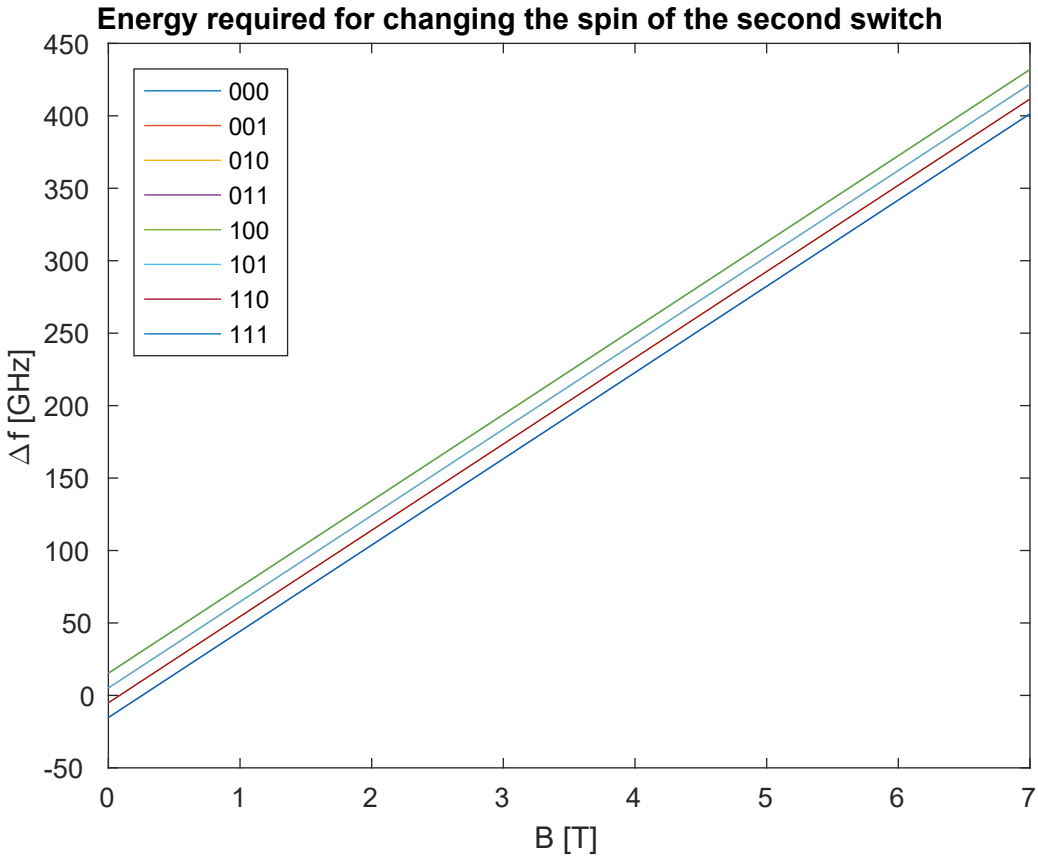

Figure 2.32: Rotation energies for the second switch spin in the three-qubit complex.

The notation puts in evidence that the $S_{\text{sw}} = \left|-\frac{1}{2}\right\rangle$ state is separated from those of qubits and that the scalar contribution due to the additional phase can be passed to the vector states of qubits according to one property of Kronecker tensor product. The main problem is due to the fact that it is not clear whether rotating wave approximation validates the unitary operator 2.2 for the switch treated as a qubit vector. If that approximated operator is not valid, coefficients different from c_{11} may be modified in absence of resonance. Since the unitary matrix of the gate is

$$\begin{bmatrix} 1 & 0 & 0 & 0 \\ 0 & 1 & 0 & 0 \\ 0 & 0 & 1 & 0 \\ 0 & 0 & 0 & \mathrm{e}^{\mathrm{i}\phi} \end{bmatrix}, \tag{2.47}$$

it has been chosen to describe the dynamics of the gate through the cascade of two matrices (one for each π transition)

$$M = \begin{bmatrix} \mathrm{e}^{\mathrm{i}P_{00}\frac{\phi}{2}} & 0 & 0 & 0 \\ 0 & \mathrm{e}^{\mathrm{i}P_{01}\frac{\phi}{2}} & 0 & 0 \\ 0 & 0 & \mathrm{e}^{\mathrm{i}P_{10}\frac{\phi}{2}} & 0 \\ 0 & 0 & 0 & \mathrm{e}^{\mathrm{i}P_{11}\frac{\phi}{2}} \end{bmatrix}, \tag{2.48}$$

where P_{ij} is the transition probability in each case, computed using equation 2.33. The Controlled-ϕ gate matrix is defined in this approximated model as

$$\text{C-}\phi \equiv M^2 = \begin{bmatrix} \mathrm{e}^{\mathrm{i}P_{00}\phi} & 0 & 0 & 0 \\ 0 & \mathrm{e}^{\mathrm{i}P_{01}\phi} & 0 & 0 \\ 0 & 0 & \mathrm{e}^{\mathrm{i}P_{10}\phi} & 0 \\ 0 & 0 & 0 & \mathrm{e}^{\mathrm{i}P_{11}\phi} \end{bmatrix}. \tag{2.49}$$

If each magnetic pulse has $\omega = \omega_{11}$ and $\omega_1\tau = \pi$, $P_{11} = 1$, so that $\mathrm{e}^{\mathrm{i}P_{11}\phi} = \mathrm{e}^{\mathrm{i}\phi}$, while in the other three cases $P_{ij} \ll \frac{1}{\phi}$ and $\mathrm{e}^{\mathrm{i}P_{ij}\phi} \approx 1$. In conclusion, the gate matrix is

approximately

$$\text{C-}\phi \approx \begin{bmatrix} 1 & 0 & 0 & 0 \\ 0 & 1 & 0 & 0 \\ 0 & 0 & 1 & 0 \\ 0 & 0 & 0 & \mathrm{e}^{\mathrm{i}\phi} \end{bmatrix}. \tag{2.50}$$

The CZ gate is derived from equation 2.49 with $\phi = \pi$. The CNOT gate can be obtained by the sequence of gates

$$\text{CNOT} = H \cdot C_Z \cdot H. \tag{2.51}$$

Chapter 3

Quantum computer architecture

In the proposed computer architecture the Cr_7Ni-Co-Cr_7Ni supramolecular complex is an execution unit excited by EPR pulses. The operations are organized according to the microprogramming paradigm, where the single qubit rotations and the C-ϕ interaction are the only two microinstructions over which it is possible to create more complex instructions. The program is stored in RAM and it refers to a sequence of

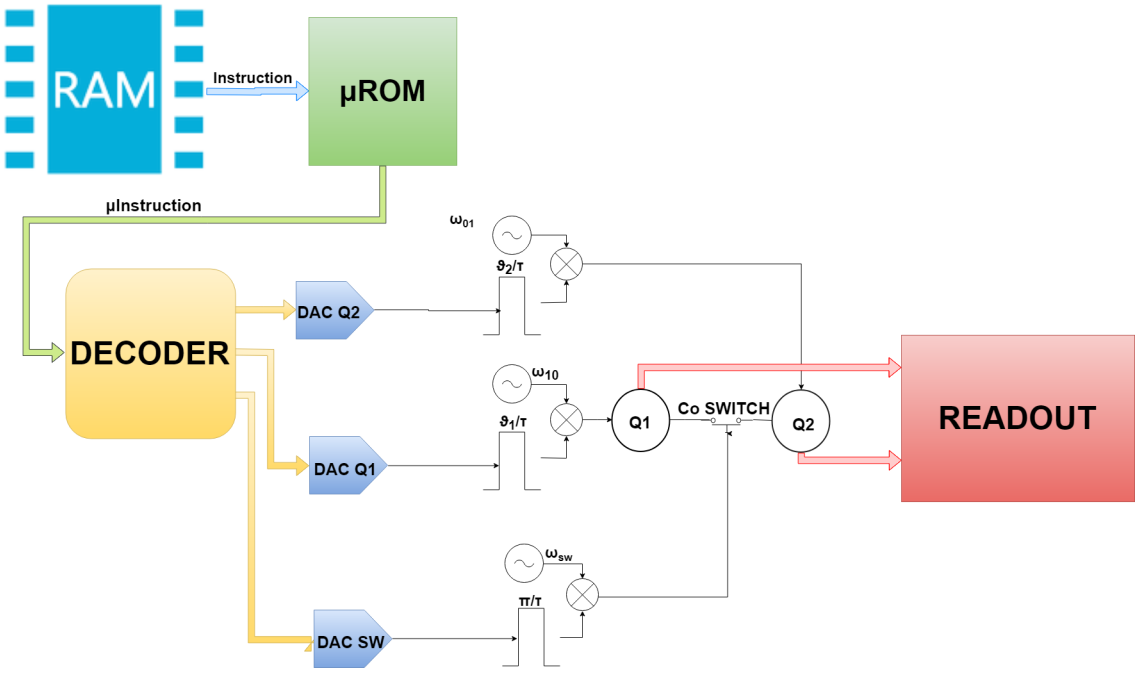

Figure 3.1: Block scheme of the proposed quantum computer architecture.

spin manipulations through AM magnetic resonance. Quantum instructions must contain parameters about the phase of the carrier and spin's rotation amount θ, that is equal - according to the magnetic resonance theory - to the product between the precession frequency around the xy plane ω_1 and the time duration τ (supposing

a modulating rectangular pulse). Since τ is supposed to be fixed, ω_1 is the only variable parameter and instructions must contain either ω_1 or θ or the amplitude of the magnetic pulse $B_1 = \frac{\omega_1}{\gamma}$. Regardless of the what is stored inside memory, Digital-to-Analog converters must provide a pulse proportional to B_1 as output. In simulations, it has been assumed that the time durations for single rotations in two-qubits and three-qubits molecule are 5 ns and 2.3 ns respectively, similar to that for the Gaussian pulse in [7]. Moreover, these values ensure the satisfaction of the condition

$$\Delta\omega_0\tau \gg 2\pi, \tag{3.1}$$

related to the fact that the frequency spectrum of modulating signal must not have too high contributions at transition frequencies different from the chosen one, since undesired spin rotations can take place. For $\tau = 2.3\,\text{ns}$ and static field $B = 6\,\text{T}$, the ratio $\frac{\Delta\omega_0\tau}{2\pi} \simeq 43$. The field values for X and Y gates in the two qubits are reported in Table 3.1. The Co switch requires a field $2B_1 = 33.6\,\text{G}$ along the y-axis for the execution of the C-ϕ gate.

	$2B_{1_X}$ [G]	$2B_{1_Y}$ [G]
{Cr_7Ni-O_2C-terpy} (1)	80.26	80.26
{Cr_7Ni-O_2C-py} (3)	82.10	80.26

Table 3.1: Pulses required for X and Y gates with oscillating field.

The architecture could totally satisfy the DiVincenzo criteria in future:

1. "*A scalable physical system with well characterized qubits*". Qubits are defined on spins of molecular nanomagnets and researchers are studying the scalability in terms of parallelism and decoherence timescales.

2. "*The ability to initialize of the state of the qubits to a simple fiducial state, such as* $|00\cdots0\rangle$". For molecular spin clusters, initialization in the ground state $|00\rangle$ or $|000\rangle$ can be achieved by rapidly cooling the sample from high down to low temperatures ($\sim 0.04\,\text{K}$) in a magnetostatic field [27].

3. "*Long relevant decoherence times, much longer than the gate operation time*". This topic is analyzed in Sections 4.2 and 4.3. It is anticipated that single gates

involving one or two qubits can be executed on time intervals significantly lower than T_2.

4. "*A "universal" set of quantum gates*". Single rotations and CNOT - implementable on the considered supramolecular complex - form a universal set of gates.

5. "*A qubit-specific measurement capability*". The measurement of magnetic qubits can be done by Superconducting Quantum Interference Devices (SQUID), which are flux-to-voltage superconducting transducers. SQUID consists of two parallel Josephson junctions and it may be configured as a magnetometer to detect magnetic fields in the order of magnitude of 1×10^{-14} T. If a constant biasing current is maintained in the SQUID device (Figure 3.2), the measured voltage oscillates with the phase changes at the two junctions, depending upon the change in the magnetic flux. Counting the voltage oscillations allows the evaluation of the flux change which has occurred. The magnetic response of a sample - in terms of flux variations - to an AC magnetic field can be measured and a single spin qubit could be coupled to an individual microSQUID. Since SQUIDs are superconducting devices based on Josephson junctions, they can only be used below their critical temperature, that can be of the same order of magnitude of those employed for the Cr_7Ni supramolecular complexes. An overview of the molecular spin measurement with these devices is available in [22].

The front-end and back-end instrumentation for initialization, manipulation and measuring is not object of this thesis; the attention is focused only on the quantum execution unit, in particular on the simulation of a single or a sequence of gates/instructions on molecules, providing the complex coefficients of the state vector after the excitation as outputs.
An example of a possible Assembler code is reported: if the instruction set contains a high-level CNOT instruction with target `Q2`, that can presumably written in a pseudo-Assembler language as

```
CNOT Q2 Q1
```

it must be translated into a sequence of microinstructions

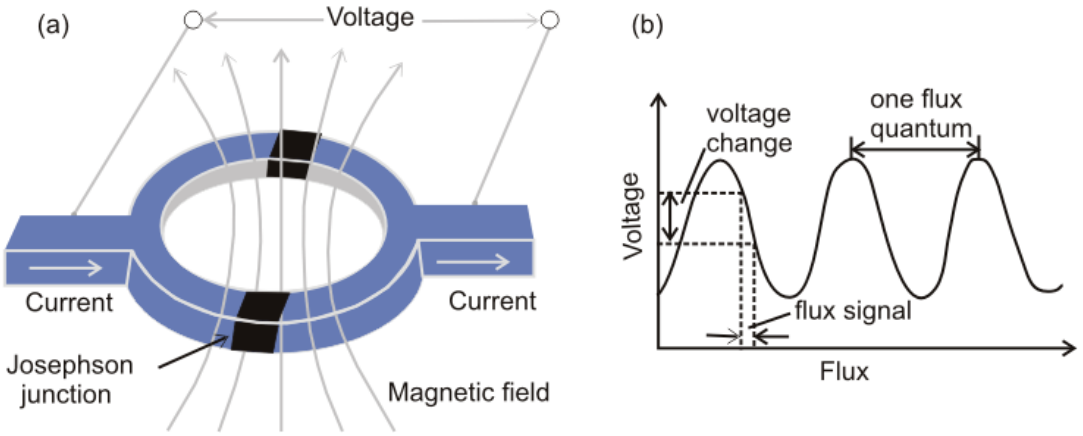

Figure 3.2: SQUID device. One period of voltage variation corresponds to an increase of one flux quantum. From http://www.geocities.ws/pranab_muduli/squid.html.

```
Y Q2 -PI/2 0
X Q2 PI 0
CZ Q2 Q1
Y Q2 -PI/2 0
X Q2 PI 0
```

where the terms refer to the name of the instruction, the target, the rotation amount $\omega_1\tau$ and the phase ϕ respectively. The instruction `CZ Q2 Q1` can be written in terms of spin rotations as

```
X SW1 PI PI
X SW1 PI 0
```

with the switch `SW1` as target. The Quantum Assembler is not described in this thesis work: the goal is to define a set of quantum operations and algorithms - strarting from the single-qubit gates and the C-ϕ - to be implemented on the supramolecular complex and to be simulated on MATLAB, with magnetic resonance quantities[1] and qubit value as inputs of MATLAB functions.

```
function [ final_state] = rotation( qubit,f_0,f_d,f,t,phi)

delta_f = f_0 - f;
V=2*pi*f_d;
theta = V*t/2;

if (delta_f == 0) && (phi==0) % resonance (X)
    U=cos(theta)*eye(2) - i*sin(theta)*[0 1;1 0];
elseif (delta_f == 0) && (phi==pi/2) % resonance (Y)
    U=[cos(theta),-sin(theta);sin(theta),cos(theta)];
elseif (delta_f == 0) && (phi==-pi/2)
    U=[cos(theta),sin(theta);-sin(theta),cos(theta)];
else % general case
    Omega = 2*pi*sqrt(f_d^2 + delta_f^2);
    alpha=Omega*t/2;
    U=[(cos(alpha) - i*(2*pi*delta_f/Omega)*sin(Omega*t/2)) ,
          (-i*V/Omega*sin(alpha))*exp(-i*phi);
     (-i*V/Omega*sin(alpha))*exp(i*phi) , (cos(alpha) +
           i*(2*pi*delta_f/Omega)*sin(alpha))];
end

final_state = U*qubit;
```

[1]The ordinary frequencies $f = \frac{\omega}{2\pi}$ are employed as input parameters, instead of the angular ones.

The function describing one of the two transitions for the C-ϕ gate implementation - exploiting Equation 2.48 - is the following

```
function [ state_n ] = transition( state,transitions,f,f1,phase,tau )

delta_f = transitions-f*ones(4,1); % difference between each transition frequency
      (00,...,11) and carrier frequency, required for the computation of
      transition probabilities
angle=zeros(4,1);
U_phase = eye(4);
for k=1:length(delta_f)
    tmp = sqrt((delta_f(k))^2 + f1^2);
    angle(k) = phase*( (f1/tmp)^2 *(sin(tau*2*pi*tmp/2))^2); % external phase
          multiplied by each transition probability (2-levels equation)
    U_phase(k,k) = exp(i*angle(k));
end
state_n = U_phase*state; % output state

end
```

For each gate, the complex output coefficients c_{ij} computed by MATLAB functions and the probability difference $\Delta|c_{ij}|^2$ - between the output computed by the functions and those computed by the ideal unitary matrices - will be reported for each vector state of the basis. It must be observed that the results are always affected by uncertainty of MATLAB computation. Since the implemented model is based on many approximations - as the evolution operator of the C-ϕ gate - that have not been established to provide a negligible error, it has been chosen to not truncate *a priori* the majority of digits (*e.g.* all digits of weight $< 10^{-4}$), but to report values up to **the most significant digit of the minimum number, regardless if it is a real or imaginary part**.

3.1 Fundamental gates and microinstructions

The identity gate is simply implemented by not applying any pulse on the qubit; the "echo" identity gate (XX) is avoided, in order to analyze the worst-case scenario. Moreover, it is supposed that on the timescales of interest the decoherence errors are kept under thresholds that do not change significantly the results in the two implementations.

The elementary rotations $R_x(\theta)$, $R_y(\theta)$ and $R_z(\theta)$ (in the following description they will be referred in terms of Pauli matrices X, Y and Z) are implemented through

the unitary evolution operator in Equation 2.25, while the C-ϕ is obtained from Equation 2.49. The combinations of these elementary functions define other fundamental quantum gates, that must be exploited for the implementation of complex algorithms. Since the output coefficients do not change with different transition frequencies, the results are reported for one qubit. It is recalled that the $-\mathrm{i}Z$ gate is obtained by a cascade of $-\mathrm{i}Y$ and $-\mathrm{i}X$ gates.

$$(-\mathrm{i}X)\cdot(-\mathrm{i}Y) = -X\cdot Y = -\mathrm{i}Z.$$

Table 3.2: $-\mathrm{i}X$ gate output coefficients.

$|\psi\rangle = \begin{bmatrix}1\\0\end{bmatrix}$

	$c_{i_{\mathrm{mol}}}$	$\Delta\lvert c_i\rvert^2$ $[\cdot 10^{-32}]$
$\lvert 0\rangle$	0	-0.4
$\lvert 1\rangle$	-1 i	0

$|\psi\rangle = \begin{bmatrix}0\\1\end{bmatrix}$

	$c_{i_{\mathrm{mol}}}$	$\Delta\lvert c_i\rvert^2$ $[\cdot 10^{-32}]$
$\lvert 0\rangle$	-1 i	0
$\lvert 1\rangle$	0	-0.4

Table 3.3: $-\mathrm{i}Y$ gate output coefficients.

$|\psi\rangle = \begin{bmatrix}1\\0\end{bmatrix}$

	$c_{i_{\mathrm{mol}}}$	$\Delta\lvert c_i\rvert^2$ $[\cdot 10^{-32}]$
$\lvert 0\rangle$	0	-0.4
$\lvert 1\rangle$	-1 i	0

$|\psi\rangle = \begin{bmatrix}0\\1\end{bmatrix}$

	$c_{i_{\mathrm{mol}}}$	$\Delta\lvert c_i\rvert^2$ $[\cdot 10^{-32}]$
$\lvert 0\rangle$	-1 i	0
$\lvert 1\rangle$	0	-0.4

Table 3.4: $-\mathrm{i}Z$ gate output coefficients.

$|\psi\rangle = \begin{bmatrix}1\\0\end{bmatrix}$

	$c_{i_{\mathrm{mol}}}$	$\Delta\lvert c_i\rvert^2$ $[\cdot 10^{-32}]$
$\lvert 0\rangle$	-1 i	-0.7
$\lvert 1\rangle$	0	0

$|\psi\rangle = \begin{bmatrix}0\\1\end{bmatrix}$

	$c_{i_{\mathrm{mol}}}$	$\Delta\lvert c_i\rvert^2$ $[\cdot 10^{-32}]$
$\lvert 0\rangle$	0	0
$\lvert 1\rangle$	1 i	-0.7

The Hadamard gate is obtained by the cascade of $Y^{-1/2}$ and X gates. The resultant gate is shifted by $\mathrm{e}^{-\mathrm{i}\frac{\pi}{2}}$, so it is properly a $-\mathrm{i}H$. The responses of the gate to the state vectors belonging to the basis are in Table 3.5. The combination of

Table 3.5: Hadamard gate output coefficients.

$|\psi\rangle = \begin{bmatrix}1\\0\end{bmatrix}$

	$c_{i_{\mathrm{mol}}}$	$\Delta\lvert c_i\rvert^2$ $[\cdot 10^{-15}]$
$\lvert 0\rangle$	-0.7071 i	0
$\lvert 1\rangle$	-0.7071 i	-0.2

$|\psi\rangle = \begin{bmatrix}0\\1\end{bmatrix}$

	$c_{i_{\mathrm{mol}}}$	$\Delta\lvert c_i\rvert^2$ $[\cdot 10^{-15}]$
$\lvert 0\rangle$	-0.7071 i	-0.2
$\lvert 1\rangle$	+0.7071 i	0

Hadamard and C-Z gates makes a CNOT gate. It can be easily proved that the

implemented gate is properly a $-$CNOT through the matrix product of the unitary matrices of the constituting gates

$$-\mathrm{i}H_2 \cdot \text{C-}Z \cdot -\mathrm{i}H_2 = -H_2 \cdot \text{C-}Z \cdot H_2 = -\text{CNOT}.$$

The response of the CNOT gate to the vectors belonging to the basis are reported in the following tables.

Table 3.6: CNOT outputs coefficents for the two-qubits vector basis.

$|\psi\rangle = \begin{bmatrix}1\\0\\0\\0\end{bmatrix}$

	$c_{ij_{\text{mol}}}$	$\Delta\lvert c_{ij}\rvert^2$ $[\cdot 10^{-10}]$
$\lvert 00\rangle$	-0.9999999960 - 0.0000892659 i	0.3
$\lvert 01\rangle$	0.0000000005 - 0.0000051047 i	-0.3
$\lvert 10\rangle$	0	0
$\lvert 11\rangle$	0	0

$|\psi\rangle = \begin{bmatrix}0\\1\\0\\0\end{bmatrix}$

	$c_{ij_{\text{mol}}}$	$\Delta\lvert c_{ij}\rvert^2$ $[\cdot 10^{-8}]$
$\lvert 00\rangle$	0.0000000005 - 0.0000051047 i	-0.3
$\lvert 01\rangle$	-0.9999999960 - 0.0000892659 i	0.3
$\lvert 10\rangle$	0	0
$\lvert 11\rangle$	0	0

$|\psi\rangle = \begin{bmatrix}0\\0\\1\\0\end{bmatrix}$

	$c_{ij_{\text{mol}}}$	$\Delta\lvert c_{ij}\rvert^2$ $[\cdot 10^{-11}]$
$\lvert 00\rangle$	0	0
$\lvert 01\rangle$	0	0
$\lvert 10\rangle$	0.000000002 - 0.000048834 i	-0.2
$\lvert 11\rangle$	-0.999999998 - 0.000048834 i	0.2

$|\psi\rangle = \begin{bmatrix}0\\0\\0\\1\end{bmatrix}$

	$c_{ij_{\text{mol}}}$	$\Delta\lvert c_{ij}\rvert^2$ $[\cdot 10^{-8}]$
$\lvert 00\rangle$	0	0
$\lvert 01\rangle$	0	0
$\lvert 10\rangle$	-0.999999998 - 0.000048834 i	0.2
$\lvert 11\rangle$	0.000000002 - 0.000042081 i	-0.2

3.2 Gates/instructions derived from C-ϕ and CNOT

From single rotation gates ($-\mathrm{i}X$, $-\mathrm{i}Y$ and $-\mathrm{i}Z$) and two-qubits gates such as C-Z, CNOT, C-$Z^{1/2}$ and C-$Z^{1/4}$, it has been possible to create a library of elementary gates to be simulated on the Cr_7Ni-Co-Cr_7Ni complex. The definition of a library of quantum gates has also permitted the **simulation** on two and three qubits molecules

of Grover's search algorithm and Quantum Fourier Transform (QFT), with qubits supposed to be ideal in terms of decoherence and residual interaction.
For the definition of new gates, it must be precised that C-Z gates with swapped control and target qubits have the same unitary matrix of the standard ones. The

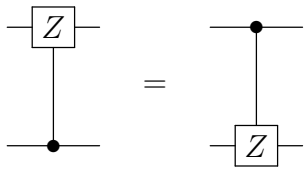

Figure 3.3: Equivalence of C-Z gates.

CNOT-21 gate, that presents swapped control and target qubits with the respect to the standard CNOT gate, can be implemented by the following quantum circuit.

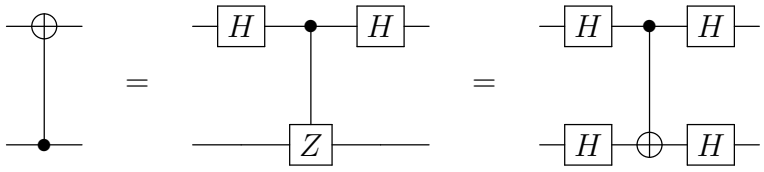

Figure 3.4: CNOT-21 gate. A pair of Hadamard gates is put before and after each qubit involved by the gate.

The SWAP gate is obtained as a cascade of three CNOT gates, according to the quantum circuit in Figure 3.5.

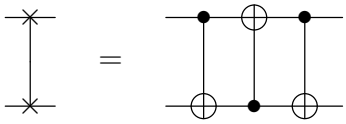

Figure 3.5: SWAP gate made of three CNOT gates.

The CNOT-13 gate, that has the control and target on the first and the third qubits respectively of the considered circuit, can be written as a sequence of CNOT-12 and CNOT-23 (Figure 3.6).

It is possible to generalize the definition of controlled quantum gates between non-adjecent qubits by exploiting SWAP gates. The values obtained for the C-$Z^{1/4}$ with third qubit as target controlled by the first one are reported.

Table 3.7: CNOT-21 outputs coefficents for the two-qubits vector basis.

$|\psi\rangle = \begin{bmatrix}1\\0\\0\\0\end{bmatrix}$

	$c_{ij_{\text{mol}}}$	$\Delta\lvert c_{ij}\rvert^2$ $[\cdot 10^{-11}]$
$\lvert 00\rangle$	-0.9999999954 - 0.0000960190 i	-0.3
$\lvert 01\rangle$	0	0
$\lvert 10\rangle$	-0.0000000002 + 0.0000016484 i	-0.3
$\lvert 11\rangle$	0	-0.03

$|\psi\rangle = \begin{bmatrix}0\\1\\0\\0\end{bmatrix}$

	$c_{ij_{\text{mol}}}$	$\Delta\lvert c_{ij}\rvert^2$ $[\cdot 10^{-8}]$
$\lvert 00\rangle$	0	0
$\lvert 01\rangle$	0.000000002 - 0.000042081 i	-0.2
$\lvert 10\rangle$	0	0
$\lvert 11\rangle$	-0.999999998 - 0.000042081 i	-0.2

$|\psi\rangle = \begin{bmatrix}0\\0\\1\\0\end{bmatrix}$

	$c_{ij_{\text{mol}}}$	$\Delta\lvert c_{ij}\rvert^2$ $[\cdot 10^{-11}]$
$\lvert 00\rangle$	-0.0000000002 + 0.0000016484 i	-0.3
$\lvert 01\rangle$	0	0
$\lvert 10\rangle$	-0.9999999954 - 0.0000960190 i	-0.3
$\lvert 11\rangle$	0	0

$|\psi\rangle = \begin{bmatrix}0\\0\\0\\1\end{bmatrix}$

	$c_{ij_{\text{mol}}}$	$\Delta\lvert c_{ij}\rvert^2$ $[\cdot 10^{-8}]$
$\lvert 00\rangle$	0	0
$\lvert 01\rangle$	-0.9999999982 - 0.000042080 i	0.2
$\lvert 10\rangle$	0	0
$\lvert 11\rangle$	0.000000002 - 0.000042081 i	-0.2

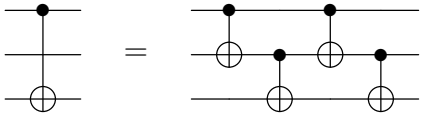

Figure 3.6: CNOT-13 gate

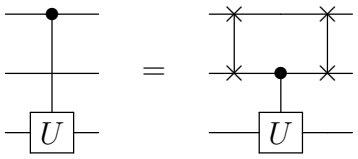

Figure 3.7: Generalized C-U gate.

Table 3.8: SWAP outputs coefficents for the two-qubits vector basis.

$|\psi\rangle = \begin{bmatrix}1\\0\\0\\0\end{bmatrix}$

	$c_{ij_{\text{mol}}}$	$\Delta\lvert c_{ij}\rvert^2$ $[\cdot 10^{-10}]$
$\lvert 00\rangle$	-0.9999999623 - 0.0002745507 i	0.55
$\lvert 01\rangle$	0.0000000016 - 0.0000051047 i	0.26
$\lvert 10\rangle$	0.0000000008 - 0.0000051047 i	0.26
$\lvert 11\rangle$	0.0000000001 + 0.0000016484 i	-0.03

$|\psi\rangle = \begin{bmatrix}0\\1\\0\\0\end{bmatrix}$

	$c_{ij_{\text{mol}}}$	$\Delta\lvert c_{ij}\rvert^2$ $[\cdot 10^{-10}]$
$\lvert 00\rangle$	0.0000000016 - 0.0000051047 i	-0.3
$\lvert 01\rangle$	-0.0000000093 - 0.000042081 i	-17.7
$\lvert 10\rangle$	-0.9999999816 - 0.000180180 i	41.8
$\lvert 11\rangle$	0.0000000088 - 0.000048834 i	-23.8

$|\psi\rangle = \begin{bmatrix}0\\0\\1\\0\end{bmatrix}$

	$c_{ij_{\text{mol}}}$	$\Delta\lvert c_{ij}\rvert^2$ $[\cdot 10^{-10}]$
$\lvert 00\rangle$	0.0000000008 - 0.0000051047 i	-0.3
$\lvert 01\rangle$	-0.9999999817 - 0.0001801801 i	41.8
$\lvert 10\rangle$	0.0000000083 - 0.0000420806 i	-17.7
$\lvert 11\rangle$	0.0000000115 - 0.0000488337 i	-23.8

$|\psi\rangle = \begin{bmatrix}0\\0\\0\\1\end{bmatrix}$

	$c_{ij_{\text{mol}}}$	$\Delta\lvert c_{ij}\rvert^2$ $[\cdot 10^{-10}]$
$\lvert 00\rangle$	-0.0000000001 + 0.0000016484 i	-0.03
$\lvert 01\rangle$	0.0000000088 - 0.0000488337 i	-23.85
$\lvert 10\rangle$	0.0000000115 - 0.0000488337 i	-23.85
$\lvert 11\rangle$	-0.9999999789 - 0.0001936863 i	47.72

Table 3.9: CNOT-13 outputs coefficents for the three-qubits vector basis.

$|\psi\rangle = \begin{bmatrix}1\\0\\0\\0\\0\\0\\0\\0\end{bmatrix}$

	$c_{ij_{\text{mol}}}$	$\Delta\lvert c_{ij}\rvert^2$ $[\cdot 10^{-15}]$
$\lvert 000\rangle$	1.00000000000 + 0.0000000197 i	0.4441
$\lvert 001\rangle$	-0.0000000009 i	-0.0008
$\lvert 010\rangle$	-0.0000000089 i	-0.0781
$\lvert 011\rangle$	-0.0000000089 i	-0.0781
$\lvert 100\rangle$	0	0
$\lvert 101\rangle$	0	0
$\lvert 110\rangle$	0	0
$\lvert 111\rangle$	0	0

$|\psi\rangle = \begin{bmatrix}0\\1\\0\\0\\0\\0\\0\\0\end{bmatrix}$

	$c_{ij_{\text{mol}}}$	$\Delta\lvert c_{ij}\rvert^2$ $[\cdot 10^{-15}]$
$\lvert 000\rangle$	-0.0000000009 i	-0.0008
$\lvert 001\rangle$	1.00000000000 + 0.0000000197 i	0.4441
$\lvert 010\rangle$	-0.0000000089 i	-0.0781
$\lvert 011\rangle$	-0.0000000089 i	-0.0781
$\lvert 100\rangle$	0	0
$\lvert 101\rangle$	0	0
$\lvert 110\rangle$	0	0
$\lvert 111\rangle$	0	0

$|\psi\rangle = \begin{bmatrix}0\\0\\1\\0\\0\\0\\0\\0\end{bmatrix}$

	$c_{ij_{\text{mol}}}$	$\Delta\lvert c_{ij}\rvert^2$ $[\cdot 10^{-15}]$
$\lvert 000\rangle$	-0.0000000089 i	-0.08
$\lvert 001\rangle$	-0.0000000089 i	-0.08
$\lvert 010\rangle$	0.99999999999 + 0.0000000036 i	0.44
$\lvert 011\rangle$	-0.0000000018 i	-0.32
$\lvert 100\rangle$	0	0
$\lvert 101\rangle$	0	0
$\lvert 110\rangle$	0	0
$\lvert 111\rangle$	0	0

$|\psi\rangle = \begin{bmatrix}0\\0\\0\\1\\0\\0\\0\\0\end{bmatrix}$

	$c_{ij_{\text{mol}}}$	$\Delta\lvert c_{ij}\rvert^2$ $[\cdot 10^{-15}]$
$\lvert 000\rangle$	-0.0000000089 i	-0.08
$\lvert 001\rangle$	-0.0000000089 i	-0.08
$\lvert 010\rangle$	-0.0000000018 i	-0.32
$\lvert 011\rangle$	0.99999999999 + 0.0000000036 i	0.44
$\lvert 100\rangle$	0	0
$\lvert 101\rangle$	0	0
$\lvert 110\rangle$	0	0
$\lvert 111\rangle$	0	0

$|\psi\rangle =$

	$c_{ij_{\mathrm{mol}}}$	$\Delta\lvert c_{ij}\rvert^2$ $[\cdot 10^{-15}]$
$\lvert 000\rangle$	0	0
$\lvert 001\rangle$	0	0
$\lvert 010\rangle$	0	0
$\lvert 011\rangle$	0	0
$\lvert 100\rangle$	0.0000000085 i	-0.0723
$\lvert 101\rangle$	1.0000000000 + 0.0000000107 i	0.4441
$\lvert 110\rangle$	0.0000000005 i	-0.0003
$\lvert 111\rangle$	0.0000000005 i	-0.0003

$|\psi\rangle =$

	$c_{ij_{\mathrm{mol}}}$	$\Delta\lvert c_{ij}\rvert^2$ $[\cdot 10^{-15}]$
$\lvert 000\rangle$	0	0
$\lvert 001\rangle$	0	0
$\lvert 010\rangle$	0	0
$\lvert 011\rangle$	0	0
$\lvert 100\rangle$	1.0000000000 + 0.0000000107 i	0.4441
$\lvert 101\rangle$	0.0000000085 i	-0.0723
$\lvert 110\rangle$	0.0000000005 i	-0.0003
$\lvert 111\rangle$	0.0000000005 i	-0.0003

$|\psi\rangle =$

	$c_{ij_{\mathrm{mol}}}$	$\Delta\lvert c_{ij}\rvert^2$ $[\cdot 10^{-15}]$
$\lvert 000\rangle$	0	0
$\lvert 001\rangle$	0	0
$\lvert 010\rangle$	0	0
$\lvert 011\rangle$	0	0
$\lvert 100\rangle$	0.0000000006 i	-0.0003
$\lvert 101\rangle$	0.0000000006 i	-0.0003
$\lvert 110\rangle$	0.0000000085 i	-0.0723
$\lvert 111\rangle$	1.0000000000 + 0.0000000107 i	0.2220

$|\psi\rangle =$

	$c_{ij_{\mathrm{mol}}}$	$\Delta\lvert c_{ij}\rvert^2$ $[\cdot 10^{-15}]$
$\lvert 000\rangle$	0	0
$\lvert 001\rangle$	0	0
$\lvert 010\rangle$	0	0
$\lvert 011\rangle$	0	0
$\lvert 100\rangle$	0.0000000006 i	-0.0003
$\lvert 101\rangle$	0.0000000006 i	-0.0003
$\lvert 110\rangle$	1.0000000000 + 0.0000000107 i	0.2220
$\lvert 111\rangle$	0.0000000085 i	-0.0723

Table 3.10: C-$Z^{1/4}$ outputs coefficents for the three-qubits vector basis.

$$|\psi\rangle = \begin{bmatrix}1\\0\\0\\0\\0\\0\\0\\0\end{bmatrix}$$

	$c_{ij_{\text{mol}}}$	$\Delta\lvert c_{ij}\rvert^2$ $[\cdot 10^{-15}]$
$\lvert 000\rangle$	0.9999999999 + 0.0000000376 i	0.88818
$\lvert 001\rangle$	0	0
$\lvert 010\rangle$	0	0
$\lvert 011\rangle$	-0.0000000177 i	-0.31255
$\lvert 100\rangle$	-0.0000000177 i	-0.31255
$\lvert 101\rangle$	0	0
$\lvert 110\rangle$	-0.0000000009 i	-0.00081
$\lvert 111\rangle$	0	0

$$|\psi\rangle = \begin{bmatrix}0\\1\\0\\0\\0\\0\\0\\0\end{bmatrix}$$

	$c_{ij_{\text{mol}}}$	$\Delta\lvert c_{ij}\rvert^2$ $[\cdot 10^{-15}]$
$\lvert 000\rangle$	0	0
$\lvert 001\rangle$	0.99999999999 + 0.0000000036 i	0.8882
$\lvert 010\rangle$	0	0
$\lvert 011\rangle$	-0.0000000018 i	-0.3126
$\lvert 100\rangle$	0	0
$\lvert 101\rangle$	0.0000000063 - 0.0000000151 i	-0.2668
$\lvert 110\rangle$	0	0
$\lvert 111\rangle$	0.0000000003 - 0.0000000008 i	-0.0007

$$|\psi\rangle = \begin{bmatrix}0\\0\\1\\0\\0\\0\\0\\0\end{bmatrix}$$

	$c_{ij_{\text{mol}}}$	$\Delta\lvert c_{ij}\rvert^2$ $[\cdot 10^{-15}]$
$\lvert 000\rangle$	-0.000000018 i	0.313
$\lvert 001\rangle$	0	0
$\lvert 010\rangle$	0.999999999 + 0.000000037 i	-0.888
$\lvert 011\rangle$	0	0
$\lvert 100\rangle$	0.000000018 i	-0.320
$\lvert 101\rangle$	0	0
$\lvert 110\rangle$	0.000000001 i	-0.001
$\lvert 111\rangle$	0	0

$$|\psi\rangle = \begin{bmatrix}0\\0\\0\\1\\0\\0\\0\\0\end{bmatrix}$$

	$c_{ij_{\text{mol}}}$	$\Delta\lvert c_{ij}\rvert^2$ $[\cdot 10^{-15}]$
$\lvert 000\rangle$	0	0
$\lvert 001\rangle$	-0.0000000177 i	-0.313
$\lvert 010\rangle$	0	0
$\lvert 011\rangle$	0.9999999999 + 0.0000000374 i	0
$\lvert 100\rangle$	0	0
$\lvert 101\rangle$	-0.0000000063 + 0.0000000153 i	-0.273
$\lvert 110\rangle$	0	0
$\lvert 111\rangle$	-0.0000000004 + 0.0000000010 i	-0.001

$$|\psi\rangle = \begin{bmatrix} 0 \\ 0 \\ 0 \\ 0 \\ 1 \\ 0 \\ 0 \\ 0 \end{bmatrix}$$

	$c_{ij_{\mathrm{mol}}}$	$\Delta\lvert c_{ij}\rvert^2$ $[\cdot 10^{-15}]$
$\lvert 000\rangle$	-0.000000018 i	-0.313
$\lvert 001\rangle$	0	0
$\lvert 010\rangle$	0.000000018 i	-0.320
$\lvert 011\rangle$	0	0
$\lvert 100\rangle$	0.9999999999 + 0.000000042 i	0.444
$\lvert 101\rangle$	0	0
$\lvert 110\rangle$	0.000000001 i	-0.001
$\lvert 111\rangle$	0	0

$$|\psi\rangle = \begin{bmatrix} 0 \\ 0 \\ 0 \\ 0 \\ 0 \\ 1 \\ 0 \\ 0 \end{bmatrix}$$

	$c_{ij_{\mathrm{mol}}}$	$\Delta\lvert c_{ij}\rvert^2$ $[\cdot 10^{-15}]$
$\lvert 000\rangle$	0	0
$\lvert 001\rangle$	0.0000000063 - 0.0000000151 i	0.8882
$\lvert 010\rangle$	0	0
$\lvert 011\rangle$	-0.0000000063 + 0.0000000153 i	-0.3126
$\lvert 100\rangle$	0	0
$\lvert 101\rangle$	0.7071067549 + 0.7071068074 i	-0.2668
$\lvert 110\rangle$	0	0
$\lvert 111\rangle$	-0.0000000008 + 0.0000000008 i	-0.0007

$$|\psi\rangle = \begin{bmatrix} 0 \\ 0 \\ 0 \\ 0 \\ 0 \\ 0 \\ 1 \\ 0 \end{bmatrix}$$

	$c_{ij_{\mathrm{mol}}}$	$\Delta\lvert c_{ij}\rvert^2$ $[\cdot 10^{-15}]$
$\lvert 000\rangle$	-0.0000000009 i	-0.0008
$\lvert 001\rangle$	0	0
$\lvert 010\rangle$	0.0000000011 i	-0.0013
$\lvert 011\rangle$	0	0
$\lvert 100\rangle$	0.0000000011 i	-0.0013
$\lvert 101\rangle$	0	0
$\lvert 110\rangle$	1.0000000000 + 0.000000008 i	0.4441
$\lvert 111\rangle$	0	0

$$|\psi\rangle = \begin{bmatrix} 0 \\ 0 \\ 0 \\ 0 \\ 0 \\ 0 \\ 0 \\ 1 \end{bmatrix}$$

	$c_{ij_{\mathrm{mol}}}$	$\Delta\lvert c_{ij}\rvert^2$ $[\cdot 10^{-15}]$
$\lvert 000\rangle$	0	0
$\lvert 001\rangle$	0.0000000003 - 0.0000000008 i	-0.0007
$\lvert 010\rangle$	0	0
$\lvert 011\rangle$	-0.0000000004 + 0.0000000010 i	-0.0011
$\lvert 100\rangle$	0	0
$\lvert 101\rangle$	-0.0000000008 + 0.0000000008 i	-0.0013
$\lvert 110\rangle$	0	0
$\lvert 111\rangle$	0.7071067787 + 0.7071067837 i	0.2220

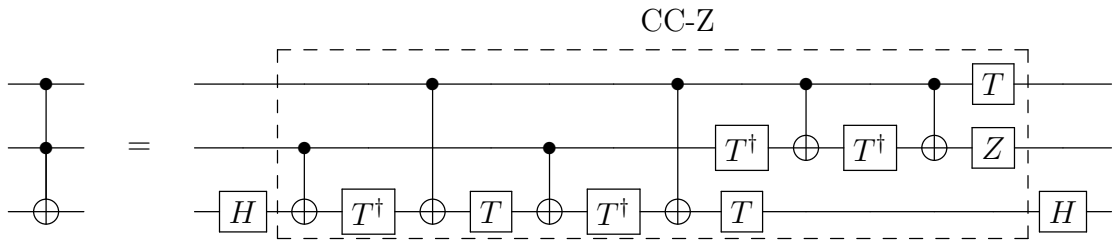

Figure 3.8: Toffoli gate obtained from CNOT gates.

The previous gates permit to create a quantum circuit that behaves as a Toffoli gate (Figure 3.8) where

$$T = \begin{bmatrix} 1 & 0 \\ 0 & \mathrm{e}^{\mathrm{i}\frac{\pi}{4}} \end{bmatrix} \qquad T^\dagger = \begin{bmatrix} 1 & 0 \\ 0 & \mathrm{e}^{-\mathrm{i}\frac{\pi}{4}} \end{bmatrix} \tag{3.2}$$

and the dashed box refers to the circuit implementing the Controlled-Controlled-Z gate

$$\text{CC-}Z = \begin{bmatrix} 1 & 0 & 0 & 0 & 0 & 0 & 0 & 0 \\ 0 & 1 & 0 & 0 & 0 & 0 & 0 & 0 \\ 0 & 0 & 1 & 0 & 0 & 0 & 0 & 0 \\ 0 & 0 & 0 & 1 & 0 & 0 & 0 & 0 \\ 0 & 0 & 0 & 0 & 1 & 0 & 0 & 0 \\ 0 & 0 & 0 & 0 & 0 & 1 & 0 & 0 \\ 0 & 0 & 0 & 0 & 0 & 0 & 1 & 0 \\ 0 & 0 & 0 & 0 & 0 & 0 & 0 & -1 \end{bmatrix}. \tag{3.3}$$

The implemented Toffoli gate presents an additional scalar term $\mathrm{e}^{-\mathrm{i}\frac{\pi}{8}}$.

Table 3.11: Toffoli gate outputs coefficents for the three-qubits vector basis.

$$|\psi\rangle = \begin{bmatrix}1\\0\\0\\0\\0\\0\\0\\0\end{bmatrix}$$

	$c_{ij_{\text{mol}}}$	$\Delta\lvert c_{ij}\rvert^2$ $[\cdot 10^{-14}]$
$\lvert 000\rangle$	0.9238795540 - 0.3826833804 i	0.1998
$\lvert 001\rangle$	-0.0000000012 + 0.0000000005 i	-0.0002
$\lvert 010\rangle$	- 0.0000000394 i	-0.1555
$\lvert 011\rangle$	0	0
$\lvert 100\rangle$	0	0
$\lvert 101\rangle$	0	0
$\lvert 110\rangle$	0	0
$\lvert 111\rangle$	0	0

$$|\psi\rangle = \begin{bmatrix}0\\1\\0\\0\\0\\0\\0\\0\end{bmatrix}$$

	$c_{ij_{\text{mol}}}$	$\Delta\lvert c_{ij}\rvert^2$ $[\cdot 10^{-14}]$
$\lvert 000\rangle$	0.0000000012 - 0.0000000005 i	-0.0002
$\lvert 001\rangle$	0.9238795557 - 0.3826833764 i	0.1776
$\lvert 010\rangle$	0.0000000115 - 0.0000000048 i	-0.0156
$\lvert 011\rangle$	0.0000000115 - 0.0000000115 i	-0.0267
$\lvert 100\rangle$	0	0
$\lvert 101\rangle$	0	0
$\lvert 110\rangle$	0	0
$\lvert 111\rangle$	0	0

$$|\psi\rangle = \begin{bmatrix}0\\0\\1\\0\\0\\0\\0\\0\end{bmatrix}$$

	$c_{ij_{\text{mol}}}$	$\Delta\lvert c_{ij}\rvert^2$ $[\cdot 10^{-14}]$
$\lvert 000\rangle$	-0.000000028 - 0.000000028 i	-0.155
$\lvert 001\rangle$	-0.000000012 + 0.000000005 i	-0.016
$\lvert 010\rangle$	0.923879590 - 0.382683293 i	0.200
$\lvert 011\rangle$	0	0
$\lvert 100\rangle$	0	0
$\lvert 101\rangle$	0	0
$\lvert 110\rangle$	0	0
$\lvert 111\rangle$	0	0

$$|\psi\rangle = \begin{bmatrix}0\\0\\0\\1\\0\\0\\0\\0\end{bmatrix}$$

	$c_{ij_{\text{mol}}}$	$\Delta\lvert c_{ij}\rvert^2$ $[\cdot 10^{-14}]$
$\lvert 000\rangle$	0	0
$\lvert 001\rangle$	-0.00000002	-0.3
$\lvert 010\rangle$	0	0
$\lvert 011\rangle$	0.92387956 - 0.38268337 i	0.4
$\lvert 100\rangle$	0	0
$\lvert 101\rangle$	0	0
$\lvert 110\rangle$	0	0
$\lvert 111\rangle$	0	0

$$|\psi\rangle = \begin{bmatrix}0\\0\\0\\0\\1\\0\\0\\0\end{bmatrix}$$

	$c_{ij_{\text{mol}}}$	$\Delta\lvert c_{ij}\rvert^2$ $[\cdot 10^{-14}]$
$\lvert 000\rangle$	0	0
$\lvert 001\rangle$	0	0
$\lvert 010\rangle$	0	0
$\lvert 011\rangle$	0	0
$\lvert 100\rangle$	0.9238795461 - 0.3826833996 i	0.1554
$\lvert 101\rangle$	0.0000000107 - 0.0000000044 i	-0.0134
$\lvert 110\rangle$	-0.0000000023 + 0.0000000005 i	-0.0005
$\lvert 111\rangle$	0.0000000005 + 0.0000000012 i	-0.0002

$$|\psi\rangle = \begin{bmatrix}0\\0\\0\\0\\0\\1\\0\\0\end{bmatrix}$$

	$c_{ij_{\text{mol}}}$	$\Delta\lvert c_{ij}\rvert^2$ $[\cdot 10^{-14}]$
$\lvert 000\rangle$	0	0
$\lvert 001\rangle$	0	0
$\lvert 010\rangle$	0	0
$\lvert 011\rangle$	0	0
$\lvert 100\rangle$	-0.0000000107 + 0.0000000044 i	-0.01339
$\lvert 101\rangle$	0.9238795372 - 0.3826834209 i	0.17764
$\lvert 110\rangle$	-0.0000000002 - 0.0000000005 i	-0.00003
$\lvert 111\rangle$	-0.0000000016 + 0.0000000002 i	-0.00025

$$|\psi\rangle = \begin{bmatrix}0\\0\\0\\0\\0\\0\\1\\0\end{bmatrix}$$

	$c_{ij_{\text{mol}}}$	$\Delta\lvert c_{ij}\rvert^2$ $[\cdot 10^{-14}]$
$\lvert 000\rangle$	0	0
$\lvert 001\rangle$	0	0
$\lvert 010\rangle$	0	0
$\lvert 011\rangle$	0	0
$\lvert 100\rangle$	0.0000000005 + 0.0000000012 i	-0.002
$\lvert 101\rangle$	0.0000000012 - 0.0000000009 i	-0.002
$\lvert 110\rangle$	-0.0000000194 + 0.0000000080 i	-0.440
$\lvert 111\rangle$	0.9238795514 - 0.3826833867 i	0.222

$$|\psi\rangle = \begin{bmatrix}0\\0\\0\\0\\0\\0\\0\\1\end{bmatrix}$$

	$c_{ij_{\text{mol}}}$	$\Delta\lvert c_{ij}\rvert^2$ $[\cdot 10^{-14}]$
$\lvert 000\rangle$	0	0
$\lvert 001\rangle$	0	0
$\lvert 010\rangle$	0	0
$\lvert 011\rangle$	0	0
$\lvert 100\rangle$	0.0000000020 - 0.0000000012 i	-0.00055
$\lvert 101\rangle$	-0.0000000002 - 0.0000000005 i	-0.00003
$\lvert 110\rangle$	0.9238795446 - 0.3826834032 i	0.13323
$\lvert 111\rangle$	0.0000000194 - 0.0000000080 i	-0.04398

Since the CNOT and Toffoli gates are available, it is possible to implement a reversible half-adder through the **Peres gate**, whose circuit is reported in the

following figure.

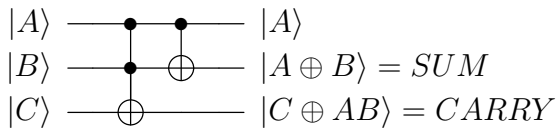

Figure 3.9: Peres Gate, that behaves as a reversible Half Adder for $|C\rangle = |0\rangle$.

The implemented gate is shifted by $\frac{7\pi}{8}$; the half-adder is obtained for $|C\rangle = |0\rangle$. The definition of quantum gates through equivalences is not optimal, since some operations (*e.g.* the Toffoli and CNOT13 gates) require a quite high number of pulses to be provided to the molecule. It is the responsibility of physicists and chemists to make a molecule characterized by an interaction capable to simplify these gates.

Table 3.12: Half adder outputs coefficents for the three-qubits vector basis.

$$|\psi\rangle = \begin{bmatrix}1\\0\\0\\0\\0\\0\\0\\0\end{bmatrix}$$

	$c_{ij_{\text{mol}}}$	$\Delta\lvert c_{ij}\rvert^2$ $[\cdot 10^{-14}]$
$\lvert 000\rangle$	-0.9238795575 + 0.3826833721 i	0.2442
$\lvert 001\rangle$	0.0000000012 - 0.0000000005 i	-0.0002
$\lvert 010\rangle$	0.0000000034+ 0.0000000476 i	-0.2277
$\lvert 011\rangle$	0	0
$\lvert 100\rangle$	0	0
$\lvert 101\rangle$	0	0
$\lvert 110\rangle$	0	0
$\lvert 111\rangle$	0	0

$$|\psi\rangle = \begin{bmatrix}0\\0\\1\\0\\0\\0\\0\\0\end{bmatrix}$$

	$c_{ij_{\text{mol}}}$	$\Delta\lvert c_{ij}\rvert^2$ $[\cdot 10^{-14}]$
$\lvert 000\rangle$	0.000000031 + 0.000000037 i	-0.23
$\lvert 001\rangle$	0.000000012 - 0.000000005 i	-0.02
$\lvert 010\rangle$	-0.923879594 + 0.382683284 i	0.24
$\lvert 011\rangle$	0	0
$\lvert 100\rangle$	0	0
$\lvert 101\rangle$	0	0
$\lvert 110\rangle$	0	0
$\lvert 111\rangle$	0	0

$$|\psi\rangle = \begin{bmatrix}0\\0\\0\\0\\1\\0\\0\\0\end{bmatrix}$$

	$c_{ij_{\text{mol}}}$	$\Delta\lvert c_{ij}\rvert^2$ $[\cdot 10^{-14}]$
$\lvert 000\rangle$	0	0
$\lvert 001\rangle$	0	0
$\lvert 010\rangle$	0	0
$\lvert 011\rangle$	0	0
$\lvert 100\rangle$	0.0000000021 - 0.0000000010 i	-0.0005
$\lvert 101\rangle$	-0.0000000005 - 0.0000000012 i	-0.0002
$\lvert 110\rangle$	-0.9238795463 + 0.3826833990 i	0.1776
$\lvert 111\rangle$	-0.0000000107 + 0.0000000044 i	-0.0134

$$|\psi\rangle = \begin{bmatrix}0\\0\\0\\0\\0\\0\\1\\0\end{bmatrix}$$

	$c_{ij_{\text{mol}}}$	$\Delta\lvert c_{ij}\rvert^2$ $[\cdot 10^{-15}]$
$\lvert 000\rangle$	0	0
$\lvert 001\rangle$	0	0
$\lvert 010\rangle$	0	0
$\lvert 011\rangle$	0	0
$\lvert 100\rangle$	0.0000000194 - 0.0000000080 i	-0.440
$\lvert 101\rangle$	-0.9238795516 + 0.3826833862 i	0.222
$\lvert 110\rangle$	-0.0000000005 - 0.0000000012 i	-0.002
$\lvert 111\rangle$	-0.0000000015 + 0.0000000004 i	-0.002

3.3 Grover's search algorithm

Given an unsorted array of N elements, the computational cost for finding a particular element with a classical computer is $O(N)$. Lov Grover proved that an algorithm capable to solve the same problem with a cost $O(\sqrt{N})$ on a quantum computer. The Grover's algorithm is based on an iteration - repeated $O(\sqrt{N})$ times - consisting of two steps:

- **phase inversion**, that changes the phase of the desired state;
- **inversion about mean**, that boosts the separation of the phases.

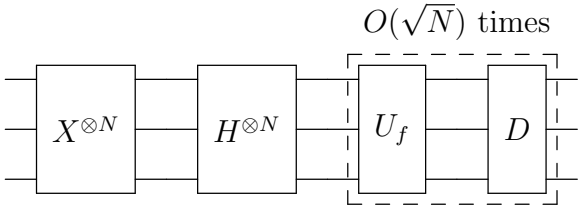

Figure 3.10: Generic Grover's search algorithm involving three qubits.

Phase inversion requires the definition of a **oracle function**, that provides as output with input $|x\rangle$ and target $|x_0\rangle$

$$f(|x\rangle) = \begin{cases} 1 & \text{for } |x\rangle = |x_0\rangle \\ & \\ 0 & \text{otherwise} \end{cases} . \tag{3.4}$$

Oracle is exploited for the definition of two different phase inversion operations

$$\begin{aligned} |x\rangle \otimes |b\rangle &\xrightarrow{f_{\text{flip}}} |x\rangle \otimes |b \otimes f(|x\rangle)\rangle \\ |x\rangle &\xrightarrow{O_f^{\pm}} (-1)^{f(|x\rangle)} |x\rangle = \begin{cases} -|x\rangle & \text{for } |x\rangle = |x_0\rangle \\ & \\ |x\rangle & \text{otherwise} \end{cases} . \end{aligned} \tag{3.5}$$

The f_{flip} operation requires an additional bit to use for the output computation, in the second case it is absent. In the implemented circuit, the $O_f^{\pm}$ is exploited to avoid

the annoyance of the extra bit. From a circuit point of view, the oracle is nothing but a C-Z gate. If it is looking for a target $|x_0\rangle \neq |11\rangle$, it would be sufficient to insert X gates before and after the controlled gate on qubits associated to a 0 in the binary representation of $|x_0\rangle$: in the case of $|01\rangle$ the oracle is

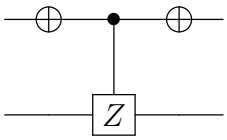

while for $|10\rangle$ it is

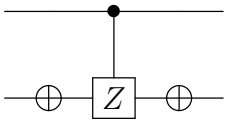

The inversion about mean is the amplification of the probability of obtaining the target as circuit output. It is based on the diffusion operator defined to have the mapping

$$\sum_{x=0}^{N-1} \alpha_x |x\rangle \xrightarrow{D} \sum_{x=0}^{N-1} (2\mu - \alpha_x) |x\rangle , \tag{3.6}$$

where μ is the average of the amplitudes. At the initialization, each value has coefficient $\frac{1}{\sqrt{N}}$, so the condition must be achieved by a sequence of Hadamard gates on each qubit initialized to $|0\rangle$.

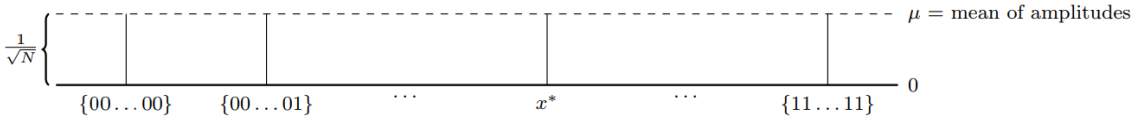

Figure 3.11: Equal superposition of states, with target value x^*. From https://www.cs.cmu.edu/~odonnell/quantum15/lecture04.pdf.

The phase inversion changes the target coefficient into $-\frac{1}{\sqrt{N}}$. The average at the first iteration is

$$\mu = \frac{\sum \alpha_x}{N} = \frac{(N-1)\cdot\frac{1}{\sqrt{N}} - \frac{1}{\sqrt{N}}}{N} = \frac{N-2}{N}\cdot\frac{1}{\sqrt{N}} \sim \frac{1}{\sqrt{N}},$$

for $N \gg 1$, so the coefficients $2\mu - \alpha_x$ are

$$\alpha_x \sim \begin{cases} \frac{3}{\sqrt{N}} & \text{for } |x\rangle = |x_0\rangle \\ \frac{1}{\sqrt{N}} & \text{otherwise} \end{cases}.$$

Applying the Grover diffusion for the second time, the average is

$$\mu = \frac{(N-1) \cdot \frac{1}{\sqrt{N}} - \frac{3}{\sqrt{N}}}{N} = \frac{N-4}{N} \cdot \frac{1}{\sqrt{N}} \sim \frac{1}{\sqrt{N}},$$

for $N \gg 4$ and the coefficients are

$$\alpha_x \sim \begin{cases} \frac{5}{\sqrt{N}} & \text{for } |x\rangle = |x_0\rangle \\ \frac{1}{\sqrt{N}} & \text{otherwise} \end{cases}.$$

At every step t the coefficient of the target $|x_0\rangle$ becomes $\sim \frac{2t+1}{\sqrt{N}}$, with $N \to \infty$, and it is ~ 1 for $t = \frac{\sqrt{N}}{2}$, thus proving the computational cost $O(\sqrt{N})$.

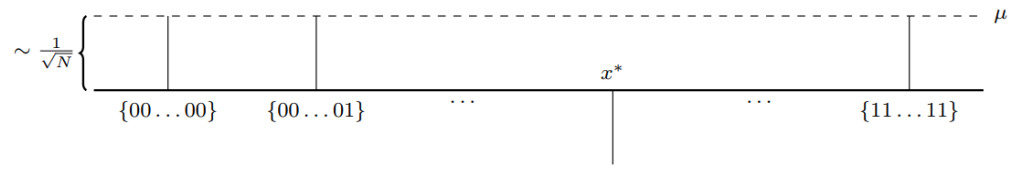

(a) Phase inversion 1

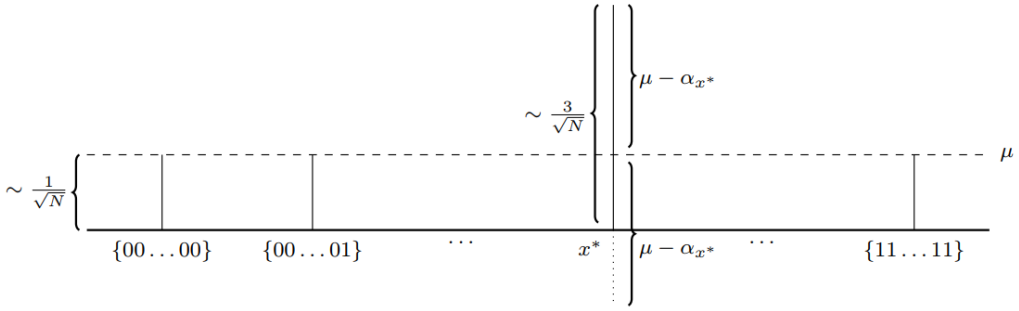

(b) Inversion about mean 1

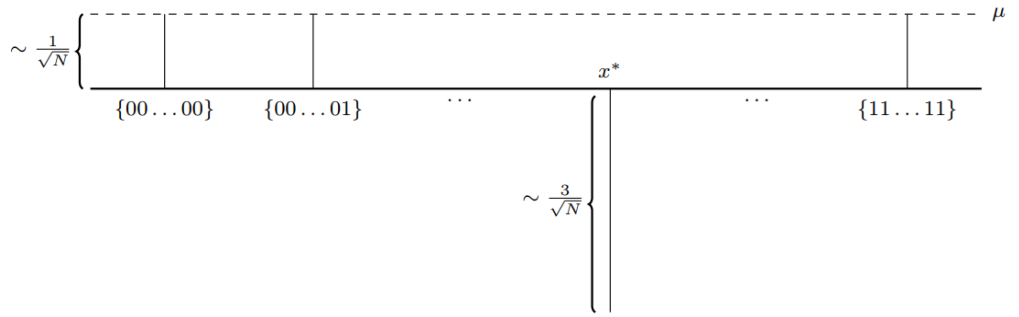

(c) Phase inversion 2

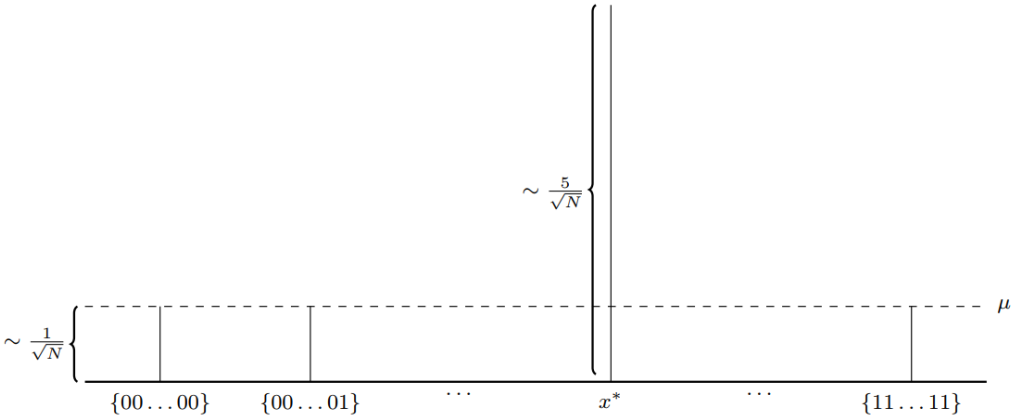

(d) Inversion about mean 2

Figure 3.12: Steps of Grover's search algorithm. Image taken from this reference.

The diffusion operator can be obtained by the quantum circuit

$$D = H^{\otimes N} Z_0 H^{\otimes N}, \tag{3.7}$$

where $H^{\otimes N}$ is the Hadamard gate applied on all N qubits and Z_0 is nothing but the C-Z for $|x_0\rangle = |000\cdots0\rangle$

$$Z_0 = \begin{cases} -|x\rangle & \text{for } |x\rangle = |0\cdots0\rangle \\ \\ |x\rangle & \text{otherwise} \end{cases}. \tag{3.8}$$

The combination of gates in D is

$$H^{\otimes N} Z_0 H^{\otimes N} = H^{\otimes N}(2\,|0\rangle\langle 0| - I)H^{\otimes N} = 2\,|\psi\rangle\langle\psi| - I, \tag{3.9}$$

that applied on a general state $\sum_x \alpha_x$ produces

$$\sum_x \left[-\alpha_x + 2\langle\alpha\rangle\right], \tag{3.10}$$

where $\langle\alpha\rangle = \frac{\sum_x \alpha_x}{N}$ is the mean value of coefficients, so the whole operation is the desired diffusion. The Z_0 gate can be derived from a standard C-Z by applying the X gate before and after the controlled gate on all qubits

$$Z_0 = X^{\otimes N}\text{C-}ZX^{\otimes N}, \tag{3.11}$$

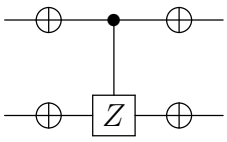

so that

$$D = H^{\otimes N} X^{\otimes N}\text{C-}ZX^{\otimes N} H^{\otimes N}. \tag{3.12}$$

In order to reduce the number of gates, it is possible to prove an equivalent circuits with $X^{\otimes N}$ put at the beginning of the circuit, *i.e.* with qubits initialized to $|111\cdots1\rangle$

(see 3.14).
In order to establish the number of iterations required to maximize the probability of the target state, it is convenient to visualize the Grover iteration $G = DU_f$ from a geometric point of view: two normalized states are defined

$$\begin{aligned} |\alpha\rangle &= \frac{1}{\sqrt{N-M}} \sum |x''\rangle \\ |\beta\rangle &= \frac{1}{\sqrt{M}} \sum |x'\rangle \end{aligned} , \tag{3.13}$$

where N is the total number of states, M the number of solutions (Grover's search can theoretically exploited for searching more targets in the same database), $\sum |x''\rangle$ the sum over all states that are not solution and $\sum |x'\rangle$ the sum over all states that are solution. The initial state may be expressed as

$$|\psi\rangle = \sqrt{\frac{N-M}{N}} |\alpha\rangle + \sqrt{\frac{M}{N}} |\beta\rangle . \tag{3.14}$$

In the following it is supposed $M = 1$, so

$$|\psi\rangle = \sqrt{\frac{N-1}{N}} |\alpha\rangle + \sqrt{\frac{1}{N}} |\beta\rangle . \tag{3.15}$$

Equation 3.15 can be written as

$$|\psi\rangle = \cos\left(\frac{\theta}{2}\right) |\alpha\rangle + \sin\left(\frac{\theta}{2}\right) |\beta\rangle , \tag{3.16}$$

with $\theta = 2 \arccos\left(\sqrt{\frac{N-1}{N}}\right)$; it can be easily proved that the angle $\theta \leq \frac{\pi}{2}$ for $M \leq \frac{N}{2}$. Grover operator G is a rotation in the two-dimensional space with base vectors $|\alpha\rangle$ and $|\beta\rangle$ (Figure 3.13):

- phase inversion U_f reflects the state vector $|\psi\rangle$ about the vector $|\alpha\rangle$, so $U_f(a\,|\alpha\rangle + b\,|\beta\rangle) = |\alpha\rangle - b\,|\beta\rangle$;

- inversion about mean D performs a reflection about $|\psi\rangle$.

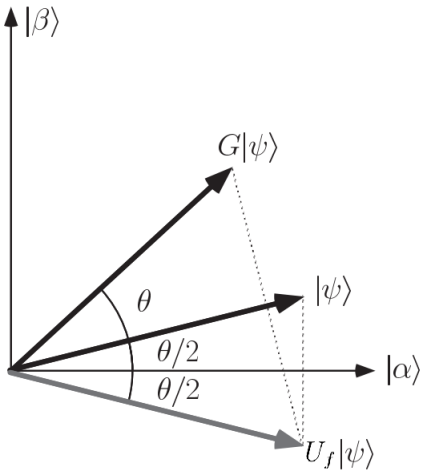

Figure 3.13: Geometric visualization of Grover iteration. Adapted from Nielsen and Chuang, 2011.

The first Grover iteration takes $|\psi\rangle$ to

$$|\psi\rangle = \cos\left(\frac{3}{2}\theta\right)|\alpha\rangle + \sin\left(\frac{3}{2}\theta\right)|\beta\rangle\,, \tag{3.17}$$

so it rotates $|\psi\rangle$ by θ; more in general after the k^{th} iteration the state vector is

$$|\psi\rangle = \cos\left(\frac{2k+1}{2}\theta\right)|\alpha\rangle + \sin\left(\frac{2k+1}{2}\theta\right)|\beta\rangle\,. \tag{3.18}$$

The goal of Grover's algorithm is to maximize the probability of $|\beta\rangle$. Since $M \leq \frac{N}{2}$ and $M \ll N$ in practical cases, the approximation

$$\sin\left(\frac{\theta}{2}\right) \approx \frac{\theta}{2} = \sqrt{\frac{M}{N}}. \tag{3.19}$$

can be exploited. When the angle approaches $\frac{\pi}{2}$ after k iterations, the probability of finding the target is close to 1

$$k\theta \approx 2k\sqrt{\frac{M}{N}} \approx \frac{\pi}{2}. \tag{3.20}$$

For this reason, it is possible to say that the number of iterations required is

$$R \leq \left\lceil \frac{\pi}{4}\sqrt{\frac{N}{M}} \right\rceil , \tag{3.21}$$

thus proving the $O(\sqrt{N})$ computational cost. For $M = 1$, the inequation becomes

$$R \leq \left\lceil \frac{\pi}{4}\sqrt{N} \right\rceil . \tag{3.22}$$

thus proving the $O(\sqrt{N})$ computational cost. The following values provide the maximum value of R for from two to eight qubits.

n	$\left\lceil \frac{\pi}{4}\sqrt{2^n} \right\rceil$
2	2
3	3
4	4
5	5
6	7
7	9
8	13

Table 3.13: Maximum number of iterations in function of the number of qubits N.

A pseudo-code for the Grover's algorithm can be finally written.

```
qubits_init = 0;
qubits = X(qubits_init);
for (k=1;k<ceil(pi/4*sqrt(2^n));k++){
        qubits_phase_inv = C_multiple-Z(qubits,target); //phase inversion

        /* inversion about mean */

        qubits_phase_inv_H = H(qubits_phase_inv);
        qubits_inv_mean = C-multiple-Z(qubits_phase_inv_H,0);
        qubits = H(qubits_inv_mean);
}
result = measure(qubits);
```

The quantum circuits for Grover's search involing two and three qubits are reported in the following figure. The sequence of quantum gates is provided to the molecules for the implementation of the algorithm.

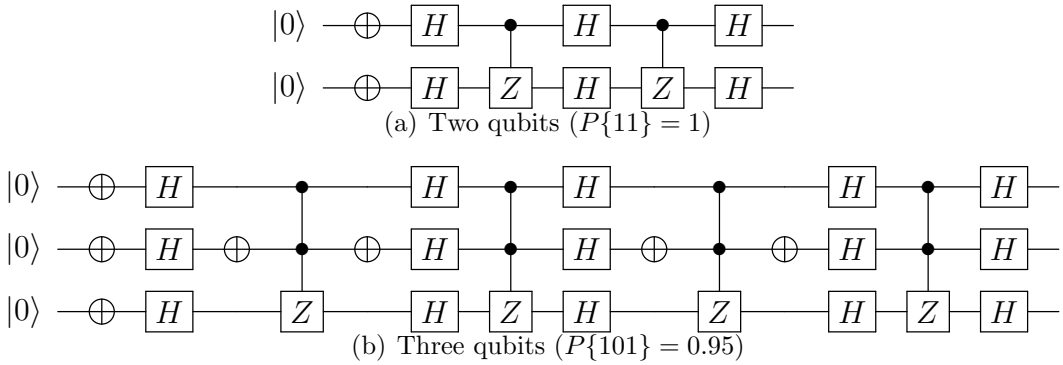

(a) Two qubits ($P\{11\} = 1$)

(b) Three qubits ($P\{101\} = 0.95$)

Figure 3.14: Grover's algorithm quantum circuit.

For the ideal two-qubits circuit, the final probabilities are

$$P = \begin{cases} 1 & \text{for } |x\rangle = |x_0\rangle \\ 0 & \text{otherwise} \end{cases}, \tag{3.23}$$

while or the three-qubits case they are

$$P = \begin{cases} 0.9453 & \text{for } |x\rangle = |x_0\rangle \\ 0.0078 & \text{otherwise} \end{cases}. \tag{3.24}$$

In the following tables the results of the MATLAB simulations for all possible circuits are reported. It has been decided to report the magnitude of complex coeffients $|c_{ijk_{\text{mol}}}|$, obtained by the simulation of the quantum circuit with the molecule, and the difference of probability values obtained by the molecule and the ideal gates $\Delta|c_{ijk}|^2 = |c_{ijk_{\text{mol}}}|^2 - |c_{ijk_{\text{ideal}}}|^2$.

Two-qubits circuits provide more accurate results than the three-qubits ones, since the absolute error is at most in the order of magnitude of 10^{-9}. However, the numerical results obtained in the three-qubits simulations are reliable, since the absolute error is always kept under 10^{-2} for the target event, that is the most probable at the end of the circuit.

Table 3.14: Two-qubits Grover's algorithm implemented on the supramolecular complex: magnitude of coefficients and probability error.

	$\lvert c_{ij_{\text{mol}}}\rvert$	$\Delta\lvert c_{ij}\rvert^2$ $[\cdot 10^{-8}]$		$\lvert c_{ij_{\text{mol}}}\rvert$	$\Delta\lvert c_{ij}\rvert^2$ $[\cdot 10^{-8}]$
$\lvert 00\rangle$	0.999999998	-0.3378944680	$\lvert 00\rangle$	0.000041103	0.1689472834
$\lvert 01\rangle$	0.000041103	0.1689472834	$\lvert 01\rangle$	0.999999998	-0.3378944680
$\lvert 10\rangle$	0.000041103	0.1689472834	$\lvert 10\rangle$	0.000000002	0.0000000004
$\lvert 11\rangle$	0.000000002	0.0000000004	$\lvert 11\rangle$	0.000041103	0.1689472834
	$\lvert c_{ij_{\text{mol}}}\rvert$	$\Delta\lvert c_{ij}\rvert^2$ $[\cdot 10^{-8}]$		$\lvert c_{ij_{\text{mol}}}\rvert$	$\Delta\lvert c_{ij}\rvert^2$ $[\cdot 10^{-8}]$
$\lvert 00\rangle$	0.000041103	0.1689472834	$\lvert 00\rangle$	0.000000002	0.0000000004
$\lvert 01\rangle$	0.000000002	0.0000000004	$\lvert 01\rangle$	0.000041103	0.1689472834
$\lvert 10\rangle$	0.999999998	-0.3378944680	$\lvert 10\rangle$	0.000041103	0.1689472834
$\lvert 11\rangle$	0.000041103	0.1689472834	$\lvert 11\rangle$	0.999999998	-0.3378944680

Table 3.15: Three-qubits Grover's algorithm implemented on the supramolecular complex: magnitude of coefficients and probability error.

	$\lvert c_{ijk_{\text{mol}}}\rvert$	$\Delta\lvert c_{ijk}\rvert^2$ $[\cdot 10^{-4}]$		$\lvert c_{ijk_{\text{mol}}}\rvert$	$\Delta\lvert c_{ijk}\rvert^2$ $[\cdot 10^{-4}]$
$\lvert 000\rangle$	0.97	-0.238	$\lvert 000\rangle$	0.09	0.02
$\lvert 001\rangle$	0.09	-0.021	$\lvert 001\rangle$	0.97	-0.68
$\lvert 010\rangle$	0.09	-0.099	$\lvert 010\rangle$	0.09	0.06
$\lvert 011\rangle$	0.09	0.112	$\lvert 011\rangle$	0.09	0.07
$\lvert 100\rangle$	0.09	-0.027	$\lvert 100\rangle$	0.09	0.06
$\lvert 101\rangle$	0.09	0.008	$\lvert 101\rangle$	0.09	0.09
$\lvert 110\rangle$	0.09	0.054	$\lvert 110\rangle$	0.09	0.15
$\lvert 111\rangle$	0.09	- 0.210	$\lvert 111\rangle$	0.09	0.22
	$\lvert c_{ijk_{\text{mol}}}\rvert$	$\Delta\lvert c_{ijk}\rvert^2$ $[\cdot 10^{-4}]$		$\lvert c_{ijk_{\text{mol}}}\rvert$	$\Delta\lvert c_{ijk}\rvert^2$ $[\cdot 10^{-4}]$
$\lvert 000\rangle$	0.09	-0.01	$\lvert 000\rangle$	0.09	-0.1
$\lvert 001\rangle$	0.09	0.04	$\lvert 001\rangle$	0.09	0.2
$\lvert 010\rangle$	0.97	-1.14	$\lvert 010\rangle$	0.09	0.3
$\lvert 011\rangle$	0.09	0.28	$\lvert 011\rangle$	0.97	-2.1
$\lvert 100\rangle$	0.09	0.13	$\lvert 100\rangle$	0.09	0.2
$\lvert 101\rangle$	0.09	0.15	$\lvert 101\rangle$	0.09	0.3
$\lvert 110\rangle$	0.09	0.22	$\lvert 110\rangle$	0.09	0.4
$\lvert 111\rangle$	0.09	0.32	$\lvert 111\rangle$	0.09	0.5

Table 3.16: Three-qubits Grover's algorithm implemented on the supramolecular complex: magnitude of coefficients and probability error.

	$\lvert c_{ijk_{\mathrm{mol}}}\rvert$	$\Delta\lvert c_{ijk}\rvert^2$ $[\cdot 10^{-4}]$		$\lvert c_{ijk_{\mathrm{mol}}}\rvert$	$\Delta\lvert c_{ijk}\rvert^2$ $[\cdot 10^{-4}]$
$\lvert 000\rangle$	0.09	-0.027	$\lvert 000\rangle$	0.09	0.06
$\lvert 001\rangle$	0.09	0.008	$\lvert 001\rangle$	0.09	0.09
$\lvert 010\rangle$	0.09	0.054	$\lvert 010\rangle$	0.09	0.16
$\lvert 011\rangle$	0.09	0.210	$\lvert 011\rangle$	0.09	0.22
$\lvert 100\rangle$	0.97	-0.238	$\lvert 100\rangle$	0.09	0.02
$\lvert 101\rangle$	0.09	-0.021	$\lvert 101\rangle$	0.97	-0.68
$\lvert 110\rangle$	0.09	-0.099	$\lvert 110\rangle$	0.09	0.06
$\lvert 111\rangle$	0.09	0.111	$\lvert 111\rangle$	0.09	0.06
	$\lvert c_{ijk_{\mathrm{mol}}}\rvert$	$\Delta\lvert c_{ijk}\rvert^2$ $[\cdot 10^{-4}]$		$\lvert c_{ijk_{\mathrm{mol}}}\rvert$	$\Delta\lvert c_{ijk}\rvert^2$ $[\cdot 10^{-4}]$
$\lvert 000\rangle$	0.09	0.13	$\lvert 000\rangle$	0.09	0.2
$\lvert 001\rangle$	0.09	0.15	$\lvert 001\rangle$	0.09	0.3
$\lvert 010\rangle$	0.09	0.22	$\lvert 010\rangle$	0.09	0.4
$\lvert 011\rangle$	0.09	0.32	$\lvert 011\rangle$	0.09	0.5
$\lvert 100\rangle$	0.09	-0.01	$\lvert 100\rangle$	0.09	0.1
$\lvert 101\rangle$	0.09	0.04	$\lvert 101\rangle$	0.09	0.2
$\lvert 110\rangle$	0.97	-1.14	$\lvert 110\rangle$	0.09	0.3
$\lvert 111\rangle$	0.09	0.28	$\lvert 111\rangle$	0.97	-2.0

3.4 Quantum Fourier Transform

The Quantum Fourier Transform (QFT) does exactly the same transformation of the Discrete Fourier Transform (DFT), that takes a vector of complex numbers $[x_0, \cdots, x_{N-1}]$ with length N providing an output complex vector $[y_0, \cdots, y_{N-1}]$ defined by

$$y_k \equiv \frac{1}{\sqrt{N}} \sum_{j=0}^{N-1} x_j \mathrm{e}^{\mathrm{i}2\pi j \frac{k}{N}} \tag{3.25}$$

The main difference between these Fourier transforms is that the Quantum is not upon a set of data as samples of a signal in the time domain, but upon the system state, so the QFT is a DFT on the amplitudes of a quantum state. The QFT is a linear operator on an orthonormal basis $|0\rangle, \cdots, |2^n - 1\rangle$ with the following action on the basis states

$$\sum_{j=0}^{2^n-1} x_j |j\rangle \rightarrow \frac{1}{\sqrt{2^n}} \sum_{k=0}^{2^n-1} \left(\sum_{j=0}^{2^n-1} x_j \mathrm{e}^{\mathrm{i}2\pi j \frac{k}{2^n}} \right) |k\rangle . \tag{3.26}$$

The unitary matrix associated to the QFT is

$$\mathrm{QFT} = \frac{1}{\sqrt{2^n}} \begin{bmatrix} 1 & 1 & 1 & \cdots & 1 \\ 1 & \Omega & \Omega^2 & \cdots & \Omega^{2^n-1} \\ 1 & \Omega^2 & \Omega^4 & \cdots & \Omega^{2(2^n-1)} \\ 1 & \Omega^3 & \Omega^6 & \cdots & \Omega^{3(2^n-1)} \\ & & \vdots & & \\ 1 & \Omega^{2^n-1} & \Omega^{2(2^n-1)} & \cdots & \Omega^{(2^n-1)(2^n-1)} \end{bmatrix}, \tag{3.27}$$

where $\Omega = \mathrm{e}^{\mathrm{i}\frac{2\pi}{2^n}}$. In the following analysis, a fractional binary representation with n qubits $|j_1, \cdots, j_n\rangle = \sum_k \frac{j_k}{2^k} |k\rangle$ is employed. It is possible to prove that Equation 3.26 can be written in a product representation

$$\mathrm{QFT}\left(|j_1, \cdots, j_n\rangle\right) = \frac{\left(|0\rangle + \mathrm{e}^{\mathrm{i}2\pi 0.j_n} |1\rangle\right) \otimes \left(|0\rangle + \mathrm{e}^{\mathrm{i}2\pi 0.j_{n-1}j_n} |1\rangle\right) \otimes \cdots \otimes \left(|0\rangle \mathrm{e}^{\mathrm{i}2\pi 0.j_1 j_2 \cdots j_n} |1\rangle\right)}{\sqrt{2^n}}. \tag{3.28}$$

where the first state of the output basis - corresponding to $|j_1\rangle$ of the input basis - is $\left(|0\rangle + \mathrm{e}^{\mathrm{i}2\pi 0.j_n}|1\rangle\right)$, the second state is $\left(|0\rangle + \mathrm{e}^{\mathrm{i}2\pi 0.j_{n-1}j_n}|1\rangle\right)$ (corresponding to $|j_2\rangle$), and so on. With this notation, the three-qubits quantum Fourier transform can be expressed as

$$\mathrm{QFT}\left(|j_1,j_2,j_3\rangle\right) = \frac{\left(|0\rangle + \mathrm{e}^{\mathrm{i}2\pi 0.j_3}|1\rangle\right) \otimes \left(|0\rangle + \mathrm{e}^{\mathrm{i}2\pi 0.j_2 j_3}|1\rangle\right) \otimes \left(|0\rangle + \mathrm{e}^{\mathrm{i}2\pi 0.j_1 j_2 j_3}|1\rangle\right)}{\sqrt{2^3}}. \tag{3.29}$$

The QFT can be implemented by the following quantum circuit.

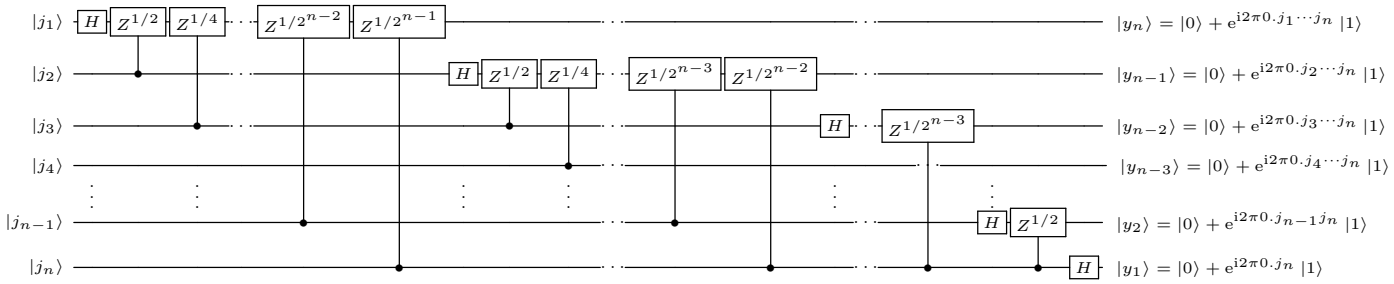

Figure 3.15: Quantum Fourier Transform circuit with n qubits.

The SWAP gates - that reverse the order of the qubits - are not shown. Considering the first qubit j_1, if the Hadamard gate is applied on it, the state $|j\rangle = |j_1 \cdots j_n\rangle$ can be written as

$$\frac{1}{\sqrt{2}}\left(|0\rangle + \mathrm{e}^{\mathrm{i}2\pi 0.j_1}|1\rangle\right)|j_2 \cdots j_n\rangle\,, \tag{3.30}$$

with $\mathrm{e}^{\mathrm{i}2\pi 0.j_1} = -1$ for $j_1 = 1$ ($\mathrm{e}^{\mathrm{i}2\pi(0.1)_2} = \mathrm{e}^{\mathrm{i}2\pi\frac{1}{2}} = -1$) and $+1$ otherwise. The C-$Z^{1/2}$ gate is controlled by j_2, producing the state

$$\frac{1}{\sqrt{2}}\left(|0\rangle + \mathrm{e}^{\mathrm{i}2\pi 0.j_1 j_2}|1\rangle\right)|j_2 \cdots j_n\rangle\,,$$

and at the end of the sequence of C-$Z^{1/2^{1\leq k\leq n-1}}$ gates on j_1 the state is

$$\frac{1}{\sqrt{2}}\left(|0\rangle + \mathrm{e}^{\mathrm{i}2\pi 0.j_1 j_2 \cdots j_n}|1\rangle\right)|j_2 \cdots j_n\rangle\,. \tag{3.31}$$

A similar procedure is performed on j_2, with a resulting state

$$\frac{1}{\sqrt{2^2}}\left(|0\rangle + e^{i2\pi 0.j_1 j_2 \cdots j_n}|1\rangle\right)\left(|0\rangle + e^{i2\pi 0.j_2 \cdots j_n}|1\rangle\right)|j_3 \cdots j_n\rangle\,. \tag{3.32}$$

The same operations are done for the remaining qubits - with $j_{m<n}$ subjected to a sequence of Hadamard and C-$Z^{1/2^{1\leq k\leq n-m}}$ gates, each one controlled by a downer qubit, and j_n to the Hadamard gate only - and the final state can be written as Equation 3.28. It is possible to prove that the same operation can be implemented by a quantum circuit symmetric to that in Figure 3.15, where SWAP gates are at the beginning and the controlled gates have control bits upper than the targets. The complete implemented circuits of the QFT involving two and three qubits (QFT_2 and QFT_3) are reported.

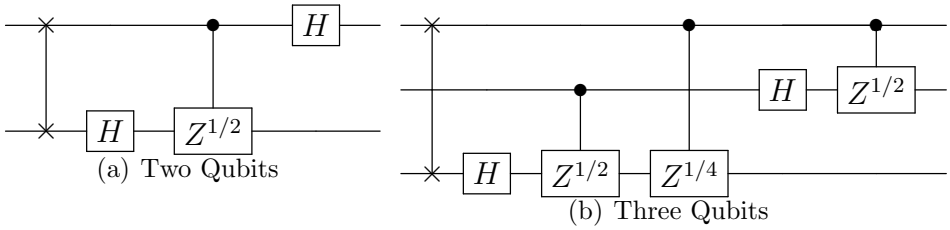

(a) Two Qubits (b) Three Qubits

Figure 3.16: Implemented QFT circuits.

The pseudo-code for a generic QFT_n can be finally written.

```
if (n%2 == 0){
for (k=1; k<=n/2; k++){
        SWAP(qubits(k),qubits(n+1-k));
}}
else{
for (k=1; k<n/2; k++){
        SWAP(qubits(k),qubits(n+1-k));
}}

for (k=n; k>1; k--){
        hadamard(qubits(k));
        for(l=1; l <= n-k; l++){
                CZ(qubits(k),qubits(k-l),l); // CZ^(1/2^l)
        }
}

hadamard(qubits(1);
```

Considering that the gates implemented on the supramolecular complex are affected by phase shifts - described by scalar coefficients $e^{i\phi}$, the implemented algorithms are $-\mathrm{QFT}_2$ and QFT_3. The following tables report the results obtained for different states, in particular:

- magnitude of output coefficients $|c_{ijk_{\mathrm{mol}}}|$;
- output probabilities $|c_{ijk}|^2$;
- difference of magnitude of complex coeffients obtained by the molecule and the ideal gates $\Delta|c_{ijk}| = |c_{ijk_{\mathrm{mol}}}| - |c_{ijk_{\mathrm{ideal}}}|$;
- phase difference $\Delta\phi$ between the ideal output and the implemented one affected by an angular correction that balances the scalar coefficients $e^{i\phi}$.

$|\psi\rangle = \frac{1}{2} \cdot \begin{bmatrix} 1 \\ 1 \\ 1 \\ 1 \end{bmatrix}$

	$\lvert c_{ij_{\mathrm{mol}}}\rvert$	$\lvert c_{ij}\rvert^2$	$\Delta\lvert c_{ij}\rvert$ $[\cdot 10^{-4}]$	$\Delta\phi$ [°]
$\lvert 00\rangle$	0.99999	1	0.00003	-0.01
$\lvert 01\rangle$	0.00003	0	-0.29976	1.51
$\lvert 10\rangle$	0.00007	0	-0.65184	-0.01
$\lvert 11\rangle$	0.00003	0	-0.29971	-6.58

$|\psi\rangle = \frac{1}{2} \cdot \begin{bmatrix} 1 \\ 0 \\ \sqrt{2} \\ 1 \end{bmatrix}$

	$\lvert c_{ij_{\mathrm{mol}}}\rvert$	$\lvert c_{ij}\rvert^2$	$\Delta\lvert c_{ij}\rvert$ $[\cdot 10^{-4}]$	$\Delta\phi$ [°]
$\lvert 00\rangle$	0.85	0.73	0.00001	-0.0119
$\lvert 01\rangle$	0.27	0.07	0.19492	-0.0006
$\lvert 10\rangle$	0.35	0.13	-0.00001	-0.0166
$\lvert 11\rangle$	0.27	0.07	-0.19494	-0.0007

$|\psi\rangle = \frac{1}{2} \cdot \begin{bmatrix} \sqrt{3} \\ 0 \\ 0 \\ 1 \end{bmatrix}$

	$\lvert c_{ij_{\mathrm{mol}}}\rvert$	$\lvert c_{ij}\rvert^2$	$\Delta\lvert c_{ij}\rvert$ $[\cdot 10^{-4}]$	$\Delta\phi$ [°]
$\lvert 00\rangle$	0.68	0.47	0.00003	-0.01
$\lvert 01\rangle$	0.50	0.25	0.34892	-0.01
$\lvert 10\rangle$	0.18	0.03	-0.00011	-0.03
$\lvert 11\rangle$	0.50	0.25	-0.34889	-0.01

Some values present a very high error phase (*e.g.* 292.72° in the table for $|\psi\rangle = \frac{1}{\sqrt{8}} \cdot [11111111]^T$, due to the uncertainty of MATLAB phase computation with very low numbers, where the first significant digits for real and imaginary parts are of the order of magnitude of 10^{-7}; since the magnitudes of the complex numbers affected

$$|\psi\rangle = \tfrac{1}{2} \cdot \begin{bmatrix} 0 \\ \sqrt{2} \\ \sqrt{2} \\ 0 \end{bmatrix}$$

	$\lvert c_{ij_{\mathrm{mol}}}\rvert$	$\lvert c_{ij}\rvert^2$	$\Delta\lvert c_{ij}\rvert$ [$\cdot 10^{-4}$]	$\Delta\phi$ [°]
$\lvert 00\rangle$	0.70711	0.50	0.0000002	-0.01
$\lvert 01\rangle$	0.49999	0.25	0.1258409	-0.01
$\lvert 10\rangle$	0.00001	0	-0.1341848	-180
$\lvert 11\rangle$	0.50001	0.25	-0.1258356	-0.01

$$|\psi\rangle = \tfrac{1}{\sqrt{2}} \cdot \begin{bmatrix} 1 \\ 1 \end{bmatrix} \otimes \begin{bmatrix} 1 \\ 0 \end{bmatrix} \otimes \tfrac{1}{\sqrt{2}} \cdot \begin{bmatrix} 1 \\ -i \end{bmatrix}$$

	$\lvert c_{ijk_{\mathrm{mol}}}\rvert$	$\lvert c_{ijk}\rvert^2$	$\Delta\lvert c_{ij}\rvert$ [$\cdot 10^{-3}$]	$\Delta\phi$ [°]
$\lvert 000\rangle$	0.49999	0.25	0.008	-0.09
$\lvert 001\rangle$	0.00005	0	-0.047	-24.99
$\lvert 010\rangle$	0.70706	0.50	0.047	-0.06
$\lvert 011\rangle$	0.00006	0	-0.055	-9.96
$\lvert 100\rangle$	0.50007	0.25	-0.074	-0.072
$\lvert 101\rangle$	0.00004	0	-0.035	11.91
$\lvert 110\rangle$	0.00017	0	-0.166	0.39
$\lvert 111\rangle$	0.00002	0	-0.020	-75.04

$$|\psi\rangle = \tfrac{1}{\sqrt{3}} \cdot \begin{bmatrix} \sqrt{2} \\ 1 \end{bmatrix} \otimes \tfrac{1}{\sqrt{2}} \cdot \begin{bmatrix} 1 \\ i \end{bmatrix} \otimes \begin{bmatrix} 1 \\ 0 \end{bmatrix}$$

	$\lvert c_{ijk_{\mathrm{mol}}}\rvert$	$\lvert c_{ijk}\rvert^2$	$\Delta\lvert c_{ij}\rvert$ [$\cdot 10^{-3}$]	$\Delta\phi$ [°]
$\lvert 000\rangle$	0.49281	0.243	-0.006	-0.09
$\lvert 001\rangle$	0.00004	0	-0.036	29.44
$\lvert 010\rangle$	0.49270	0.243	0.104	-0.07
$\lvert 011\rangle$	0.11959	0.014	-0.014	-0.09
$\lvert 100\rangle$	0.49293	0.243	-0.135	-0.07
$\lvert 101\rangle$	0.00006	0	-0.057	10.00
$\lvert 110\rangle$	0.49275	0.243	0.045	-0.07
$\lvert 111\rangle$	0.11959	0.014	-0.016	-0.09

$$|\psi\rangle = \tfrac{1}{\sqrt{8}} \cdot \begin{bmatrix} 1 \\ 1 \\ 1 \\ 1 \\ 1 \\ 1 \\ 1 \\ 1 \end{bmatrix}$$

	$\lvert c_{ijk_{\mathrm{mol}}}\rvert$	$\lvert c_{ijk}\rvert^2$	$\Delta\lvert c_{ij}\rvert$ [$\cdot 10^{-4}$]	$\Delta\phi$ [°]
$\lvert 000\rangle$	0.9999999	1	0.000001	-0.09
$\lvert 001\rangle$	0.0000037	0	-0.036663	63.10
$\lvert 010\rangle$	0.0000112	0	-0.111981	104.71
$\lvert 011\rangle$	0.0000026	0	-0.026310	292.72
$\lvert 100\rangle$	0.0000006	0	-0.006117	-0.06
$\lvert 101\rangle$	0.0000026	0	-0.026292	69.81
$\lvert 110\rangle$	0.0000112	0	-0.112008	-104.86
$\lvert 111\rangle$	0.0000037	0	-0.036668	-52.60

$$|\psi\rangle = \frac{1}{\sqrt{8}} \cdot \begin{bmatrix} 0 \\ i \\ 0 \\ \sqrt{2} \\ 0 \\ 0 \\ 2 \\ 1 \end{bmatrix}$$

	$\lvert c_{ijk_{\mathrm{mol}}}\rvert$	$\lvert c_{ijk}\rvert^2$	$\Delta\lvert c_{ij}\rvert$ [$\cdot 10^{-4}$]	$\Delta\phi$ [°]
$\lvert 000\rangle$	0.57	0.32	-0.02	-0.09
$\lvert 001\rangle$	0.18	0.03	0.06	-0.08
$\lvert 010\rangle$	0.48	0.23	-0.31	-0.06
$\lvert 011\rangle$	0.20	0.04	0.15	-0.05
$\lvert 100\rangle$	0.14	0.02	-0.88	-0.08
$\lvert 101\rangle$	0.40	0.16	0.05	-0.05
$\lvert 110\rangle$	0.33	0.11	0.65	-0.06
$\lvert 111\rangle$	0.31	0.09	0.02	0.06

$$|\psi\rangle = \frac{1}{\sqrt{8}} \cdot \begin{bmatrix} -\mathrm{i}\frac{1}{\sqrt{5}} \\ \frac{1}{\sqrt{5}} \\ \mathrm{i}\frac{1}{\sqrt{5}} \\ \sqrt{2} \\ \frac{1}{\sqrt{5}} \\ \frac{1}{\sqrt{5}} \\ 2 \\ 1 \end{bmatrix}$$

	$\lvert c_{ijk_{\mathrm{mol}}}\rvert$	$\lvert c_{ijk}\rvert^2$	$\Delta\lvert c_{ij}\rvert$ [$\cdot 10^{-4}$]	$\Delta\phi$ [°]
$\lvert 000\rangle$	0.72	0.52	-0.02	-0.09
$\lvert 001\rangle$	0.31	0.09	0.08	-0.08
$\lvert 010\rangle$	0.36	0.13	-0.26	-0.07
$\lvert 011\rangle$	0.23	0.05	0.34	-0.04
$\lvert 100\rangle$	0.11	0.01	0.31	359.89 (-0.11)
$\lvert 101\rangle$	0.35	0.12	0.47	-0.05
$\lvert 110\rangle$	0.21	0.04	0.45	-0.07
$\lvert 111\rangle$	0.16	0.03	0.24	-0.06

$$|\psi\rangle = \frac{1}{\sqrt{8}} \cdot \begin{bmatrix} \frac{1}{\sqrt{3}} \\ -\mathrm{i}\frac{1}{\sqrt{3}} \\ \frac{1}{\sqrt{3}} \\ \sqrt{2} \\ 0 \\ 0 \\ 2 \\ 1 \end{bmatrix}$$

	$\lvert c_{ijk_{\mathrm{mol}}}\rvert$	$\lvert c_{ijk}\rvert^2$	$\Delta\lvert c_{ij}\rvert$ [$\cdot 10^{-4}$]	$\Delta\phi$ [°]
$\lvert 000\rangle$	0.70	0.490	0.01	-0.09
$\lvert 001\rangle$	0.21	0.044	0.17	-0.07
$\lvert 010\rangle$	0.35	0.123	-0.35	-0.06
$\lvert 011\rangle$	0.31	0.096	-0.28	-0.05
$\lvert 100\rangle$	0.12	0.014	0.50	-0.03
$\lvert 101\rangle$	0.17	0.030	0.27	-0.04
$\lvert 110\rangle$	0.44	0.195	0.19	-0.06
$\lvert 111\rangle$	0.09	0.008	-0.26	-0.07

by phase error are much lower than the others (6×10^{-7} in the example case), the effect of the phase error is negligible and it does not affect significantly the result of the QFT_3.
The following figures plot the phase coefficients of QFT_2 and QFT_3 with an with input quantum state changing as a sawtooth signal. In both cases, eight iterations are taken into account, so in the two-qubits case the input state changes from $|00\rangle$ to $|11\rangle$ two times (`[0:3,0:3]` according to MATLAB notation) and in the other case there is one period from $|000\rangle$ to $|111\rangle$ (`[0:7]` according to MATLAB notation).

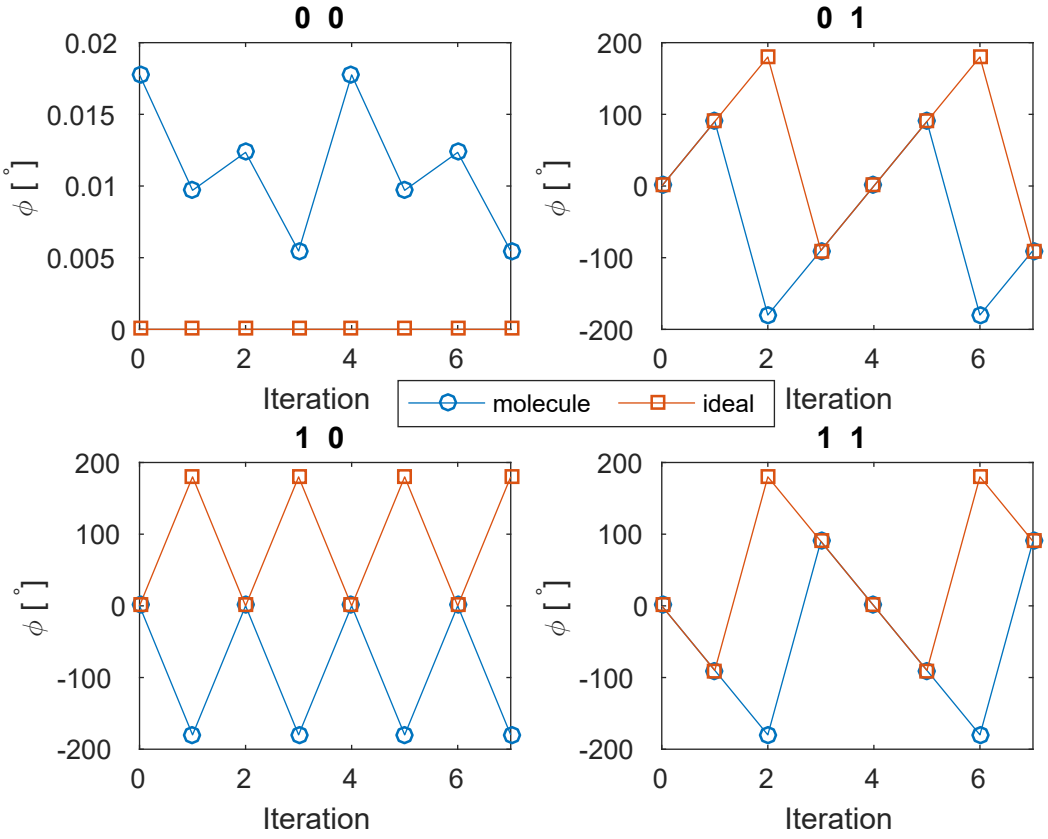

Figure 3.17: Phase evolution of the output coefficients of QFT_2 (sawtooth input state).

In the majority of cases the curves are superposed. Even though some couples of phase look like different, they are the same; in fact, in all these cases the phases are $-\pi$ are $+\pi$ that refer to the same angle on the trigonometric circonference.

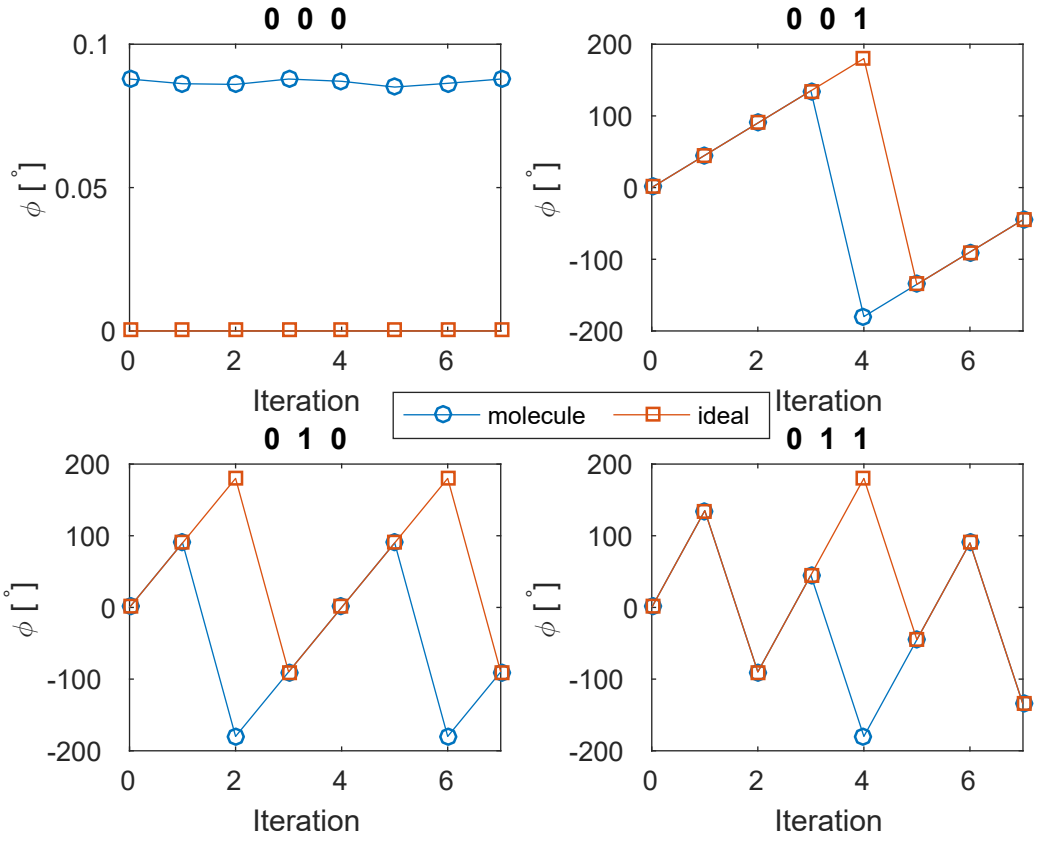

Figure 3.18: Phase evolution of the output coefficients $|0ij\rangle$ of QFT_3 (sawtooth input state).

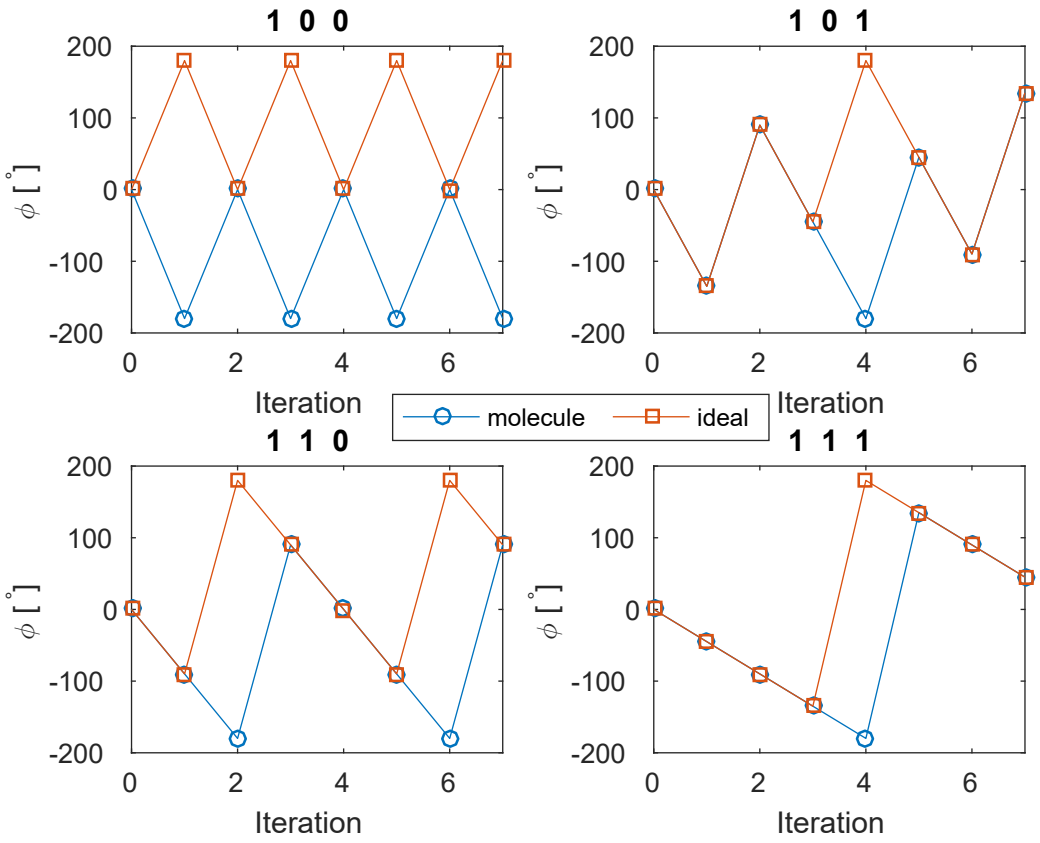

Figure 3.19: Phase evolution of the output coefficients $|1ij\rangle$ of QFT_3 (sawtooth input state).

3.5 Quantum teleportation circuit

Quantum teleportation circuit in Section 1.2.5 has been simulated through a MATLAB script.

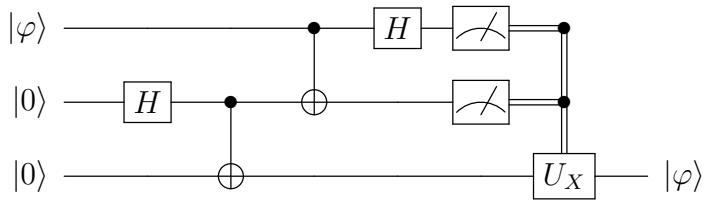

It is recalled that quantum teleportation permits to transmit an unknown quantum state of a qubit on another one with the destruction of the original state. Let $|\varphi\rangle = a\,|0\rangle + b\,|1\rangle$ the state of the qubit to be transmitted. The other two qubits - both initialized to $|0\rangle$ - are entangled by a Hadamard gate and a CNOT. The result is the **Bell state**

$$\left|\Phi^+\right\rangle = \frac{1}{\sqrt{2}}(|00\rangle + |11\rangle). \tag{3.33}$$

Since $|\varphi\rangle$ and $|\Phi^+\rangle$ are separate

$$|\varphi\rangle \otimes \left|\Phi^+\right\rangle = \frac{1}{\sqrt{2}}(a\,|000\rangle + a\,|011\rangle + b\,|100\rangle + b\,|111\rangle). \tag{3.34}$$

A CNOT-12 gate and the Hadamard on the first qubit determine the following state

$$|\psi\rangle = \frac{1}{2}[|00\rangle\,(a\,|0\rangle + b\,|1\rangle) + |01\rangle\,(a\,|1\rangle + b\,|0\rangle) + |10\rangle\,(a\,|0\rangle - b\,|1\rangle) + |11\rangle\,(a\,|1\rangle - b\,|0\rangle)]. \tag{3.35}$$

The first two qubits have equal probability $\frac{1}{4}$ of being $|00\rangle, \cdots, |11\rangle$. When the measurement is done, the third qubit collapses to $a\,|0\rangle + b\,|1\rangle, \cdots, a\,|1\rangle - b\,|0\rangle$. A final correcting gate may be required, in order to obtain $|\varphi\rangle = a\,|0\rangle + b\,|1\rangle$ on the third qubit.

Measure	State collapsed	Gate
00	$a\,\|0\rangle + b\,\|1\rangle$	I (no gate)
01	$a\,\|1\rangle + b\,\|0\rangle$	X
10	$a\,\|0\rangle - b\,\|1\rangle$	Z
11	$a\,\|1\rangle - b\,\|0\rangle$	Y

After the eventual application of the correcting gate, the third qubit is in state $|\varphi\rangle$ and the state on the first one is lost.
Teleportation requires measurements on two qubits to be completed. However, it has not been defined a measurement mechanism for this architecture, so it is not possible to establish whether this circuit is implementable on the three-qubits molecule. Moreover, the measure must be provided to a control system for the evaluation of the corrective rotation and the latency of this procedure cannot be established. Some examples - one for each measure - are reported in the following tables. Since this analysis is preliminary, the measurement and the evaluation of the correction are supposed to be ideal: they are executed on an infinitesimal time interval and measurement mechanism is described by a Dirac delta. For these reasons, the results cannot be considered definitive. As in the other circuits, the effect of real gates is to provide the additional scalar phase contribution $e^{i\phi}$, that does not affect the probabilities of the third qubit, that are $|a|^2$ and $|b|^2$ for $|0\rangle$ and $|1\rangle$ respectively.

Table 3.17: Quantum teleportation examples, one per each possible measure.

$$|\psi\rangle = \frac{1}{\sqrt{2}} \cdot \begin{bmatrix} 1 \\ 1 \end{bmatrix} \; M = 00$$

	$c_{ijk_{\text{mol}}}$	$\Delta\lvert c_{ijk}\rvert^2$ $[\cdot 10^{-4}]$
$\lvert 000\rangle$	-0.7071 - 0.0059 i	0.12
$\lvert 001\rangle$	-0.7071 - 0.0009 i	0.04
$\lvert 010\rangle$	0	0
$\lvert 011\rangle$	0	0
$\lvert 100\rangle$	0	0
$\lvert 101\rangle$	0	0
$\lvert 110\rangle$	0	0
$\lvert 111\rangle$	0	0

$$|\psi\rangle = \frac{1}{\sqrt{5}} \cdot \begin{bmatrix} 2 \\ 1 \end{bmatrix} \; M = 01$$

	$\lvert c_{ijk_{\mathrm{mol}}} \rvert$	$\Delta \lvert c_{ijk} \rvert^2$ [$\cdot 10^{-5}$]
$\lvert 000 \rangle$	0	0
$\lvert 001 \rangle$	0	0
$\lvert 010 \rangle$	-0.005 + 0.894 i	-0.6
$\lvert 011 \rangle$	-0.002 + 0.447 i	-0.2
$\lvert 100 \rangle$	0	0
$\lvert 101 \rangle$	0	0
$\lvert 110 \rangle$	0	0
$\lvert 111 \rangle$	0	0

$$|\psi\rangle = \frac{1}{\sqrt{3}} \cdot \begin{bmatrix} \sqrt{5} \\ 2\mathrm{i} \end{bmatrix} \; M = 10$$

	$\lvert c_{ijk_{\mathrm{mol}}} \rvert$	$\Delta \lvert c_{ijk} \rvert^2$
$\lvert 000 \rangle$	0	0
$\lvert 001 \rangle$	0	0
$\lvert 010 \rangle$	0	0
$\lvert 011 \rangle$	0	0
$\lvert 100 \rangle$	-0.004 + 0.748 i	0.003
$\lvert 101 \rangle$	-0.668 - 0.002 i	0.002
$\lvert 110 \rangle$	0	0
$\lvert 111 \rangle$	0	0

$$|\psi\rangle = \frac{1}{\sqrt{11}} \cdot \begin{bmatrix} 2 \\ \sqrt{7}\mathrm{i} \end{bmatrix} \; M = 11$$

	$\lvert c_{ijk_{\mathrm{mol}}} \rvert$	$\Delta \lvert c_{ijk} \rvert^2$ [$\cdot 10^{-3}$]
$\lvert 000 \rangle$	0	0
$\lvert 001 \rangle$	0	0
$\lvert 010 \rangle$	0	0
$\lvert 011 \rangle$	0	0
$\lvert 100 \rangle$	0	0
$\lvert 101 \rangle$	0	0
$\lvert 110 \rangle$	0.603 + 0.003 i	0.6
$\lvert 111 \rangle$	-0.003 + 0.797 i	0.6

Chapter 4

Molecule characterization

In order to validate the instruction set architecture, it must be required that non-idealities do not affect significantly the system, thus not changing the results. Three dynamic effects must be taken into account:

- spin relaxation;
- spin decoherence;
- residual inter-qubit interaction, that does not ensure the complete insulation of the qubits when the switch is off.

These phenomena can be described by time constants, that are useful for the definition of a time duration on which they are negligible.
It is recalled that spin relaxation has a response equivalent to the voltage discharge on a capacitor. In fact, if the qubit is set to $|1\rangle$ (high energy state), the probability of being in that state is

$$P_1 = \mathrm{e}^{-\frac{t}{T_1}}. \tag{4.1}$$

For the molecular magnet [7] $T_1 = (17.73 \pm 0.33)$ µs, a value much greater than those associated to relaxation and residual interaction; for this reason, spin relaxation will be always neglected. The following sections focus their attention on the other phenomena and the definition of a quasi-ideal operating point where they are all negligible.

4.1 Residual inter-qubit interaction

When the Co switch is in the off state (*i.e.* $M = -\frac{1}{2}$), it is not possible to consider the qubits isolated on an infinite timescale. In fact, a residual interaction is always

present and it can be described - supposing that the static field is applied on the z axis - by the following Hamiltonian[4]:

$$H = \Gamma_{xx}\hat{S}_{1x}\hat{S}_{2x} + \Gamma_{yy}\hat{S}_{1y}\hat{S}_{2y} + \lambda_1\hat{S}_{1z} + \lambda_2\hat{S}_{2z} + C \tag{4.2}$$

with

$$\Gamma_{xx} = -\frac{g_{1z}J_{1y}J_{2x}\left(g_{\mathrm{Coz}}^2 - g_{2z}^2\right) + J_{1x}\left[J_{2x}g_{\mathrm{Coz}}\left(g_{\mathrm{Coz}}^2 - g_{1z}^2 - g_{2z}^2\right) + g_{2z}J_{2y}\left(g_{\mathrm{Coz}}^2 - g_{1z}^2\right)\right]}{4\mu_B B\left(g_{\mathrm{Coz}}^2 - g_{1z}^2\right)\left(g_{\mathrm{Coz}}^2 - g_{2z}^2\right)},$$

$$\Gamma_{yy} = -\frac{g_{2z}J_{1y}J_{2x}\left(g_{\mathrm{Coz}}^2 - g_{1z}^2\right) + J_{2y}\left[J_{1y}g_{\mathrm{Coz}}\left(g_{\mathrm{Coz}}^2 - g_{1z}^2 - g_{2z}^2\right) + g_{1z}J_{1x}\left(g_{\mathrm{Coz}}^2 - g_{2z}^2\right)\right]}{4\mu_B B\left(g_{\mathrm{Coz}}^2 - g_{1z}^2\right)\left(g_{\mathrm{Coz}}^2 - g_{2z}^2\right)},$$

$$\lambda_1 = -\frac{J_{1z}}{2} - \frac{2g_{\mathrm{Coz}}J_{1x}J_{1y} + g_{1z}\left(J_{1x}^2 + J_{1y}^2\right)}{8\mu_B B\left(g_{\mathrm{Coz}}^2 - g_{1z}^2\right)},$$

$$\lambda_2 = -\frac{J_{2z}}{2} - \frac{2g_{\mathrm{Coz}}J_{2x}J_{2y} + g_{2z}\left(J_{2x}^2 + J_{2y}^2\right)}{8\mu_B B\left(g_{\mathrm{Coz}}^2 - g_{2z}^2\right)},$$

$$\hat{S}_{1k=\{x,y,z\}} = \hat{S}_{k=\{x,y,z\}} \otimes I,$$
$$\hat{S}_{2k=\{x,y,z\}} = I \otimes \hat{S}_{k=\{x,y,z\}}.$$

$\hat{S}_j$ are the spin matrices, that permit to write more compactly the spin Hamiltonian equation

$$\begin{aligned}\hat{S}_x &= \frac{\hbar}{2}X,\\ \hat{S}_y &= \frac{\hbar}{2}Y,\\ \hat{S}_z &= \frac{\hbar}{2}Z.\end{aligned} \tag{4.3}$$

Apart from a constant term, Γ_{xx} and Γ_{yy} interactions induce an unwanted evolution when the switch is turned off. The expression above shows that these can be controlled by the size of the applied field or by the size of the Co-ring exchange, in order to obtain high-fidelity single qubit gates. In the simulation of the unwanted evolution, the effect fast oscillations induced by the rotations of single spins around z (proportional to $\hat{S}_z$) must be neglected. From a practical point of view, the terms on the main diagonal of the Hamiltonian matrix must be removed through an analytic correction

$$H' = H - H_0 \tag{4.4}$$

with

$$H_0 = \begin{bmatrix} H_{11} & 0 & 0 & 0 \\ 0 & H_{22} & 0 & 0 \\ 0 & 0 & H_{33} & 0 \\ 0 & 0 & 0 & H_{44} \end{bmatrix}. \tag{4.5}$$

The unitary unwanted evolution can be written as

$$U(t) = \mathrm{e}^{-\mathrm{i}\frac{H'}{\hbar}t}. \tag{4.6}$$

In order to estimate the effect of the unwanted evolution, fidelity has been estimated. It is defined as

$$\mathcal{F}(t) = \langle \psi_I(t) \,|\, \psi(t) \rangle \,, \tag{4.7}$$

where $|\psi_I(t)\rangle$ is the ideal evolution of the quantum state and $|\psi(t)\rangle = U(t)\,|\psi(0)\rangle$ is the real evolution due to inter-qubit interaction. In the absence of residual coupling no evolution occurs, so that $|\psi_I(t)\rangle = |\psi(0)\rangle$. The fidelity for $B = 5\,\mathrm{T}$ is reported in the Figure 4.1; the two curves refer to the evolution of the molecule described in [7] and the evolution of a molecule whose $\underline{J}$ tensors are one half of those of the other molecule. A reduction by a factor of only 2 of the Co-ring exchange is sufficient to increase the timescale of the evolution by an order of magnitude, thus permitting to obtain fidelities close to 1 for longer time intervals. For the fidelity of a single gate, the effect is not very significant in both cases, since the shortest evolution (molecule [7], blue curve in Figure 4.1) occurs on a timescale of $0.5\,\mu\mathrm{s}$, that is significantly longer than the duration of a CNOT gate, that is $\sim 30\,\mathrm{ns}$ with a sequence of four Gaussian pulses [7]. In order to establish a time duration in which the effect is negligible, the time intervals T_{UE} for which $\mathcal{F} \geq 0.9$ have been determined in function of the applied magnetic field, since 4.2 depends on B. The results are reported for both molecules in Figure 4.2. As expected from the $B = 5\,\mathrm{T}$ case, the reduction of $\underline{J}$ terms by a factor two increases significantly the operating time intervals for the same magnetic field; for example, a static field $B = 3\,\mathrm{T}$ is sufficient for $T_{\mathrm{UE}} = 513\,\mathrm{ns}$ - a time duration for some hundred qubit rotations - in the $\frac{1}{2}\underline{J}$ molecule, while $T_{\mathrm{UE}} = 52\,\mathrm{ns}$ when the same field is applied to the $\underline{J}$ molecule. However, since the $\frac{1}{2}\underline{J}$ molecule has not been synthesized, the timing model in Section 4.3 will focus its attention on the molecular magnet already

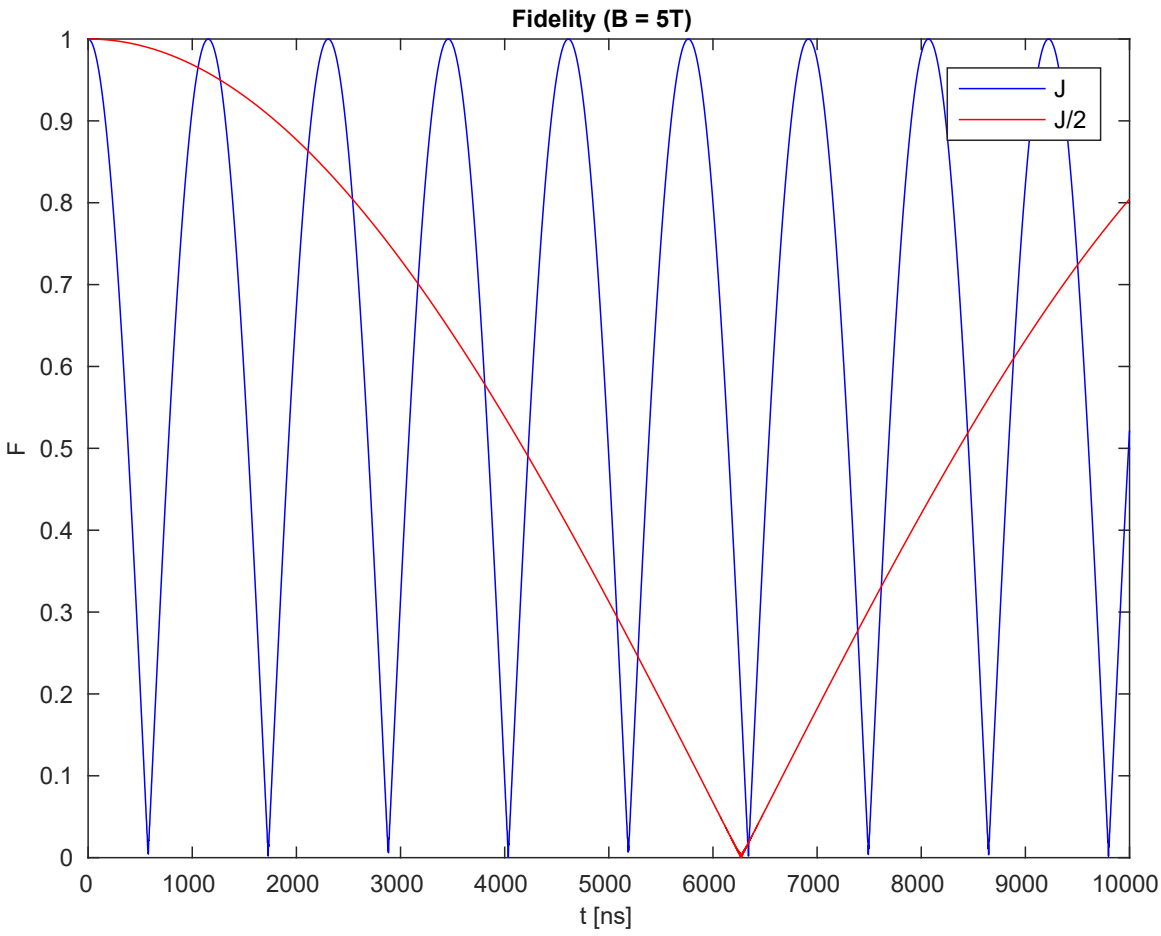

Figure 4.1: Fidelity in function of time - with $B = 5\,\mathrm{T}$ - for two different two-qubit molecules, having different different J exchange factors.

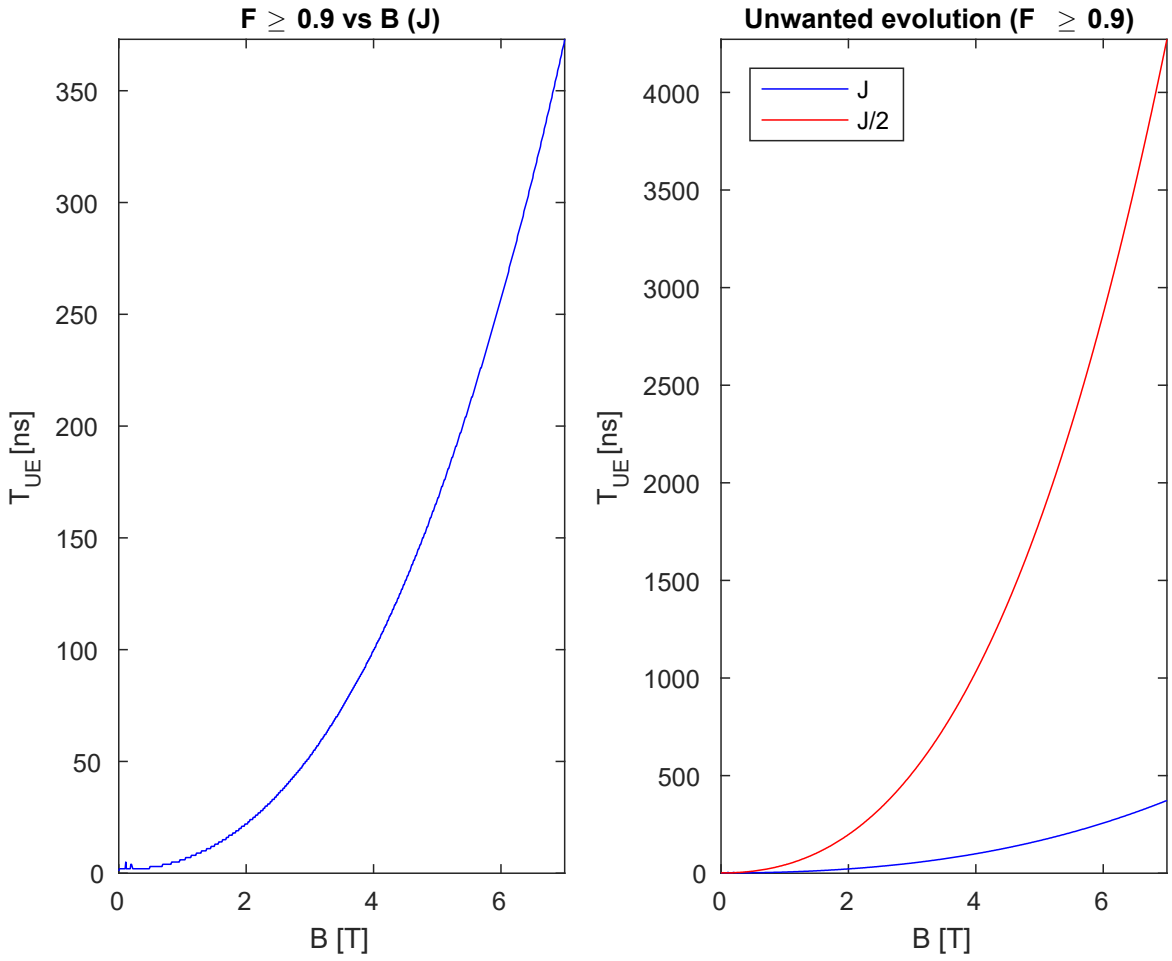

Figure 4.2: Time intervals in which $\mathcal{F} \geq 0.9$ in function of the applied magnetic field.

produced.

The dependency of T_{UE} in function of the number of qubits has been also estimated. Considering the right plot of Supplementary Figure 29 in [7], the unwanted evolution for a molecule with a number of qubits $N \geq 1$ is estimated as

$$T_{\mathrm{UE}}(N) = T_{\mathrm{UE}}(N-1) \cdot \frac{N-1}{N}. \tag{4.8}$$

Plots in Figure 4.3 report $T_{\mathrm{UE}}(N)$ - for $\underline{J}$ and $\frac{1}{2}\underline{J}$ - for $B = 5\,\mathrm{T}$ and with variable field $0\,\mathrm{T} \leq B \leq 7\,\mathrm{T}$.

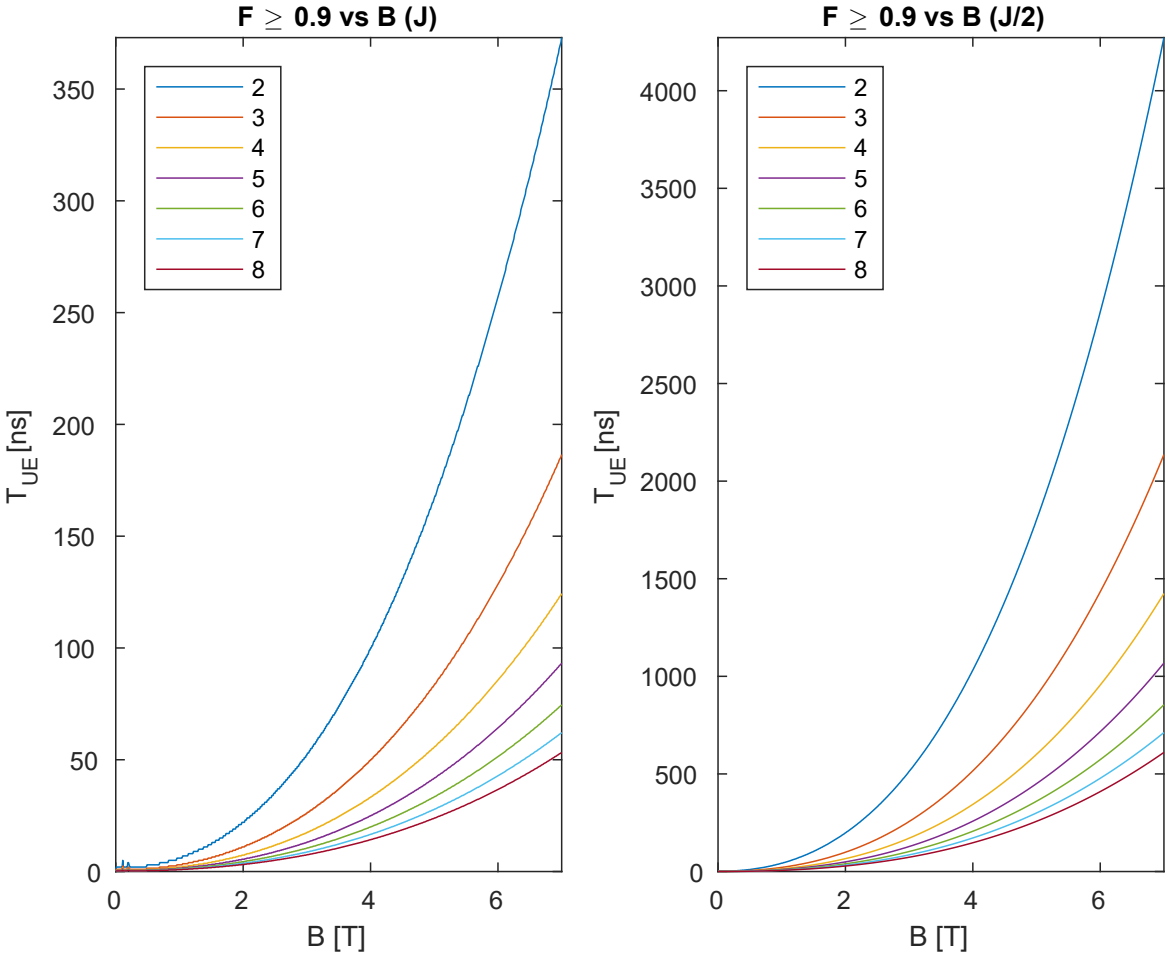

Figure 4.4: Time intervals in which $\mathcal{F} \geq 0.9$ in function of the applied field B, for molecules with different number of qubits.

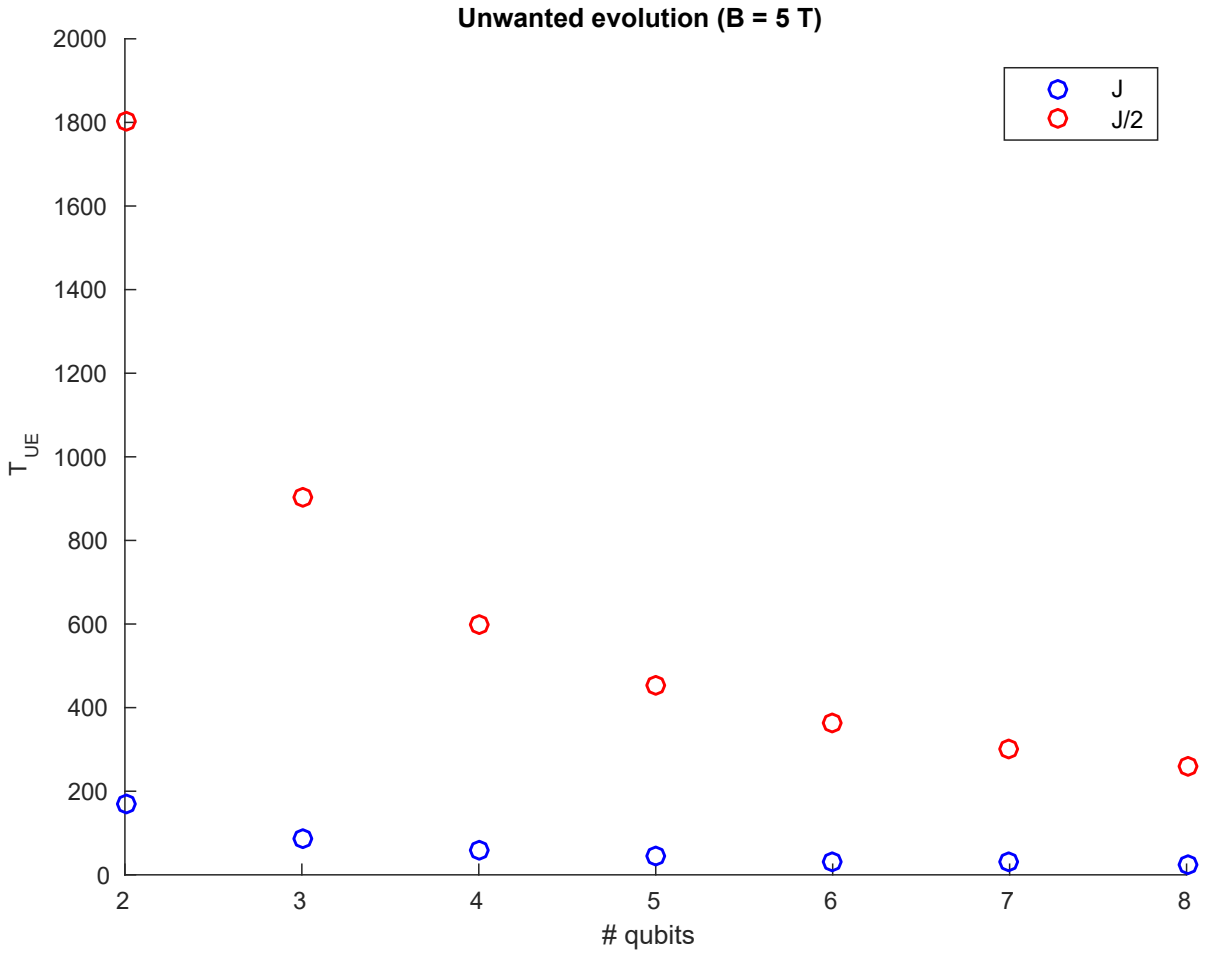

Figure 4.3: Time intervals in which $\mathcal{F} \geq 0.9$ in function of the number of qubits, with $B = 5\,\mathrm{T}$.

Molecules with more qubits are subjected to a more significant qubit-qubit interaction, thus limiting the maximum time duration keeping the fidelity of the quantum system over 0.9. As usual, the $\frac{1}{2}\underline{J}$ molecules present timescales that are one order of magnitude longer than the $\underline{J}$ ones - for the same static field - or equivalently it is possible to obtain the same T_{UE} of $\underline{J}$ molecular magnets for lower static fields; for three-qubits molecules, $T_{\mathrm{UE}} = 100\,\mathrm{ns}$ for $B = 5.4\,\mathrm{T}$ on the $\underline{J}$ molecule and $B \simeq 2\,\mathrm{T}$ for the $\frac{1}{2}\underline{J}$ one.

4.2 Decoherence

Similarly to the residual qubit-qubit interaction, a fidelity due to decoherence can be defined for non-interacting qubits subjected to Lindblad (Markovian) dynamics

$$\mathcal{F} = \sqrt{|\alpha|^4 + |\beta|^4 + 2|\alpha|^2|\beta|^2 \mathrm{e}^{-\frac{t}{2T_M}}} = \sqrt{1 - 2|\alpha|^2|\beta|^2 \left(1 - \mathrm{e}^{-\frac{t}{2T_M}}\right)}. \tag{4.9}$$

Fidelity permits to define the decoherence error

$$\epsilon = 1 - \mathcal{F}^2 = 2|\alpha|^2|\beta|^2 \left(1 - \mathrm{e}^{-\frac{t}{2T_M}}\right), \tag{4.10}$$

that is maximed for the same t in the state $|\alpha|^2 = |\beta|^2 = \frac{1}{2}$, *i.e.* on equator of the Bloch sphere

$$\epsilon = \frac{1}{2}\left(1 - \mathrm{e}^{-\frac{t}{2T_M}}\right). \tag{4.11}$$

When the molecule presents N qubits, the decoherence error is simply obtained by multiplying Equation 4.11 by N

$$\epsilon_N = \frac{N}{2}\left(1 - \mathrm{e}^{-\frac{t}{2T_M}}\right). \tag{4.12}$$

For the considered molecules, decoherence affects not only the qubits but also the Co switch. The decoherence of each qubit in molecule [7] is considered independent from the applied magnetic field and it is equal to

$$T_M = 683\,\mathrm{ns},$$

for $T = 2.8\,\mathrm{K}$, while the switch decoherence depends on B. Considering the Supplementary Table 5 of [7], a dependence $T_M(B)$ has been estimated though linear regression and it is plotted in Figure 4.5. For $B \geq 3\,\mathrm{T}$ the Co switch decoherence

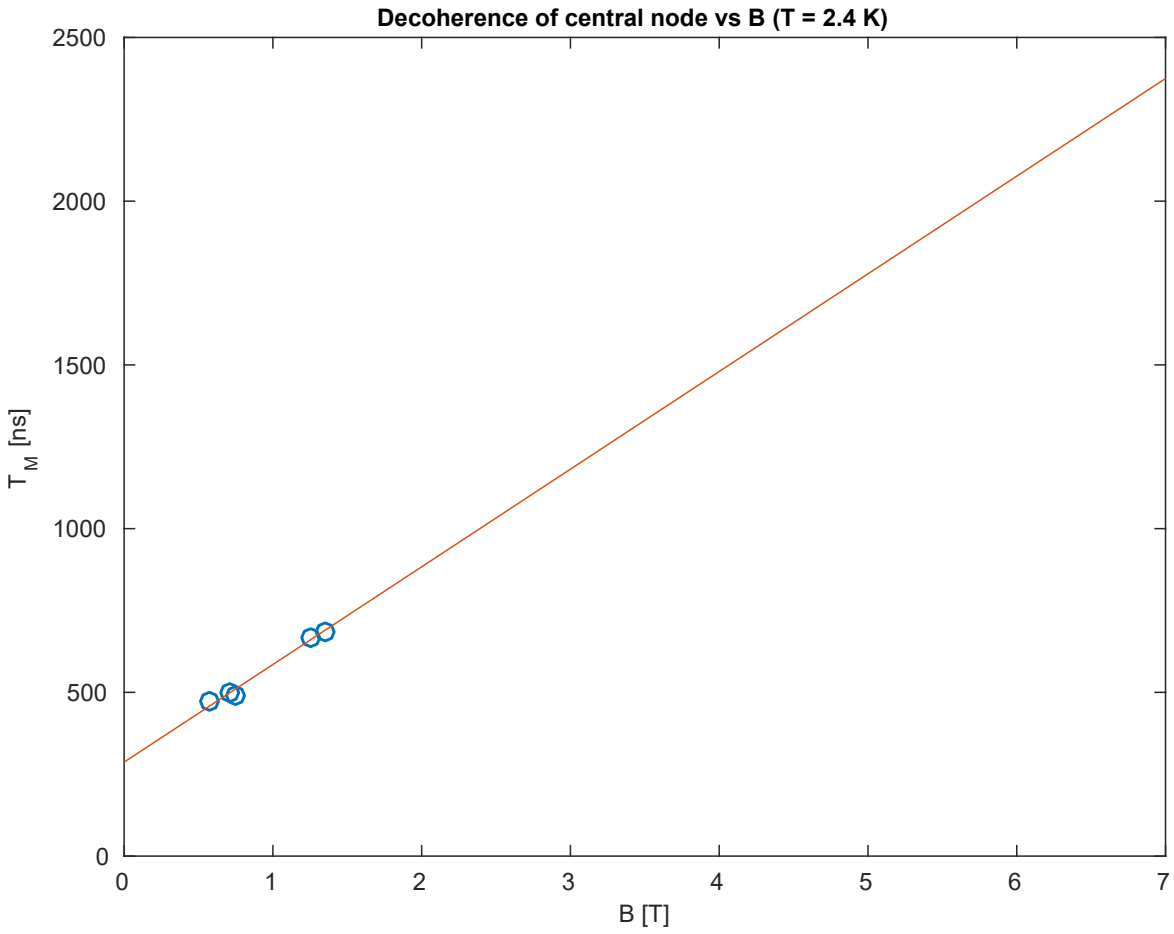

Figure 4.5: Decoherence of Co switch in function of B. The blue circles refer to measured values in [7], exploited for linear regression.

occurs on a timescale longer than that of qubits, thus permitting to consider it negligible.

In order to establish the effect of decoherence on the reliability of results, the time duration τ_M has been computed, for which the error ϵ_N - given by Equation 4.12 - is lower than 0.1 ($\mathcal{F} = 0.949$) for qubit and switch. In the first case - with T_M supposed

to be constant - τ_M has been estimated in function of the number of qubits:

$$\tau_M = \frac{2}{N} T_M \log\left(\frac{1}{1-2\epsilon}\right). \tag{4.13}$$

Since the fidelity for $\epsilon \leq 0.1$ is higher than 0.9 - the threshold exploited to obtain Figures 4.2 - larger timescales would be obtained when the maximum admitted error is that for $\mathcal{F} = 0.9$ ($\epsilon \leq 1 - 0.9^2 \leq 0.19$).

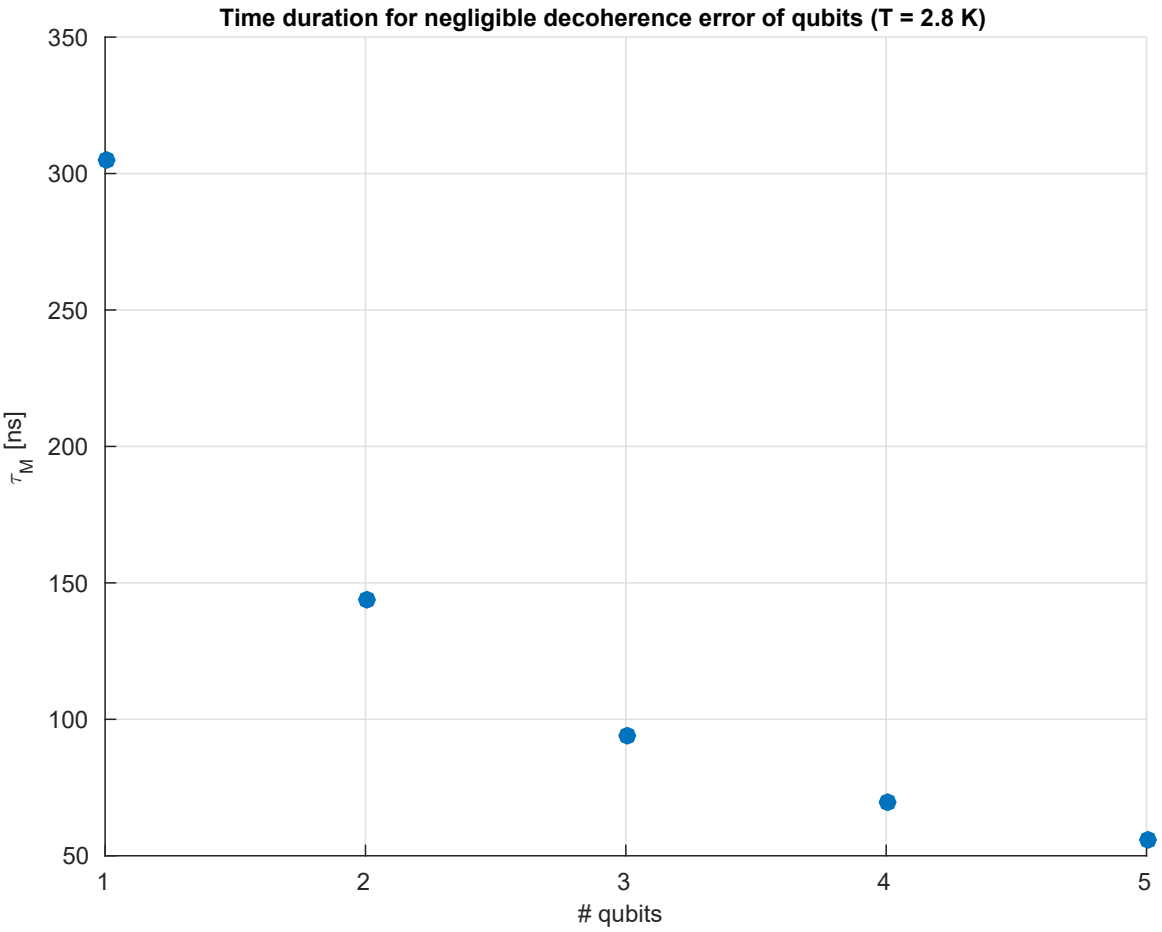

Figure 4.6: Time intervals for qubits decoherence error $\epsilon \leq 0.1$ in function of the total number of qubits in a molecule.

The predicted τ_M values for molecules with two and three qubits are exploited in Section 4.3 as timing thresholds for the execution of elementary instructions and quantum programs.
In the switch case, the decoherence error $\tau_{M_{\text{sw}}}$ has been computed in function of the applied magnetic field (Figure 4.7). It is possible to say that the switch does not

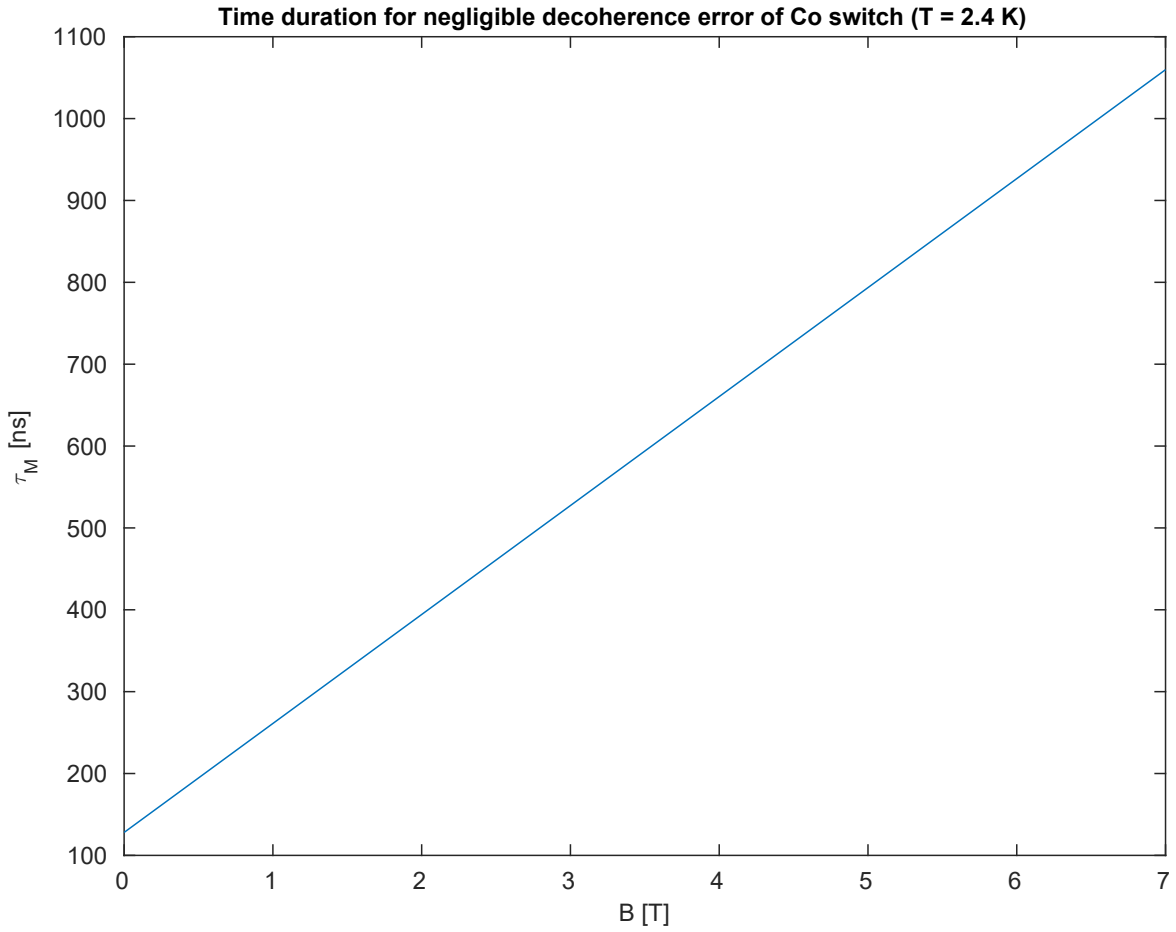

Figure 4.7: Time intervals for switch decoherence error $\epsilon \leq 0.1$ in function of the applied magnetic field.

affect significantly the functionality of the gate for $B \geq 3\,\text{T}$, since $\tau_{M_{\text{sw}}}$ is longer than both τ_M and T_{UE}.

4.3 Timing

It is possible to define a **time duration Δt for the implementation of quantum gates and algorithms** in which two and three-qubits molecules (with the parameters in [7]) can be considered quasi-ideal. It is supposed that $\tau_M < T_{\mathrm{UE}}$, *i.e.* the **shortest timescale is that associated to the qubit decoherence**; this condition can be reached by applying a sufficiently high static field ($B \sim 6\,\mathrm{T}$), with the drawback that the transition energies can belong to the infrared spectrum ($150\,\mathrm{GHz} \leq f \leq 560\,\mathrm{GHz}$ approximately). The time interval for each gate/algorithm is computed by multiplying the longest sequence of gates by the pulse duration τ, supposing that all gates are executed in sequence; it is a worst case scenario, since there are some single rotations on different qubits than can be executed in parallel. Figures 4.8 and 4.9 compare time durations of all gates in the instruction set and of the elementary algorithms with the critical time duration Δt. It is recalled that the pulse duration τ is equal to 5 ns and 2.3 ns in the two and three-qubits cases respectively. Single rotations and the two-qubits QFT can be completed during the critical time interval, even in the worst-case, while the Grover's algorithm does not always satisfy the timing requirements. In fact, differently from the pure sequential `Grover S` approach, the `Grover P` algorithm execution parallelizes single rotations on different qubits, thus keeping the latency under threshold. In the molecule with three qubits, even if the critical timescale is shorter than the corresponding for two qubits, the controlled gates involving a couple of non-adjacent qubits, the CC-Z-based gates and the three-qubits QFT can be executed on a time interval lower than the critical one. The Grover's algorithm requires a so high number of gates that the timing requirements are not satisfied in both `S` and `P` cases.

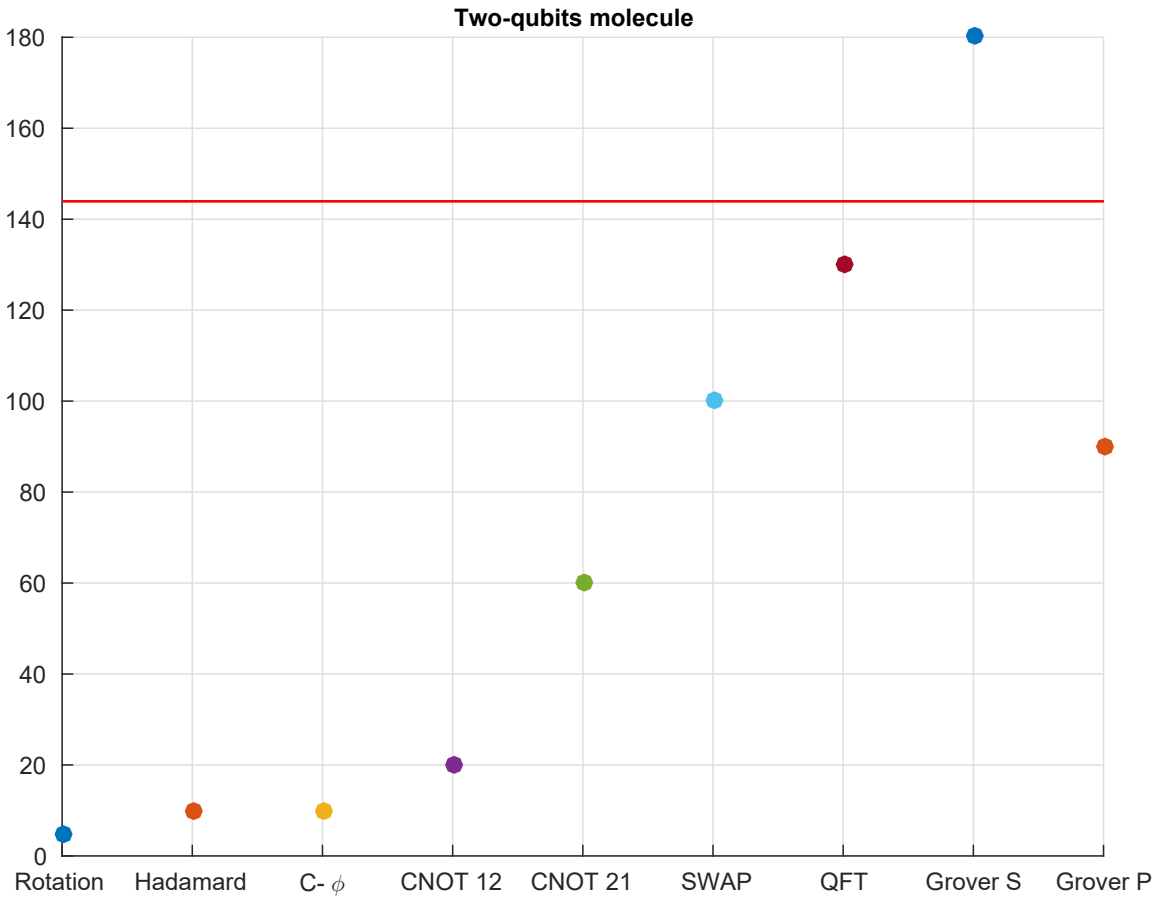

Figure 4.8: Delay estimations for $\tau = 5\,\text{ns}$. Time duration measured in nanosecond.

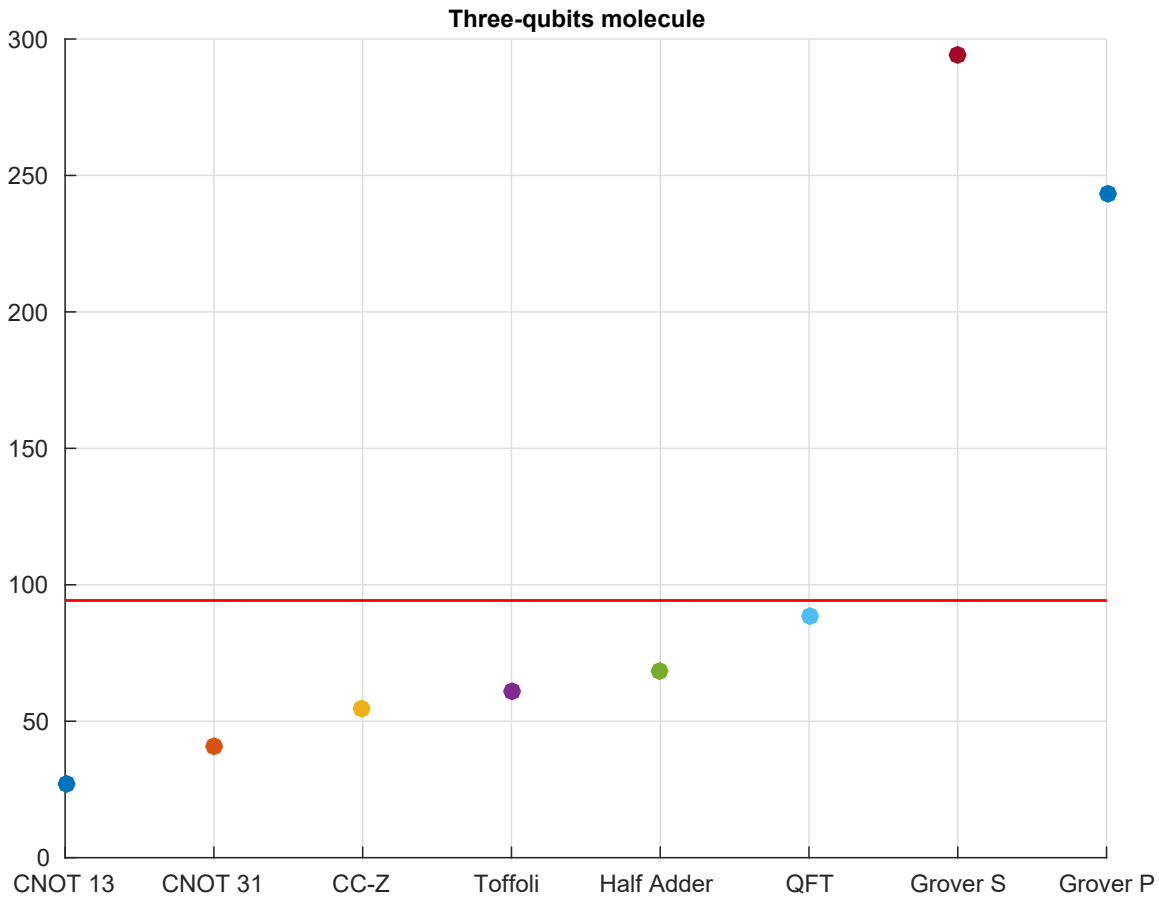

Figure 4.9: Delay estimations for $\tau = 2.3\,\text{ns}$. Time duration measured in nanosecond.

Conclusions

The execution unit of the quantum computer is studied in this thesis and a possible model for the quantum gates implementation is defined, taking care of non-idealities. It must be observed that the spin manipulation model employed in this thesis is ideal, since pulses are supposed to be rectangular with infinite frequency bandwidth and infinitesimal rising/falling edges. Real modulating signals have finite-bandwidth spectrum and they imply higher errors in the calculation of qubit complex coefficients. For these reasons, the implemented gates must be simulated through more sophisticated quantum models, where the shape of modulating pulses could be Gaussian or trapezoidal and numerical resolution of Schrödinger equations can be executed on environments as the Quantum Toolbox in Python (QuTiP) or Simulink.
The results obtained in chapters 3 and 4 can be considered optimistic for the feasibility of a quantum computer based on molecular magnets, since the DiVincenzo criteria for quantum computers could be totally satisfied in the next decades.
Microwave or infrared - depending on the complexity of the molecule, that influences the values of energy levels - magnetic fields manipulate spins for fields of few tesla. The realization of front-end and back-end of the architecture must also be defined. For the spin manipulation point of view, a reference can be the EPR spectrometer in Figure 4.10 [10], where the modulating signal can generate different pulse shapes including rectangular, triangular, Gaussian and sync from a Digital-to-Analog Converter. On the other hand, SQUID-based circuits look like to be the most serious candidates for spin qubit measurement. Moreover, the definition of the back-end circuitry would be fundamental for the estimation of the total latency of quantum teleportation in the three-qubits molecule.

Elementary arithmetic-logic operations up to an half-adder and the QFT can be executed on available molecules with negligible dynamic errors on timescales of hundreds of nanosecond. Supramolecular complexes with more than three qubits could permit the implementation of more sophisticated gates and algorithms, *e.g.* the reversible full-adder with four qubits.

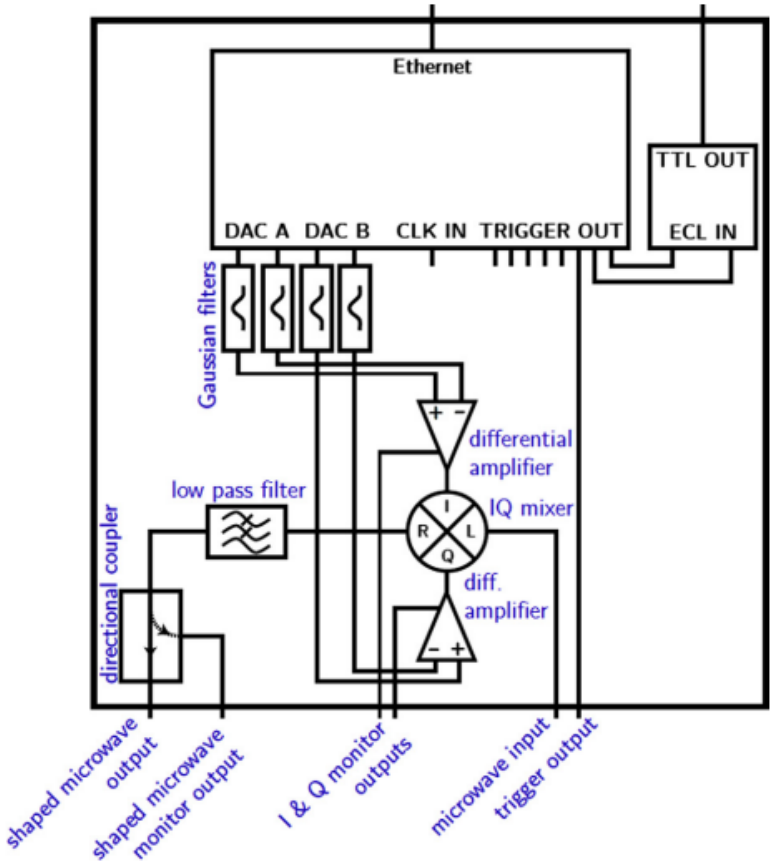

Figure 4.10: Schematic of an arbitrary waveform generation unit, where the output waveform of a DAC are employed for the modulation of a microwave carrier through a I/Q mixer. Kaufmann *et al.*, 2013.

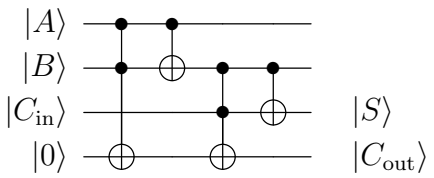

Figure 4.11: Reversible full adder.

Two-qubits Grover's algorithm can be implemented with negligible errors, if the available instrumentation permits to execute single rotations on different qubits in parallel.

In order to obtain a quantum computer reliable on larger timescales, quantum information must be protected from errors due to decoherence and other quantum noise (faulty quantum gates, faulty quantum preparation, and faulty measurements) and Quantum Error Correction (QEC) strategies can help for reaching this target.

All the considered perspectives and goals require the parallel support of chemical engineering, through the synthesis of molecules with more qubits and longer timescales for non-idealities. Cr_7Ni rings with decoherence timescales of 15 µs have been already synthesized [28] and their insertion in supramolecular complexes would be an essential step towards a reliable and scalable quantum computing architecture.

Bibliography

[1] José J Baldoví, Salvador Cardona-Serra, Juan M Clemente-Juan, Eugenio Coronado, Alejandro Gaita-Ariño, and Helena Prima-García. Coherent manipulation of spin qubits based on polyoxometalates: the case of the single ion magnet $[GdW_{30}P_5O_{110}]^{14-}$. *Chemical Communications*, 49(79):8922–8924, 2013.

[2] Lapo Bogani and Wolfgang Wernsdorfer. Molecular spintronics using single-molecule magnets. *Nature materials*, 7(3):179, 2008.

[3] Siegmund Brandt and Hans Dieter Dahmen. *The picture book of quantum mechanics*. Springer Science & Business Media, 2012.

[4] Alessandro Chiesa, Paolo Santini, and Stefano Carretta. Supramolecular complexes for quantum simulation. *Magnetochemistry*, 2(4):37, 2016.

[5] Michel H Devoret and Robert J Schoelkopf. Superconducting circuits for quantum information: an outlook. *Science*, 339(6124):1169–1174, 2013.

[6] David P DiVincenzo et al. The physical implementation of quantum computation. *arXiv preprint quant-ph/0002077*, 2000.

[7] Jesús Ferrando-Soria, Eufemio Moreno Pineda, Alessandro Chiesa, Antonio Fernandez, Samantha A Magee, Stefano Carretta, Paolo Santini, Iñigo J Vitorica-Yrezabal, Floriana Tuna, Grigore A Timco, et al. A modular design of molecular qubits to implement universal quantum gates. *Nature communications*, 7, 2016.

[8] MD Jenkins, Y Duan, B Diosdado, JJ García-Ripoll, A Gaita-Ariño, C Giménez-Saiz, PJ Alonso, E Coronado, and F Luis. Coherent manipulation of three-qubit states in a molecular single-ion magnet. *Physical Review B*, 95(6):064423, 2017.

[9] MD Jenkins, D Zueco, O Roubeau, G Aromí, J Majer, and F Luis. A scalable architecture for quantum computation with molecular nanomagnets. *Dalton Transactions*, 45(42):16682–16693, 2016.

[10] Thomas Kaufmann, Timothy J Keller, John M Franck, Ryan P Barnes, Steffen J Glaser, John M Martinis, and Songi Han. Dac-board based x-band epr spectrometer with arbitrary waveform control. *Journal of Magnetic Resonance*,

235:95–108, 2013.

[11] Michael N Leuenberger and Daniel Loss. Quantum computing in molecular magnets. *Nature*, 410(6830):789, 2001.

[12] R Maurand, X Jehl, D Kotekar-Patil, A Corna, H Bohuslavskyi, R Laviéville, L Hutin, S Barraud, M Vinet, M Sanquer, et al. A cmos silicon spin qubit. *Nature communications*, 7:13575, 2016.

[13] David McMahon. *Quantum computing explained*. John Wiley & Sons, 2007.

[14] Corrado Mencuccini and Vittorio Silvestrini. *Fisica II: Elettromagnetismo, Ottica*. Liguori, Napoli, 1988.

[15] Nakahara Mikio, Rahimi Robabeh, and Saitoh Akira. *Mathematical Aspects Of Quantum Computing 2007*, volume 1. World Scientific, 2008.

[16] David AB Miller. *Quantum mechanics for scientists and engineers*. Cambridge University Press, 2008.

[17] John JL Morton, Dane R McCamey, Mark A Eriksson, and Stephen A Lyon. Embracing the quantum limit in silicon computing. *Nature*, 479(7373):345, 2011.

[18] Mikio Nakahara and Tetsuo Ohmi. *Quantum computing: from linear algebra to physical realizations*. CRC press, 2008.

[19] A.V. Narlikar, Y.Y. Fu, and W. Wernsdorfer. Molecular nanomagnets: Towards molecular spintronics. In Anant V Narlikar and Yunyi Y Fu, editors, *Oxford Handbook of Nanoscience and Technology: Volume 3: Applications*, volume 3. Oxford University Press, 2010.

[20] Michael A. Nielsen and Isaac L. Chuang. *Quantum Computation and Quantum Information: 10th Anniversary Edition*. Cambridge University Press, New York, NY, USA, 10th edition, 2011.

[21] Peter James Joyce O'Malley. *Superconducting Qubits: Dephasing and Quantum Chemistry*. University of California, Santa Barbara, 2016.

[22] Ana María Repollés Rabinad. *Quantum computing with molecular magnets*, volume 131. Prensas de la Universidad de Zaragoza, 2016.

[23] Hiroyuki Sagawa and Nobuaki Yoshida. *Fundamentals of quantum information*. World Scientific, 2011.

[24] Roberta Sessoli, Dante Gatteschi, Andrea Caneschi, and MA Novak. Magnetic bistability in a metal-ion cluster. *Nature*, 365(6442):141, 1993.

[25] J Tejada, EM Chudnovsky, E Del Barco, JM Hernandez, and TP Spiller. Magnetic qubits as hardware for quantum computers. *Nanotechnology*, 12(2):181, 2001.

[26] Grigore A Timco, Stefano Carretta, Filippo Troiani, Floriana Tuna, Robin J Pritchard, Christopher A Muryn, Eric JL McInnes, Alberto Ghirri, Andrea Candini, Paolo Santini, et al. Engineering the coupling between molecular spin qubits by coordination chemistry. *Nature Nanotechnology*, 4(3):173–178, 2009.

[27] Filippo Troiani and Marco Affronte. Molecular spins for quantum information technologies. *Chemical Society Reviews*, 40(6):3119–3129, 2011.

[28] Christopher J Wedge, GA Timco, ET Spielberg, RE George, F Tuna, S Rigby, EJL McInnes, REP Winpenny, SJ Blundell, and A Ardavan. Chemical engineering of molecular qubits. *Physical review letters*, 108(10):107204, 2012.

[29] Karl Weighardt, Klaus Pohl, Ibrahim Jibril, and Gottfried Huttner. Hydrolysis products of the monomeric amine complex (c6h15n3) fecl3: The structure of the octameric iron (III) cation of $\{[(C_6H_{15}N_3)_6Fe_8(\mu_3\text{-}O)_2(\mu_2\text{-}OH)_{12}]Br_7(H_2O)\}Br_8H_2O$. *Angewandte Chemie International Edition*, 23(1):77–78, 1984.

[30] Noson S. Yanofsky and Mirco A. Mannucci. *Quantum Computing for Computer Scientists*. Cambridge University Press, New York, NY, USA, 1 edition, 2008.